Electronic Thesis and Dissertation Repository

9-6-2011 12:00 AM

Investigation of Hybrid Monopile-Footing Foundation Systems Subjected to Combined Loading

Mohamed El-Marassi, *The University of Western Ontario*

Supervisor: Dr. M. Hesham El-Naggar, *The University of Western Ontario*
A thesis submitted in partial fulfillment of the requirements for the Doctor of Philosophy degree
in Civil and Environmental Engineering
© Mohamed El-Marassi 2011

Follow this and additional works at: https://ir.lib.uwo.ca/etd

Part of the Geotechnical Engineering Commons

Recommended Citation

El-Marassi, Mohamed, "Investigation of Hybrid Monopile-Footing Foundation Systems Subjected to Combined Loading" (2011). *Electronic Thesis and Dissertation Repository*. 261.
https://ir.lib.uwo.ca/etd/261

INVESTIGATION OF HYBRID MONOPILE-FOOTING FOUNDATION SYSTEMS
SUBJECTED TO COMBINED LOADING

(Spine title: Hybrid Monopile-Footing Foundation Systems)

(Thesis format: Integrated-Article)

by

Mohamed El-Marassi

Graduate Program in Civil and Environmental Engineering

A thesis submitted in partial fulfillment
of the requirements for the degree of
Doctor of Philosophy

The School of Graduate and Postdoctoral Studies
The University of Western Ontario
London, Ontario, Canada

THE UNIVERSITY OF WESTERN ONTARIO
School of Graduate and Postdoctoral Studies

CERTIFICATE OF EXAMINATION

Supervisors

_____
Dr. M. Hesham El-Naggar

Co-Supervisor

_____
Dr. Timothy A. Newson

Supervisory Committee

_____
Dr. Maged A. Youssef

Examiners

_____
Dr. Leo Rothenburg

_____
Dr. Julie Q. Shang

_____
Dr. Michael F. Bartlett

_____
Dr. Tom Jenkyn

The thesis by

Mohamed Asser El-Marassi

entitled:

Investigation of Hybrid Monopile - Footing Foundation Systems Subjected to Combined Loading

is accepted in partial fulfillment of the
requirements for the degree of
Doctor of Philosophy

_____   _____
Date   Chair of the Thesis Examination Board

ii

Abstract

Laterally loaded structures such as wind turbines, offshore platforms, earth retaining structures, bridge abutments and many other structures impose complex loading regimes on the supporting foundations. These foundations are typically subjected to combinations of vertical, horizontal and moment loadings resulting from the vertical self-weight of the foundation system, superstructure, soil fill and surface surcharge, in addition to significant lateral loads and moments due to soil pressures, wind loads, waves and currents. In the case of shallow foundations, the weight and dimensions must be sufficient to resist tilting and sliding, whilst at the same time preventing failure of the subsoil and satisfying any serviceability conditions. These criteria can be achieved by controlling the width and thickness of the shallow foundation. However, this often requires the use of large and thick footings, which is a problem especially in locations with limited access and in offshore environment, where the presence of gravity bases has a large influence on the movement of the surrounding water and generates significant heave forces.

In this study, an innovative technique is proposed to improve the lateral capacity of shallow footings by providing them with a central short monopile. The interaction between the footing and the monopile in the proposed hybrid foundation system has proven to increase the lateral load resistance and decrease the dependency of the lateral resistance on the vertical load component acting on the system. The lateral load resistance of the hybrid system is generated, even at low vertical load ratios, directly by mobilizing passive lateral pressures on the embedded portion and indirectly through the restoring moment resulting by the bearing stresses underneath the footing. The two phenomena together contribute to the resistance of sliding and rotation of the whole system. An extensive 2D and 3D numerical modeling program, complemented with physical centrifuge testing have been used to study the behavior of the system under various combinations of vertical, horizontal and moment (V-H-M) loadings and generate detailed information about the failure envelopes in three-dimensional (V-H-M) load space for both drained and undrained loading. The numerical study indicates that the interaction between the structural elements of the hybrid system increased the strength and stiffness of the foundation system and mobilized high lateral load and rocking resistances, even at low strains. The resistance was found to rely mainly on the geometry of the system, especially the pile length-to-footing width ratio.

Keywords

Hybrid, monopile-footing, foundation, combined loading, failure envelopes, numerical modeling, centrifuge.

Co-Authorship Statement

This thesis has been prepared in accordance with the regulation of Integrated-Article format stipulated by the school of Graduate and Postdoctoral Studies at the University of Western Ontario. Some parts of Chapters 3 and 5 of this thesis were published in peer-reviewed conferences. All modeling process, physical testing, data analysis, and writing of initial version of this thesis were carried out by the candidate himself under supervision of his research advisors Professors Hesham El-Naggar and Tim Newson.

Substantial parts of Chapter 3, entitled "Numerical Investigation of Hybrid Monopile-Footing Foundation Systems under Drained Loading Conditions" were submitted for publication at the peer-reviewed technical journal, *Canadian Geotechnical Journal*.

Significant parts of Chapter 4 of this thesis, entitled "Numerical Investigation of Hybrid Monopile-Footing Foundation Systems under Undrained Loading Conditions" will be submitted for publication in the peer-reviewed technical journal, *ASCE Journal of Geotechnical and Geo-environmental Engineering*.

Substantial parts of Chapter 5, entitled "Physical Centrifuge Testing of Hybrid Monopile-Footing Foundation Systems on Drained Sands" will be submitted for publication in the peer-reviewed technical journal, *ASTM Geotechnical Testing Journal*.

Professors Tim Newson, Hesham El-Naggar and Kevin Stone, have reviewed the documents and contributed to the final version of the following publication:

El-Marassi, M., Newson, T., El-Naggar, H. and Stone, K. (2008). Numerical modeling of the performance of a hybrid monopiled-footing foundation. *In* Proceedings of the 61st Canadian Geotechnical Conference (GeoEdmonton 2008), Paper n. 420, pp. 97-104.

The candidate contributed, in addition to other co-authors when applicable, in the modeling, testing, analysis, writing and preparation of the final version of the following publication:

Stone, K.J.L., Newson, T.A., El-Marassi, M., El-Naggar, H., Taylor, R.N. and Goodey, R.J. (2010). An investigation of the use of a bearing plate to enhance the lateral capacity of monopile foundations. *In* Proceedings of the 2nd International Symposium on Frontiers in Offshore Geotechnics (ISFOG 2010), Perth, pp. 623 - 628.

Acknowledgments

The author would like to express his sincere appreciation and gratitude to his supervisors, Professors Hesham El-Naggar and Tim Newson. The research presented in this thesis would not have been possible without their stimulating supervision, consistent guidance and constructive advice. Professors Hesham El-Naggar and Tim Newson sincere mentorship and friendship provided the author with an enriching personal and professional experience, which shall be acknowledged forever.

The author is indebted to the University of Western Ontario and his supervisors, Professors Hesham El-Naggar and Tim Newson for financially supporting the research. The author would like to thank all his colleagues for their friendship and enjoyable, stimulating discussions. The author would like also to thank all the technical and administrative staff at the Department of Civil and Environmental Engineering, the University of Western Ontario, for their continuous help. The author is indebted to Professors Fathi Abd-Rabbo, Hassan Abou-Seeda, Adel Barakat and all the soil mechanics and foundation engineering professors at Alexandria University, who inspired him to further study in soil mechanics.

Finally, and most important, the author wishes to thank his family back home, his father, mother, brother and sister for their understanding, continuous support and encouragement throughout the course of this research. Special thanks are due to my mother, I am indebted forever to your love and encouragement; to my wife for her companionship, continuous encouragement, and great understanding in this challenging journey; and to my cute little daughter for all the sweet laughs and joyful moments. I am forever grateful and thankful for your love and support.

Table of Contents

List of Tables

List of Figures

List of Symbols

Soil parameters:

δ Interface friction angle (degrees)

ψ Angle of dilation (degrees)

ϕ Friction angle of sand (degrees)

ϕ_{cr} Critical friction angle (degrees)

ϕ_{inter} Friction angle at foundation-soil interface (degrees)

γ Unit weight of soil (F/L^3)

γ' Effective unit weight of soil (F/L^3)

γ_w Unit weight of water (F/L^3)

ν Poisson's ratio

c Cohesion of soil (F/L^2)

c_{inter} Cohesion at foundation-soil interface (F/L^2)

D_{10} Soil diameter at 10 % finer (L)

D_{50} Soil diameter at 50 % finer (L)

D_{60} Soil diameter at 60 % finer (L)

e_{max} Maximum voids ratio

e_{min} Minimum voids ratio

E Modulus of elasticity (F/L^2)

E_s Modulus of soil reaction (F/L^2)

G Shear modulus of soil (F/L^2)

Gs Specific gravity

K_a Active earth pressure coefficient

K_p Passive earth pressure coefficient

q Overburden pressure (F/L^2)

R_{inter} Strength reduction factor

S_u Undrained shear strength (F/L^2)

Bearing capacity parameters:

α Load inclination angle (degrees)

N_γ Bearing capacity factor self weight

N_c Bearing capacity factor cohesion

N_q Bearing capacity factor overburden

Foundation parameters:

A Area of footing (L^2)

D Diameter of pile (L)

e Eccentricity of moment load (L)

E_p Modulus of elasticity of pile (F/L^2)

h Depth of embedment of shallow footing (L)

I_p Moment of inertia of pile (L^3)

$K_{M\theta}$ Rotational restraint coefficient

L Embedded length of pile (L)

P Soil reaction (F)

Q Axial load on the pile (F)

R Radius of footing (L)

t Thickness of shallow footing (L)

W Width of footing (L)

y Lateral deflection of the pile (L)

Load parameters:

$\beta_1, \beta_2, \beta_3$ Dimensionless curve fitting parameter

h Dimensionless horizontal load

h_o Dimensionless ultimate horizontal load

H Horizontal load (F)

H_{max} Peak horizontal load (F)

m Dimensionless moment load

m_o Dimensionless ultimate moment load

M Moment load (FL)

M_{max} Peak moment load (FL)

v Dimensionless vertical load

v_o Dimensionless ultimate vertical load

V Vertical load (F)

V_{max} Peak Vertical load (F)

Displacement parameters:

δu Horizontal displacement (L)

δv Vertical displacement (L)

k Stiffness (F/L)

Chapter 1

1   Introduction

1.1   Background

The growth of the wind energy sector in Canada has been very rapid and the majority of wind farms constructed so far have been onshore. However, the growing opposition to the construction of wind farms in suburban and rural areas has led to the delay or cancellation of many projects, prompting a threat to Ontario's energy security. For this reason, the strategic switch to the development of offshore wind farms in the Great Lakes is a promising opportunity for further significant energy-generating projects and allows the access to highly desirable wind environments. Despite the recent reinstatement of the moratorium on wind farm development in the Great Lakes, in the larger terrain it is anticipated this development will occur rapidly.

The economic viability of offshore wind farms is highly dependent on the installation costs, which can be as much as 40% of the total field development costs (Andrews, 1998), and the selection of a suitable foundation design is a crucial factor in determining the economic viability of a wind farm. The requirements for such foundations are more demanding than for onshore developments, since they will experience complex loading states as the result of combined wind, wave, currents and self-weight loading effects, all of which must be accommodated with sufficiently small displacements to maximize the operational envelope of the turbines.

Currently, there are several types of foundation systems available to the designer of offshore wind turbines. The preferred foundation system will depend on the local seabed soil conditions and size of the turbine. In general, the choice will be between surface or near surface type foundation solutions, such as gravity base or suction caisson systems (including tripods), or large diameter mono-piles. Gravity bases can be quite large, with typical diameters of 10 to 20 m and weights of up to 2000 tons. In addition, monopiles are typically made of very large steel pipes with a diameter of 3 to 4m or more and length of 20m to 35m (Bransby and Randolph, 1998). Since both foundation types require

substantial equipment, jack-up barges or ship hire, both foundation types are expensive to install and this often constitutes the major component of wind farms installation costs. Hence, a reduction in the width or length of foundations required to resist these complex loading cases has potentially significant economic benefits.

Clearly, there is scope to develop foundation systems that are more efficient, economic and satisfactory for the particular case of resisting the combined loading induced by a wind turbine. One such approach is to develop foundation systems that combine several foundation elements to create a 'hybrid' system. This proposal concerns the investigation of such 'hybrid' foundation system, which combines a mono-pile and circular footing or foundation plate to produce a 'hybrid' monopiled-footing arrangement.

Despite the apparently obvious advantages of such hybrid systems, with the exception of some recent work reported by Stone *et al.* (2007), there is no information available in the literature to suggest that such systems have been explicitly studied. On the other hand, there is a significant body of literature available in respect to the component elements i.e. piles, surface footings and pile caps. In particular, research on the response of shallow foundations to combined loading has been developing rapidly (Bransby and Randolph 1998; Houlsby and Puzrin 1999; Gourvenec and Randolph 2003). Similarly, several methods for the analysis of piles, and in particular their response to lateral loads have been developed (e.g. Matlock and Reese 1960; Broms 1964; Poulos 1971; Reese *et al.* 1974; Randolph 1981; Duncan *et al.* 1994; Zhang *et. al* 2005).

It should also be noted that a 'hybrid' foundation system composed of a monopiled-footing is an attractive combination from an installation point of view, since the plate can be located first, and then used as a seabed guide for the installation of the pile, although the practicality of such procedure remains to be investigated. Furthermore, it has also been suggested (Stone et al., 2007) that existing monopile turbine towers could be fitted with footing or stabilizing plates as a way of upgrading their capacity to carry larger (heavier) generators.

1.2 Overall Research Objectives

The overall aim of this project is to undertake a 'proof of concept' or feasibility study of a novel foundation system for wind turbines and to develop the guidelines for its design and installation. Canada's natural abundance of potential wind farm sites makes wind energy a particularly attractive source of renewable energy. The proposed 'hybrid' monopiled-footing foundation system has the potential to significantly improve the performance of current turbine foundation design, while minimizing the installation costs and time. The main premise is that combining a foundation plate with the mono-pile not only provides additional vertical capacity, it also provides a significant increase in lateral capacity and stiffness compared to that of a single pile.

1.3 Methodology and Novelty of Approach and/or Application

In this thesis, numerical and experimental investigations are conducted with an emphasis on developing guidelines for the design of the hybrid foundation system under various vertical, horizontal and moment combinations. Extensive finite element analyses using the commercial software packages PLAXIS 2D and PLAXIS 3D Foundations are used to provide interpretation of the behavior of the hybrid foundation system and to further extend the database of findings through parametric analysis. Furthermore, the numerical results are backed up by the experimental testing on scaled physical model foundations at enhanced gravity (on a centrifuge). The centrifuge tests ensure the accurate determination of lateral load-displacement response curves for the foundation system under the action of a range of applied vertical, horizontal and moment loads.

The measurable objectives associated with the proposed test program are as follows:
- Undertake a 'proof of concept' or feasibility study of a novel foundation system to support laterally loaded structures.
- Evaluate the performance of the proposed 'hybrid' systems under drained and undrained loading conditions
- Develop guidelines for the design of HMFF at different soil conditions, while taking account of the influence of the relative geometry of the constituent

elements of the 'hybrid' system (i.e. the pile length and plate diameter) on the performance characteristics of the system.

1.4   Research Milestone

The study explores a methodology for adapting existing offshore design (from the oil and gas industry) to the particular requirements of wind turbines. In terms of economic value, the wind energy sector is now firmly established as one of the largest sectors in the energy market. The total value of new generating equipment installed globally in 2006 was $26.6 billion (CAD). There is no doubt that any technological advantage for Canada in the wind energy sector would result in significant economic gains for Ontario and Canada. The project also has much relevance to the oil and gas industry where the operating requirements (tolerable displacements) are less severe. Developing the design guidelines and the installation procedures in this study may lead to a significant interest in the industrial community, which could accelerate the research and development of such systems and further enhance offshore foundation technology.

1.5   Thesis Outline

The remainder of this thesis is divided into five main chapters.

Chapter 2 consists of a comprehensive literature review on the behavior of conventional onshore and offshore shallow and deep foundations under combined vertical, horizontal and moment loading.

Chapter 3 presents the results of an extensive 2D and 3D finite element numerical modeling program, which has studied the behavior of the system under various combinations of vertical, horizontal and moment (V-H-M) drained loadings and generated detailed information about the drained failure envelopes in the three-dimensional V-H-M load space.

Chapter 4 discusses the results of a comprehensive 2D and 3D finite element numerical modeling program, which focused on the behavior of the hybrid system under undrained V-H-M load combinations.

Chapter 5 reports on a series of small-scale centrifuge model tests designed to investigate whether the hybrid system offers a significant advantage in terms of lateral and axial load capacities to conventional shallow footings or monopiled foundation.

Chapter 6 summarizes the main findings of this research and provides recommendations for future studies and research.

1.6 References

Andrews, R. N. L. (1998). Environmental Regulation and Business "Self-Regulation." Policy Sciences, 31(3): 177-197

Bransby, M. F. and Randolph, M. F. (1998). Combined loading of skirted foundations. Geotechnique, 48 (5): 637-655.

Broms, B.B. (1964). Lateral resistance of piles in cohesionless soils. ASCE Journal of the Soil Mechanics and Foundation Division Proceedings (JSMFD), 90(SM3), 123-156.

Duncan, J. M., Evans, L. T., and Ooi, P. S. (1994). Lateral load analysis of single piles and drilled shafts. ASCE Journal of Geotechnical Engineering, 120(6): 1018-1033.

Gourvenec, S. and Randolph, M. F. (2003). Effect of strength nonhomogeneity on the shape and failure envelopes for combined loading of strip and circular foundations on clay. Geotechnique, 53(6): 575-586.

Houlsby, G. T. & Puzrin, A. M. (1999). The closed-form solutions for the bearing capacity of strip footing under combined loadings. *In* Proceedings of the Royal Society Conference, London, UK, pp. 893-916.

Matlock, H., and Reese, L. C. (1960). Generalized solutions for laterally loaded piles. ASCE Journal of Soil Mechanics and Foundations Division, 86(SM5), 63-91.

Poulos, H. G. (1971). Behaviour of laterally loaded piles: Part I-single piles. ASCE Journal of the Soil Mechanics and Foundations Division, 97(SM5), 711-731.

Randolph, M. F. (1981). The response of flexible piles to lateral loading. Géotechnique,

31(2): 247-259.

Reese, L. C., Cox, W. R., and Koop, F. D. (1974). Analysis of laterally loaded piles in sand. *In* Proceedings of the Offshore Technology Conference, Vol. II, Paper No. 2080, Houston, Texas, 473-484.

Stone, K., Newson, T. and Sandon, J. (2007). An Investigation of the Performance of a 'Hybrid' Monopile-Footing Foundation for Offshore Structures. *In* Proceedings of the 6th International Offshore Site Investigation and Geotechnics Conference, London, UK, 391-396.

Zhang, L., Silva, F. and R Grismala, R. (2005). Ultimate Lateral Resistance to Piles in Cohesionless Soils. Journal of Geotechnical and Geoenvironmental Engineering, 131(1): 78–83.

Chapter 2

2   Literature Review

Laterally loaded structures such as wind turbines, earth-retaining structures, bridge abutments and offshore structures impose complex loading combinations on the supporting foundations. These foundations are typically subjected to a combination of vertical, horizontal and moment loadings as the result of vertical self-weights of the foundation system, superstructure, soil fill and surface surcharge, in addition to lateral loads and moments due to horizontal soil pressures, wind load and waves and currents.

There are several types of foundation systems capable of supporting laterally loaded structures. The selection of a suitable foundation is a crucial factor in determining the economic viability of the design and depends on the nature of applied loads, in addition to specific soil characteristics. In the case of relatively small loads and strong supporting soils, a shallow foundation would represent the most economical solution, especially when the foundation level is above the ground water table. The weight and dimensions of the foundation must be sufficient to resist tilting and sliding, while at the same time preventing failure of the subsoil and must satisfy serviceability conditions. These criteria can be achieved by controlling the width and thickness of the shallow foundation. However, as loads increase or the bearing soil becomes weaker it becomes essential to use larger and thicker footings. This could be a problem, especially in locations with limited access, on weak, soft soils and in case of offshore foundations, where the presence of gravity bases has a large influence on the currents and movement of the surrounding water and generates significant heave forces (Zaaijer, 2003). Otherwise, large monopiles, spaced piles or continuous diaphragm walls can be used to resist the lateral loads through the generation of lateral soil pressures along their embedded length. These deep foundations are affected by the rotational restraint at the wall or pile head as well as the bending stiffness of the section.

The need to develop more efficient and economic foundation systems initiated the development of the proposed foundation system, which combines two foundation

elements to create a 'hybrid' system. The idea is to strengthen the footing plate with a central, short monopile to create a 'hybrid' monopiled-footing arrangement. The monopiled-footing concept is not dissimilar to that of a retaining wall with a stabilizing base, in that the stabilizing base acts to generate resisting moment from the underlying soil, thus enhancing the lateral stiffness of the retaining wall. For example, Carder and Brooks (1993) and Carder *et al.* (1999) and more recently Powrie and Daly (2007) examined this concept, although perhaps a closer analogy is that of a single capped pile. Poulos and Randolph (1983) developed methods for analyzing the relative influence of the pile and pile cap under axial loading, and some studies of the influence of the pile cap on the lateral performance of single piles has also been reported (e.g., Kim et al. 1979; Mokwa 1999; Maharaj 2003).

Apart from a few studies discussing the effect of shear keys on the resistance of shallow footings to sliding (Horvath, 1991) and recent work by Stone *et al.,* (2007), there is little in the literature that suggests that such systems have been comprehensively studied. The NAVFAC DM-7.02 design manual entitled "Foundations and Earth Structures" mentioned briefly that the sliding resistance of a retaining wall may be improved by installing a shear key below the foundation. The manual gave a brief recommendation of calculating the resultant of the passive earth pressures in front of the key, which does not take account for the foundation response or resistance under the combined vertical, horizontal and moment loading regime that is anticipated to act on a retaining wall foundation. The DM-7.02 did not provide any guidelines in regard of sizing the keyed foundation. Moreover, the DM-7.02 restricted the use of shear keys to the case of walls bearing on rock or very stiff clay without providing any justifications or giving any consideration for the cases of softer clays and sandy soils.

On the other hand, there is a significant body of literature available in respect to the component elements, i.e. a pile and surface footing that will be introduced in the following subsections. In particular, research on the response of shallow foundations to combined loading (Bransby and Randolph 1998; Houlsby and Puzrin 1999), and more recently, the use of sophisticated numerical modeling (Gourvenec and Randolph 2003) has led to the development of design aids for circular footings under combined loading.

Similarly, several methods for the analysis of piles, and in particular their response to lateral loads have been developed (e.g.: Matlock and Reese, 1960; Broms, 1964; Poulos 1971; Reese *et al.,* 1974; Randolph 1981; Duncan *et al.,* 1994; Zhang *et al.,* 2005).

2.1 Offshore Foundations

The offshore industry has evolved to a stage where the use of advanced technology has become increasingly important to reduce costs and improve safety and efficiency of offshore structures. It is not uncommon to place offshore structures in remote, harsh environments to exploit new promising natural energy resources, which are inaccessible to exploit with existing technologies. Many of the newly discovered oil and gas fields are small and their economic development is challenging since the cost of production with the existing technologies is unattractive. The ever increasing social need to extract these vital energy resources, in these harsh environments, has initiated the development of new structures and concepts. The design of the supporting foundations of these structures necessitates some special precautions to overcome the anticipated complex loading regimes associated with the environmental hazards of wind, waves and current forces in addition to the self weight of the structure.

The growth of the wind energy sector in Canada has been very rapid with the majority of wind farms constructed onshore. However, the growing opposition to the construction of wind farms in shoreline areas has led to the delay or cancellation of many projects, prompting a threat to Ontario's energy security. For this reason, the strategic switch to developing offshore wind farms in the Great Lakes is a promising opportunity for further significant energy generating projects and allows the access to highly desirable wind environments. Numerous studies have investigated support structures for offshore structures in general and recently for offshore wind turbines.

In general, the cost of offshore foundations is significantly higher than traditional onshore foundations. The reason for this higher cost is attributed to the fact that offshore foundations must support taller towers (because of the additional height due to water depth), withstand forces and overturning moments from waves, currents and winds and finally be capable of being constructed offshore quickly at the lowest possible costs. In

particular, the design of offshore wind turbine foundations is troublesome since it implies the use of more strict displacement tolerance criteria. Moreover, self-weights are typically small in comparison to horizontal loads and moments due to wind, waves and currents.

2.1.1   Gravity Base Foundations

Gravity base foundations are efficiently used to support offshore structures located in shallow waters (Malhotra, 2007). Although gravity bases are usually constructed onshore and subsequently installed offshore as a single unit, they are similar in concept to concrete pad foundations constructed in-situ onshore. The weight of a gravity base has to be sufficient to avoid uplift, tilting and sliding, while at the same time avoiding failure of the subsoil. The main parameters to achieve this balance are the diameter and height of the gravity base. The performance of the foundation may be enhanced by adding ballast after placement.

However, such foundations are likely to be too expensive for deeper waters in which the waves or wind significantly increase the overturning moments and in shallow waters where the sea bed condition requires special preparation (dredging of soft soil and replacement with compacted coarse matters). It is notable that the interference of the large gravity bases with the surrounding water currents produces excessive heave forces on the base itself (Zaaijer, 2003) resulting in considerable heave forces, which significantly decrease the stability and alter the design.

2.1.2   Monopile Foundations

Monopiles are the most common form of foundation at intermediate water depths. The piles, typically 4m or more in diameter and 20m to 35m long are installed by drilling and grouting, or by driving, or a combination of drilling and driving (e.g.: Byrne and Houlsby, 2002 and 2003). In either case, substantial equipment is required for installing the piles (Figure 2-1). A special jack-up barge is usually required, and the cost of the foundation depends as much on the cost of installation as on the materials used. The load from the wind turbine is transferred to the surrounding soil by lateral earth pressure along

the embedded depth of the monopile. An additional advantage of monopole foundations is the ability to assess their capacity with dynamic measurement during installation.

Monopile foundations are often ductile in nature, which dampens the loads and increase the lifetime of the turbine (Malhotra, 2007). On the other hand, this ductility tends to increase the deflections in deep waters, which can exceed serviceability requirements of the wind turbine (Malhotra, 2007). Under cyclic loading, the lateral response of monopiles can result in a buildup of pore pressures adjacent to the pile, which decreases the effective confining stresses and the shear strength of the surrounding soil along the sides of the pile. Subsequently, this can increase the vertical settlement of the foundation (Malhotra, 2007). Tensioned guyed wires can be used to extend the practical range of depths to 40 m by offering additional lateral supports to the monopile (Malhotra, 2007). As the water depth increases, the monopile's diameter required to limit the lateral displacements would become so large that it would not be economically feasible to construct it.

a) Monopile on the deck   b) Hydraulic hammer on pile   c) Transition piece mounted

Figure 2-1 Installation of the Kentish Flats offshore wind farm (photographed by Chris Laurens, royalty free usage rights)

2.1.3   Suction Caissons

In a medium water depth, suction caissons represent an economically attractive foundation alternative, since they offer a simpler construction procedure compared to an equivalent monopile foundation. A suction caisson is essentially a skirted shallow foundation resembling an upturned bucket that is fabricated onshore and then floated to site. They are installed by lowering them to the seabed until they embed a small distance. Subsequently, large pumps are used to remove the water trapped inside the caisson. The differential pressures created force the caisson to rest in its final position (Byrne and Houlsby, 2002 and 2003).

From an economical as well as technical viewpoint, the use of suction caissons is limited to intermediate water depths. As water depth gets deeper, the size of suction caissons as well as the problems associated with the construction and handling of the foundation will dramatically increase, which makes this option uneconomical (Byrne and Houlsby, 2006).

2.1.4   Overview and Comparison of Foundations

Economic feasibility is a significant factor in the selection of an offshore foundation type. This feasibility is highly influenced by the type and size of the supported structure, the expected loading combinations from self-weights in addition to the environmental conditions, the properties of the seabed soil and finally the water depth, which is typically the deciding factor in foundation type. In shallow waters or locations with bedrock, gravity base foundations may be the economically feasible option. In medium waters, monopiles and suction caissons may be more appealing. Byrne and Houlsby (2006) summarized the basic diameter sizes, weights and water depth feasibility of all offshore foundation types in Table 2-1.

Byrne and Houlsby (2006) reported that for deeper waters and larger turbines, monopiles become excessively large to be handled and installed using current technologies, and similarly a caisson would become uneconomically large. In deep waters, it is more feasible to use multiple footings, either in the form of tripods (three foundations) or tetra-

pods (four foundations). In this case, the turbine's tower will be mounted on a steel connection, which in turn would be supported on multiple foundations. Even though fabricating and installing the steel connection will increase the foundation cost, this connection will shorten the free length of the tower and provides a stiffer overall structure, hence making it easier to meet the dynamic requirements.

Table 2-1 Overview of offshore foundation types (after Byrne and Houlsby, 2006)

Type of Foundation	Size (m)	Weight (ton)	Typical Water Depths (m)	Construction Sequence
Gravity Base	12 - 15	500 - 1000	0 - 15	Prepare seabed Placement Infill ballast
Monopile	3 - 6	175 - 350	0 - 30	Place pile Drive pile
Monopile with Guy wires	3 - 6	175 - 350	20 - 40	Place pile Drive pile
Tripod	15 - 20	125 - 150	20 - 40	Place frame Insert pile Drive pile
Braced frame with multiple piles	15 - 20	200 - 400	20 - 50	Place frame Insert pile Drive pile
Suction buckets	10 - 20	150 - 400	0 - 30	Place base Suction installation
Tension leg platform	10 - 20	100 - 400	> 50	Drive anchor pile or suction bucket Float tension leg platform Install anchor cables

2.2   Behavior of Laterally Loaded Single Piles

Offshore pile foundations are typically subjected to a combination of lateral loads and moments in addition to axial loads. API RP 2A (2000) recommends that pile foundations must be designed for lateral loading conditions. To design a pile foundation subjected to lateral forces and moments, three criteria must be satisfied: 1) the ultimate capacity of the surrounding soil must be sufficient, 2) the deflections should not exceed the tolerance criteria, and 3) the structural integrity of the foundation system must be insured.

Subsequently, the working lateral load on each pile adopted in the design is usually the smaller of: the load obtained by dividing the ultimate (failure) load by an adequate factor of safety and the lateral load associated with an acceptable lateral deflection.

2.2.1   Ultimate Lateral Load Resistance of Single Piles

Several theories are available to evaluate the ultimate resistance such as the methods presented by Broms (1964a, 1964b) to determine the ultimate lateral load in cohesive and cohesionless soils and recent research undertaken to predict theoretically the behavior of laterally loaded piles (Poulos and Davis, 1980; Reese, 1984; Brown and Shie, 1991). Simplified solutions by Broms (1964a, 1964b) are widely applied for evaluating the ultimate load capacity of laterally loaded piles; however these solutions are not precise.

For piles embedded in clayey soils, Broms ignored the soil resistance within the top depth of 1.5D, and considered a constant resistance value of $9S_uD$ along the remainder of the pile, where S_u is the undrained shear strength, and d is the pile diameter. This value of $9S_uD$ is close enough to best-known lower and upper bound solutions, $9.14S_uD$ and $9.20S_ud$, respectively (Randolph & Houlsby, 1984; Martin & Randolph, 2006). Researchers such as Klar and Randolph (2008) consider neglecting the upper soil resistance to be somewhat arbitrary. Other researchers such as Murff and Hamilton (1993) proved that it is not conservative to assign a resistance value of $9S_uD$ to the upper soil. For these reasons, reduction factors are commonly applied to the ultimate soil resistance near the surface in p–y curves (e.g., Matlock, 1970; Fleming *et al.,* 1992).

The prediction of the ultimate lateral resistance of piles in cohesionless soils is a challenging three-dimensional and nonlinear problem, which has drawn the attention of several researchers (Brinch Hansen 1961; Broms 1964; Reese *et al.,* 1974; Poulos and Davis 1980; Fleming *et al.,* 1992). Most of existing solutions are either semi-empirical or employ approximate analysis with considerable simplifications (Jamiolkowski and Garassino 1977). Consequently, these methods often produce significantly different ultimate resistance values (Zhang *et al.,* 2005). In Broms (1964) method, the lateral capacity of piles can be easily determined using simple charts in non-dimensional form. The simplicity of Broms method gained it a wide popularity among practitioners.

2.2.2 Analytical Methods of Predicting the Lateral Deflection of a Single Pile

The second and third criteria are concerned with estimating the lateral deflections, rotations and stresses in single piles, at working load levels. There are several analytical methods capable of providing theses estimates based on either one of the following concepts; Winkler approach, *p-y* method, elasticity theory and finite element methods (e.g. Matlock, 1970; Reese *et al.,* 1974; Poulos and Davis 1980; etc.). The following is a brief review of the most widely recognized analytical techniques.

Pile deflections and bending moments can be estimated using the widely applied Winkler approach method (also called the subgrade reaction theory), where the soil is modeled as a series of unconnected linear springs. Matlock and Reese (1960) defined the spring stiffness, E_s (also known as modulus of soil reaction or soil modulus) as a ratio of the lateral soil reaction per unit length of the pile to the lateral deflection of the pile expressed in units of force per length squared (FL^{-2}).

$$E_s = \frac{-P}{y} \tag{2-1}$$

The solution proposed by Hetenyi (1946) for elastic beams on elastic foundations produced the following beam bending equation:

$$E_p I_p \frac{d^4y}{dx^4} + Q\frac{d^2y}{dx^2} + E_s y = 0 \tag{2-2}$$

Where, E_p is the modulus of elasticity of the pile, I_p is the moment of inertia of the pile section, Q is the axial load on the pile, x is the vertical depth, and y is the lateral deflection of the pile at point x along the length of the pile.

Based on Hetenyi (1946) solution, Reddy (1993) proposed the following governing equation for the deflection of laterally loaded piles.

$$\frac{d^4y}{dx^4} + \frac{E_s}{E_p I_p}y = 0 \tag{2-3}$$

In Equation (2-3), the distribution of Es with depth is usually assumed constant for overconsolidated clays and linearly increasing for normally consolidated clays and sands. Poulos and Davis (1980) and Prakash and Sharma (1990) produced tables and charts that can be used to determine pile deflections, slopes, and moments as a function of depth for overconsolidated clays. For normally consolidated clays and sands, Matlock and Reese (1960) and Poulos and Davis (1980) proposed non-dimensional coefficients to calculate pile deflections, rotations, and bending moments for various pile-head boundary conditions. Gill and Demars (1970) produced solutions for special distributions of E_s with depth such as step functions, hyperbolic functions, and exponential functions).

Despite the frequent use of Winkler approach, the method includes several limitations. At first, these semi-empirical solutions usually ignore the effect of axial load acting on the pile. In addition, the modulus of subgrade reaction is not a unique property of the soil but rather depends on the pile characteristics and the magnitude of deflection. Finally, since the soil is modeled as independent linearly elastic Winkler springs thus the displacement at a point is unaffected by the displacements or stresses at other points (Jamiolkowski and Garassino, 1977). Several researchers proposed solutions to overcome the limitations of the original subgrade reaction approach (McClelland and Focht, 1956; Georgiadis and Butterfield, 1982; Horvath, 1984).

The p-y curve method is a modified Winkler model, which uses non-linear springs (p-y curves) to model the soil resistance with depth. In general, full-scale lateral load tests are required to derive the p-y curves. Many researchers described the shape of p-y curves for laterally loaded piles in clays such as: Matlock (1970) curves for soft clay in the presence of free water; Reese and Welch (1975) for stiff clay in the presence of free water; Welch and Reese (1972) and Reese and Welch (1975) for stiff clay with no free water. Among the studies of p-y curves in sands, Reese *et al.* (1974) studied the laterally loaded piles in sand above and below the water table. Another solution is described by the American Petroleum Institute (1987) for sand above and below the water table. Reese (1977) developed a computer program that is widely used to predict the performance of piles subjected to lateral loading based on the p-y curves. This program solves differential equation derived on the assumption that pile is linearly elastic and that the soil reaction

may be represented as a line load. In addition, the *p-y* method is implemented in commercial computer programs such as LPILE Plus 3.0 (1997) and COM624 (1993). The complete solution of the *p-y* method produces the lateral deflection (y), slope (S), bending moment (M), shear (H), and soil reaction (P) along the pile length.

The theory of elasticity was used by Poulos (1971a, 1971b) to analyze the behavior of laterally loaded pile idealized as a thin beam embedded in an ideal, elastic, homogeneous, isotropic semi-infinite continuum that represents the surrounding soil. The approach is applicable for analyzing battered piles, pile groups of any shape and dimension, layered systems, and systems in which the soil modulus varies with depth. Poulos (1980) modified the method to account for the nonlinear behavior of the soil when determining both immediate and final total movements of the pile. Poulos and Davis (1980) proposed expressions for free head and fixed head piles for a number of different soil and loading conditions. The complexity of the computation and the difficulty in determining an appropriate soil modulus, E_s are the biggest limitations of this method.

Recently, the finite element method has been widely used in analyzing complicated loading conditions on important projects and for research purposes. The method gives the ability to apply any combination of axial, torsion, and lateral loads while considering the nonlinear behavior of structure and soil and the effect of pile-soil-pile-structure interactions. Nowadays, with the presence of many commercial finite element packages dedicated to geotechnical applications and with the increased capabilities of personal computers and workstations, the finite element method is being widely used by practitioners on the professional level and for research purposes.

2.3   Lateral Resistance of Pile Caps

The main role of a pile cap is to provide a connection between a structure and the supporting piles. The cap distributes the vertical, lateral and moment loads to a group of piles. Typically in the design, the lateral load resistance of pile caps is neglected; nevertheless pile caps possess a considerable ability to resist lateral loads. Many published studies have proven that pile caps can produce significant resistance to lateral loadings for a variety of conditions including different pile and cap sizes, soil properties

and loading conditions (Beatty, 1970; Kim and Singh, 1974; Rollins *et al.,* 1997; Zafir and Vanderpool, 1998; Mokwa and Duncan, 2001).

According to Mokwa and Duncan (2001), this lateral resistance depends primarily on the stiffness and strength of the soil in front of the cap and the depth of cap embedment, which control the resisting passive pressures. Some other factors include: the base and side friction along the pile cap soil interface; the rotational restraint provided by the pile cap resulting in smaller lateral deflection in the piles; deflections for the same lateral load; in addition to the bearing stresses of the soil underneath the cap, which can reduce the rotation of the whole piles – cap foundation system.

2.3.1   Base and Side Friction

The base and side friction along the pile cap soil interface depend on normal stresses, roughness of the interface, and the angle of internal friction or adhesion stresses of the surrounding soil (Clough and Duncan, 1971; Kim *et al.,*1979; Gadre and Dobry, 1998; Rollins and Sparks, 2002; Cole, 2003). Unless a full contact between the cap and the bearing soil is guaranteed for the life span of the foundation, it is more conservative to ignore the contribution of base friction in cases where settlement is expected around the foundation (Lam *et al.,* 1991 and Cole, 2003).

2.3.2   Pile Cap Rotational Restraint

The behavior of laterally loaded piles is highly affected by the rotational restraint at the pile head. Mokwa and Duncan (2003) reported that the deflection of a free-head pile may be reduced by approximately 75% if the pile head is rigidly restrained and prevented from rotating. However, it is almost impossible to ensure a pure fixed-head condition in the field even when the piles are constrained with a pile cap stiff enough to move as a rigid body without deformation, because the cap itself rotates (Kim and Brungraber, 1976). Mokwa and Duncan (2003) described the effect of reducing the degree of fixity at the pile head on increasing the deflection of the piles and modifying the distribution of the bending moments along the piles. They concluded that assuming complete fixity at the pile head would generate underestimated values of pile-head deflection, and incorrect

magnitudes and locations of maximum pile bending moments. On the other hand, a free-head condition is an overly conservative design assumption.

In general, the rotational restraint of the pile head is somewhere in between the limiting conditions represented by fixed-head and free-head cases (as displayed in Figure 2-2). A simple approach to introduce the partially restrained boundary condition can make use of the rotational restraint coefficient $K_{M\theta}$, which was introduced by Matlock and Reese (1961) and is defined as the restraining moment at the pile head divided by the rotation ($\Delta M/\Delta\theta$). The rotational restraint coefficient of a pile may be estimated through a trial and error process by varying the value of rotational resistance $K_{M\theta}$ until the calculated values of deflection or rotation matches the observed results. Mokwa and Duncan (2003) concluded that a reasonable accuracy in the computed lateral load response may be achieved even if the value of $K_{M\theta}$ introduced in the analysis was not highly precise.
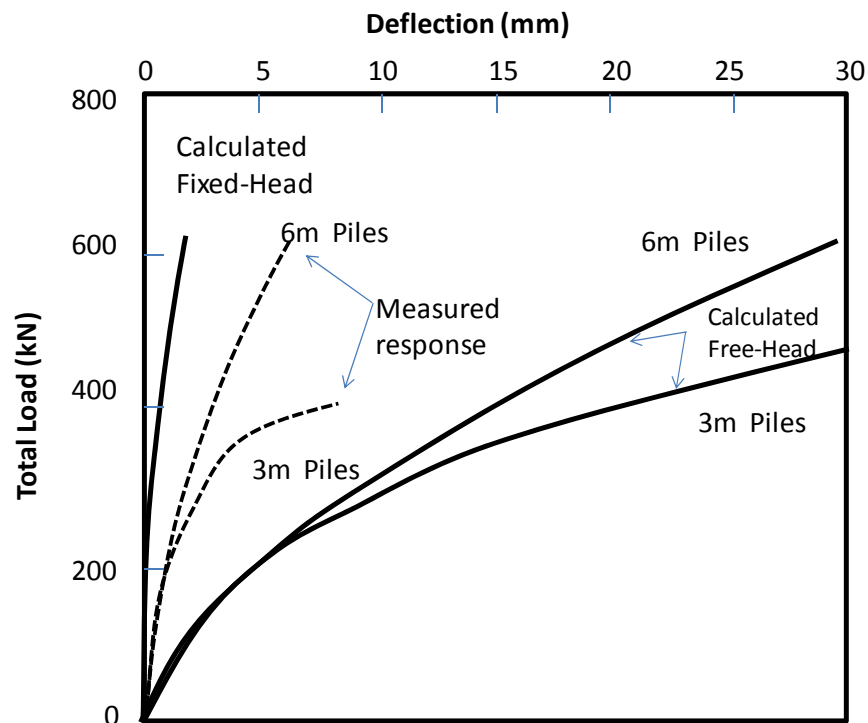
Figure 2-2 Load–deflection response of a four-pile group of 6m-long piles (After Mokwa and Duncan, 2003)

2.4   Response of Shallow Foundations to General Loading

2.4.1   Solutions Based on Theory of Elasticity

While the design of shallow foundations in general is concerned with the estimation of the ultimate capacity, the elastic behavior is also important especially to offshore foundations. At first in the preliminary design stage, elasticity theory is used to estimate the deformations caused by loads applied on the offshore foundation (Poulos, 1988). Moreover, the elastic stiffness values are used to represent the compressibility of the foundation soil in the structural analysis of offshore structures and in the calculation of the natural frequency of the structure (Hambly et al, 1990).

Poulos and Davis (1974) and Davis and Selvadurai (1996) reported a number of linear-elastic solutions for flat, rigid footings resting on a homogeneous half space. The elastic solutions of Poulos and Davis (1974) determine the elastic footing behavior for offshore structures. Bell (1991) and Ngo-Tran (1996) extended those solutions to account for the case of embedded footings, which has a significant effect on increasing the horizontal load and moment capacities due to the cross coupling of the translational and rotational degrees of freedom. Doherty and Deeks (2003) determined the stiffness coefficients for rigid caissons embedded in non-homogeneous elastic soil. Subsequently, Doherty et al. (2005) extend the analysis to account for caissons fitted with flexible skirts.

The two essential soil parameters in the elastic solutions are Poisson's ratio (ν) and the shear modulus (G). The typical values of Poisson's ratio adopted in the analysis are 0.5 and 0.2 for clays and sands respectively. For sands, in the early stage of a first loading, where the theory of elasticity is in use, it is difficult to evaluate Poisson's ratio since it is varying with strain due to particle rearrangements. Lamb and Whitman (1969) reported that the value of ν tends to have a relatively small effect on the engineering predictions.

2.4.2 Solutions Based on Empirical and Semi-Empirical Bearing Capacity Formulations

The main concern of the bearing capacity formulations is to estimate the maximum permissible load that may be applied on a footing and sustained by the soil. Prandtl (1921) published a solution for a strip footing on a weightless perfectly plastic material. Based on Prandtl's theory, Terzaghi (1943) proposed a bearing capacity formulation for the analysis of a surface continuous footing (plane strain condition) with a rough base subjected to a vertical concentric load. The equation neglected the shear resistance of the soil above the foundation level and only used an equivalent surcharge to represent its weight. The formulation considered the effects of soil weight (γ), cohesion (c) and overburden (q) in the determination of the bearing capacity. Terzaghi (1943) gave a definition to the bearing capacity factors N_c, N_q, and N_γ which are dependent on the angle of shear resistance of the supporting soil.

$$V_{max} = \left[cN_c + qN_q + \frac{1}{2}\gamma BN_\gamma \right] A_{footing} \qquad (2\text{-}4)$$

Meyerhof (1953) and Hansen (1963) have suggested alternative expressions. Although these expressions were initially limited to plane strain conditions, they can be easily modified to account for other footing shapes by using the shape factors (Meyerhof, 1953; De Beer, 1970; Hansen, 1970; Vesic, 1973).

Meyerhof (1951), Brinch Hansen (1970) and Vesic (1975) developed methods that account for load inclination and eccentricity. The vertical bearing capacity is reduced as larger horizontal and/or moment loads are applied. The API (1993) adapted the approach by Vesic for determination of the bearing capacity of shallow foundations. Different inclination factors were proposed to account for the horizontal loading by reducing the vertical bearing capacity depending on the ratio of horizontal to vertical load. It is worth mentioning that all published solutions plot parabolic envelopes in the (V/V_{max} - H/V_{max}) space. The peak values for these envelopes occur at approximately V/V_{max} = 0.42 to 0.50, though their maximum ordinates clearly differ (see Figure 2-3).
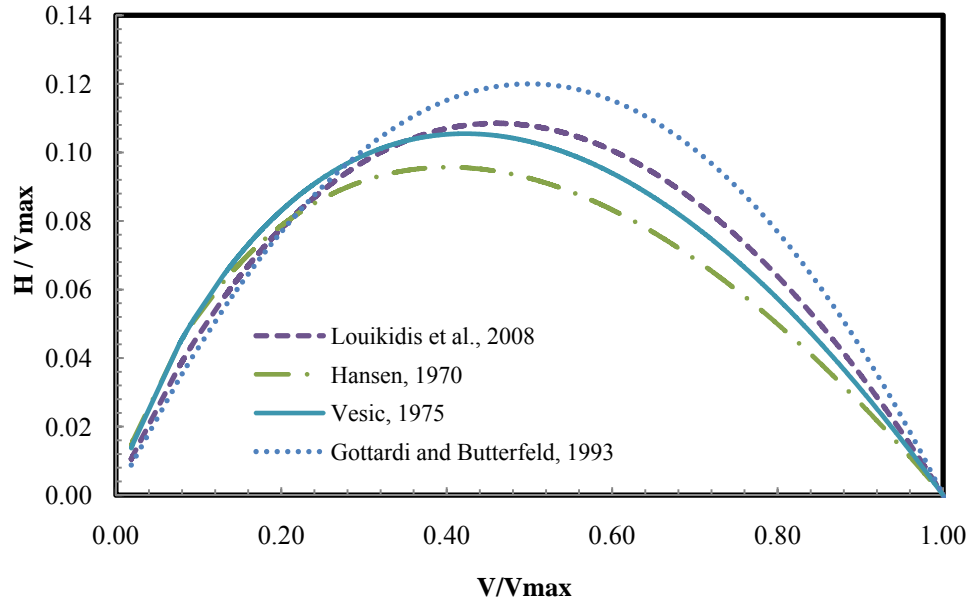
Figure 2-3 Normalized V-H failure envelopes from previous bearing capacity formulations (surface strip on sand, $\phi = 32^{\circ}$)

For the case of eccentric vertical loading, or in other words combined vertical and moment loads, the bearing capacity equations consider a reduced footing with smaller dimensions determined by the load eccentricity ($e = M/V$) in the way that the vertical load acts at the centre of the reduced footing. The idea of effective area was introduced by Meyerhof (1953), and adapted by Hansen (1970) and Vesic (1975). The plot of the (V/V_{max} - $M/W.V_{max}$) interaction diagrams are similar in shape to the (V/V_{max} - H/V_{max}) diagrams, with maximum $M/W.V_{max}$ ordinates occurring at almost 0.5 V/V_{max}. For a fully combined loading, this is introduced in the analysis as an inclined resultant acting on a the center of a reduced foundation. Further reduction factors were introduced to the bearing capacity equations to account for the effects of footing embedment, slope of ground surface and inclination of foundation base.
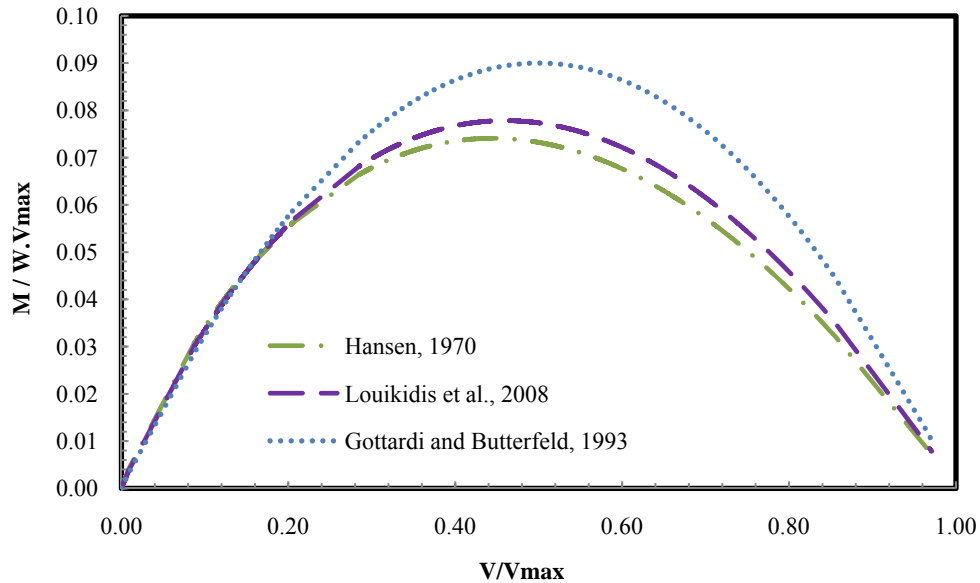
Figure 2-4 Normalized V-M failure envelopes from previous bearing capacity formulations (surface strip on sand, $\phi = 32^{o}$)

2.4.3 Solutions Based on Strain-Hardening Plasticity Theory

The empirical and semi-empirical bearing capacity formulations discussed in the previous paragraphs can hardly be implemented into a numerical analysis. Another approach is to address the bearing capacity problem in terms of the force resultants acting on the footing within a three-dimensional (*V-M-H*) load space, and the corresponding footing displacements. This kind of plasticity-based numerical model can determine the macroscopic load–displacement behavior of the footing in a manner similar to a constitutive law for a metal (or a soil) that relates stresses to strains. In order to develop a complete force resultant model, the following components must be determined:

1) A definition of yield surface in the (*V-M-H)* load space so that plastic displacements occur if the loading state acting on the foundation touches or outcrops the yield surface while it is assumed (for simplicity) that only elastic displacements occur within the yield surface.

2) A hardening law capable of identifying t*h*e size of the yield surface. While, the shape of this surface is assumed constant, the size of the surface expands as the footing is pushed further into the soil. The hardening law is expressed through a

relationship between the apex of the surface (referred to as V_{max}) and the vertical plastic displacement.

3) A flow rule, to determine the post yield relationship between stresses and plastic strains and the directions of the plastic strains increments under multi-axial loading. The simplest type of flow rule is "associated flow", in which the plastic potential is the same as the yield surface; however, a non-associated flow rule gives a more realistic presentation for the behavior of coarse soils.

4) A description of the elastic behavior of the foundation for any load combinations within the yield surface (Bell, 1992 and Ngo Tran, 1996).

Models based on the force resultant concept have been developed for dense sands (Butterfield and Gottardi, 1996), overconsolidated clays (Martin and Houlsby, 2001), and, loose carbonate sands (Byrne and Houlsby, 2001). Moreover, some of these models can be readily implemented within structural analysis packages (Cassidy, 1999).

The use of concepts of plasticity theory and exploration of the shape of yield surface within three-dimensional load space (V-M-H) was introduced by Roscoe and Schofield (1957), who studied a problem of soil-structure interaction of a short pier foundation supporting a steel framework. Ticof (1977) conducted several experimental load-controlled lateral loading tests on a rough strip footing resting on sand. Ticof fitted the data produced by a symmetric parabolic envelope in the horizontal-vertical load (V-H) plane, and an elliptical envelope in the moment-horizontal load (M-H) plane. Figure 2-5 displays the three dimensional, parabolic "cigar-shaped" yield surface in the (V-M-H) space, that was proposed by Butterfield and Ticof (1979) and later on verified by Georgiadis and Butterfield (1988) and Nova and Montrasio (1991). The size of the (V-M-H) yield surface is determined by V_{max}, the pure vertical load capacity and its biggest cross section occurs at $V/V_{max} = 0.5$ where the corresponding ratios of H/V_{max} and $M/W.V_{max}$ are 0.12 and 0.10 respectively. Nova and Montrasio (1991) developed what they called a "macro-element framework", which is a work-hardening plasticity model with a non-associated flow rule that they developed using the results of load-controlled tests with a strip footing bearing on a loose bed of silica sand.
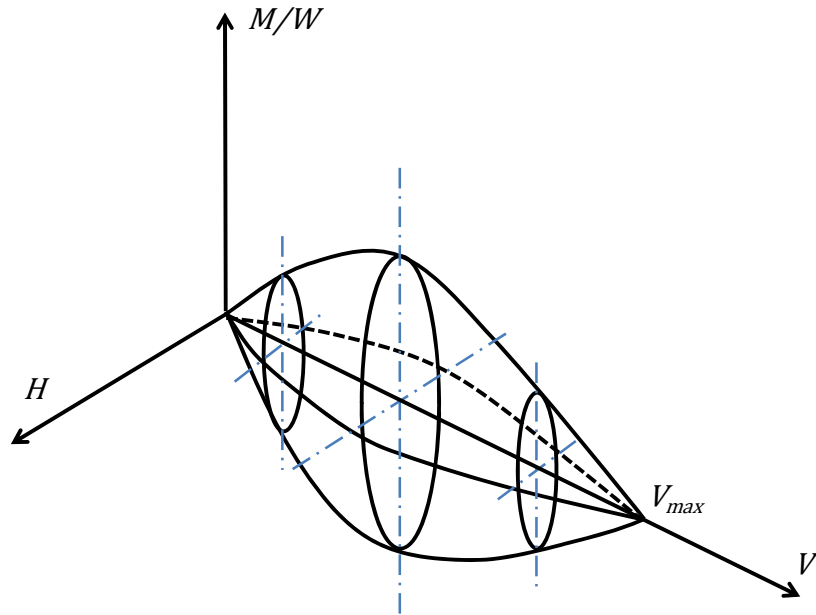
Figure 2-5 Cigar-shape of failure envelope (After Butterfield and Ticof, 1979)

Tan (1990) investigated the *V-H* yield loci for various conical and spudcan footings resting on saturated sands by conducting "sideswipe tests" in the centrifuge at Cambridge. Tan (1990) introduced the swipe tests in his study of the response of shallow foundations to combined vertical and lateral conditions, that were used later on by many researchers (Houlsby, 1997; Bransby and Randolph, 1998; Gourvenec & Randolph, 2003; Bienen et al. 2006, etc.). The swipe test Figure 2-6 typically consists of two loading stages. First, a prescribed displacement (typically vertical) is applied to the foundation until reaching the ultimate vertical load bearing capacity. Subsequently, the footing is swiped laterally (or rotated) while the vertical displacement is kept constant and the load resultants are measured. The analogy of the sideswipe test is that, when the first loading stage continues until reaching the ultimate vertical load; there should be no further increase in vertical load with increased footing penetration. This implies a zero plastic stiffness at yield. Subsequently, in the second stage the elastic stiffness is much greater than the plastic stiffness so that the loading path will follow closely the shape of the yield locus as negligible expansion of the yield locus will be required to balance the small elastic deformation (Bransby and Randolph, 1998). However, because of the elasto-plastic yielding occurring within the yield locus, the load resultants measured during the

second phase will generate a load path falling slightly within the true failure envelope (Houlsby, 1997; Gourvenec & Randolph, 2003).
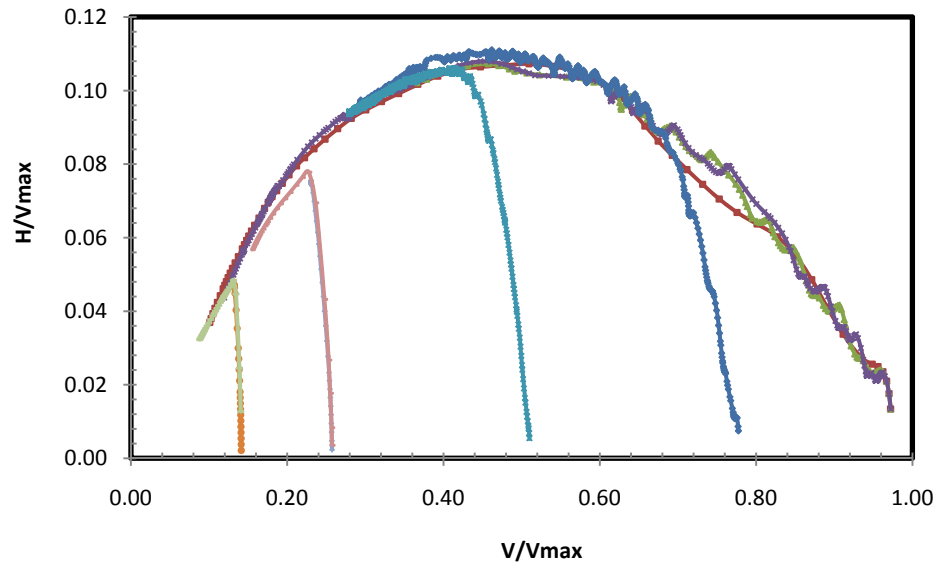
Figure 2-6 Example of a normalized H-V failure envelope obtained by sideswipe tests

Tan (1990) concluded that the shape of the *V-H* yield locus of conical footings is not symmetrical but rather had a max H/V_{max} ratio of 0.14, which occurs at $V/V_{max} \approx 0.4$. Later on Dean et al. (1992) continued Tan's work by introducing moment loadings to the analysis.

Martin (1994) used the force resultant concept to produce a plasticity model to analyze shallow and deep foundations in Kaolin clay. Martin concluded that increasing the penetration of the footing increases the size of the yield surface while its shape remains constant during expansion. The plasticity models proposed by Houlsby & Martin (1992) and Martin (1994) displayed a unique similarity with the critical-state constitutive models. According to Houlsby and Cassidy (2002), in Martin's model the vertical load corresponds to the mean normal stress, p'; whereas the horizontal load and moment correspond to the deviator stress, *q*; and finally the vertical penetration plays the same role (with a change of sign) as the voids ratio or specific volume. Martin (1994) proposed

a mathematical function (Model B) to describe the shape of the yield surface which was similar to the "cigar shape" previously suggested by Butterfield and Ticof (1979) with maximum H/V_{max} and $M/W.V_{max}$ values of 0.127 and 0.083 respectively. Martin (1994) was then able to develop a complete three-dimensional work hardening plasticity theory based on the experimental results, which was implemented in a structural analysis program suitable for analyzing jack-up units. Subsequently, Thompson (1996) integrated Martin's model in a full dynamic structural analyses package for jack-up units.

Using the three-degree-of freedom (3DOF) loading apparatus designed by Martin (1994), Gottardi and Houlsby (1995) and Gottardi et al. (1999) conducted a displacement-controlled testing program using circular flat footings on dense sand. The test results were used to develop a three-dimensional plasticity model. Based on the experimental results obtained by Gottardi et al. (1999), Cassidy (1999) and Houlsby and Cassidy (2002) were able to construct a plasticity model, referred to as "Model C", capable of predicting the response of footings subjected to drained-monotonic combined loading while tacking account for the strong non-associative response found in the experimental results using the association factors.

Houlsby (2003) extended Model C to carry out a six-degree-of-freedom (6DOF) modeling of jack-up foundations. Byrne and Houlsby (2005) designed and constructed a spatial loading apparatus to verify experimentally 6DOF models. Bienen et al. (2006) used the 6DOF apparatus to conduct horizontal, rotational and torsional swipe tests and radial displacement tests with a circular, rough flat footing on dry, loose sand. Bienen et al. (2006) used the outcomes their tests and produced a yield surface, a plastic potential and a hardening law. The parameter values of the yield surface agreed with the values obtained in previous 3DOF studies.

Gourvenec and Randolph (2003) examined the influence of soil strength non-homogeneity on the shape of the (V-M-H) failure envelope. The researchers conducted two and three-dimensional finite element displacement-controlled swipe and fixed displacement ratio probe tests on surface strip and circular footings fully bonded to an

underlying bed of a simple Tresca soil model. The shear strength of the soil varied linearly with depth according to:

$$S_u = S_{uo} + k.z \qquad (2\text{-}5)$$

Where, Su_o is the shear strength at foundation level and k is the strength gradient with depth, z. The degree of non-homogeneity was represented with strength non-homogeneity ratios, $\kappa = kD/Su_o$, between 0 and 10. The study showed that increasing the degree of strength non-homogeneity reduced the size of the normalized (*V-M-H*) failure envelope. Gourvenec and Randolph (2003) found out that in the *V-H* plane, with $M = 0$, the shape of the failure envelope was essentially independent of the foundation geometry, or the degree of non-homogeneity, and followed the classical closed-form expression of Green (1954) scaled to the magnitude of the ultimate vertical load. On the other hand, the degree of non-homogeneity was found to significantly affect the shape of the *V-M* and *H-M* failure envelopes.

Gourvenec (2007) carried out small-displacement finite element analyses with the commercially available software ABAQUS v6.5 to investigate the effect of foundation shape on the undrained bearing capacity of shallow foundations under general loading. As expected, the analyses of foundations with an interface incapable to sustain tension revealed that the three-dimensional effects only affect the vertical load and moment capacities but not the horizontal load capacity since the last is governed by simple sliding along the surface, which is independent of the foundation shape. Based on these findings, Gourvenec (2007) proposed an expression in the normalized (*V-M-H*) load space capable of defining the shape of the complete failure envelope, once scaled to the appropriate apex points.

Gourvenec (2008) extended her work to include the effect of the embedment of shallow strip foundations on the generalization of an additional horizontal load and moment capacity due to the coupling of translational and rotational degrees of freedom. This study revealed that the maximum horizontal capacity is linearly proportional to the depth of embedment, while maximum moment was proportional to the square of the embedment ratio.

2.4.3.1 Load Reference Point (LRP)

In load-resultant analysis, the shape of the yield envelopes is highly influenced by the choice of reference point for footing loads and displacements. This effect was described by Dean *et al.* (1992) in Figure 2-7 below. In this same context, Houlsby (2003) pointed out that the load-resultant analysis of complex soil-footing interaction problems may be simplified by reducing the analysis to the LRP and treating the footing as a rigid foundation bearing on an elastic soil. Standard solutions may be employed to define the stiffness factors, which relate the forces applied on the footing to corresponding displacements. This procedure allows incorporating the solution into a finite element structural analysis by connecting the foundation model to the rest of the structure.

On the other hand, changing the load reference point may modify the moment, horizontal and vertical displacements, which in turn affects the elastic stiffness coefficients and the shape of the yield surface.
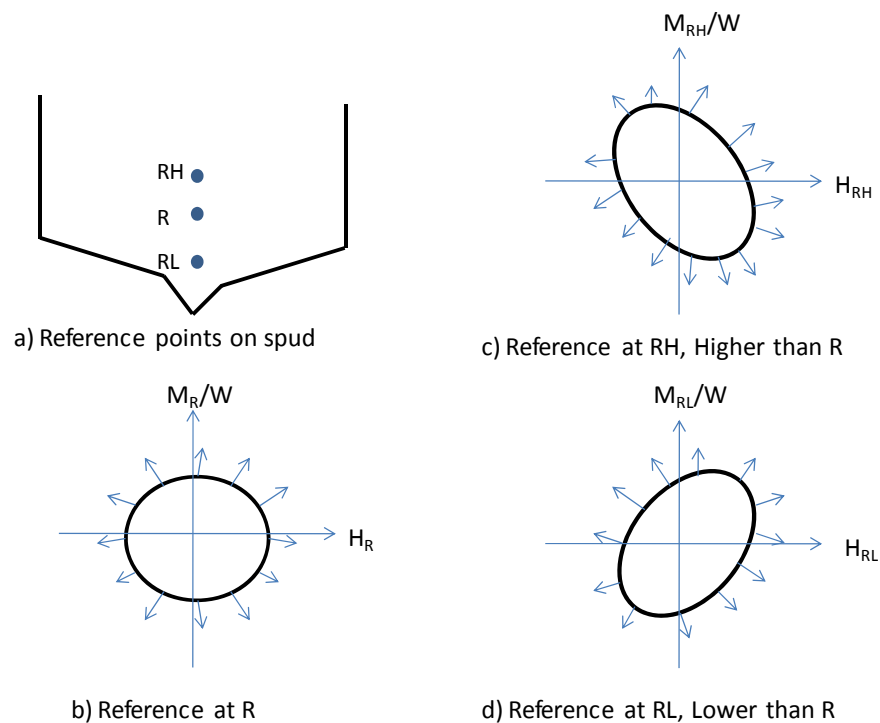
Figure 2-7 Effect of moving the load-displacement reference point on the H-M yield envelope (after Dean *et at.*, 1992)

2.5   Summary and Discussion

In some cases the nature of the structure exerts awkward and complex loading combinations on the foundation. When these complex loading regimes are accompanied by strict tolerance criteria of the allowable displacements, this combination creates a challenging problem. This necessitates a need to adopt innovative design approaches.

As previously discussed, the foundation design of an offshore wind turbine is a good demonstration of such a situation, where the vertical loads produced by the wind turbine are typically low and accompanied by a significant lateral resultant acting at a large eccentricity above grade level. Gravity base foundations rely on the vertical load component for insuring adequate resistance against sliding and overturning. Since the self-weight of a wind turbine is relatively low in comparison to the vertical loads that are required to insure the stability, the gravity base will need to be massive with common weights of up to 2 MN. These weights need to be safely transmitted to the bearing soils, which require increasing the foundation area to up to 20 m in diameter, as discussed in the literature review. This proves that the use of a traditional foundation in such an awkward situation may produce an uneconomical design.

There is a real need to develop a novel, efficient and economical foundation alternative that is capable of withstanding severe loading conditions and still produces a satisfactory response. This need is the main driving force for developing the proposed foundation system, which combines two foundation elements to create a 'hybrid' system. The idea is to strengthen the footing with a central, short monopile to create a 'hybrid monopiled-footing foundation'. This combination ensures restraining the pile head rotation which leads to a stiffened lateral response in addition to the extra gain produced by the restoring moment of the bearing stresses below the footing. This behavior is expected to increase the lateral capacity of the proposed hybrid foundation system and reduce its dependency on the applied vertical loads, which allows reducing the foundation size and lowering the associated installation costs and complexities. Apart from a few studies (Horvath, 1991 and Stone *et al.,* 2007), there is little in the literature that suggests that such systems have been comprehensively studied.

2.6 References

API RP 2A-WSD (2000). Recommended practice for planning, designing and constructing fixed offshore platforms - Working stress design. 21st edition.

Beatty, C. I. (1970). Lateral test on pile groups. Foundation Facts, VI(1), 18-21.

Bell, R. W. (1991). The analysis of offshore foundations subjected to combined loading, MSc thesis, University of Oxford, UK

Bienen, B., Byrne, B. W., Houlsby, G. T. & Cassidy, M. J. (2006). Investigating six-degree-of-freedom loading of shallow foundations on sand. Geotechnique, 56 (6): 367-379.

Bransby, M. F. and Randolph, M. F. (1998). Combined loading of skirted foundations. Geotechnique, 48 (5): 637-655.

Brinch Hansen, J. (1961). The ultimate resistance of rigid piles against transversal forces. The Danish Geotechnical Institute Bulletin 12, 5-9.

Broms, B.B. (1964a). "Lateral Resistance of Piles in Cohesive Soils," ASCE Journal of the Soil Mechanics and Foundation Division Proceedings (JSMFD), Vol. 90 SM2, pp. 27-63.

Broms, B.B. (1964b). Lateral Resistance of Piles in Cohesionless Soils. ASCE Journal of the Soil Mechanics and Foundation Division Proceedings (JSMFD), 90 SM3, 123-156.

Brown, D. A., and Shie, C.F. (1991). Some numerical experiments with a three dimensional finite element model of a laterally loaded pile. Computers and Geotechnics, vol. 12: 149-162.

Butterfield, R. and Ticof, J. (1979). Design parameters for granular soils (discussion contribution). *In* proceedings of the 7th International Conference of Soil Mechanics and Foundation Engineering, Brighton, vol. 4, pp. 259-261.

Butterfield R., Gottardi G. (1996). Simplified failure load envelopes for shallow foundation on dense sand. International Journal of Offshore and Polar Engineering, (6): 62-67.

Byrne, B.W. and Houlsby, G.T. (2001). Observations of footing behaviour on loose carbonate sands. Géotechnique, 51 (5): 463-466.

Byrne, B.W. and Houlsby, G.T. (2002). Investigating novel foundations for offshore wind turbines. *In* proceedings of the 21st International Conference on Offshore Mechanics and Arctic Engineering (OMAE'02), Oslo, Norway, Paper No. OMAE2002-28423.

Byrne, B.W. and Houlsby, G.T. (2003). Foundations for offshore wind turbines. *In* proceedings of the Philosophical Transactions of the Royal Society of London, Series A, 361, pp. 2909-2930.

Byrne, B.W. and Houlsby, G.T. (2005). Investigating six degree-of-freedom loading on shallow foundations. *In* proceedings of the International Symposium on Frontiers in Offshore Geotechnics, Perth, Australia, pp 477-482.

Byrne, B.W. and Houlsby, G.T. (2006). Assessing novel foundation options for offshore wind turbines. *In* proceedings of the World Maritime Technology Conference, London.

Carder, D. R. and Brookes, N. J. (1993). Discussion. In Retaining structures (ed. C. R. I. Clayton), pp. 498–501. London: Thomas Telford.

Carder, D. R., Watson, G. V. R., Chandler R. J. and Powrie, W. (1999). Long term performance of an embedded retaining wall with a stabilizing base. In proceedings of the Institution of Civil Engineers: Geotechnical Engineering, 137(2): 63–74

Cassidy, M.J. (1999). The nonlinear dynamic analysis of jackup platforms subjected to random waves . DPhil Thesis. Oxford University.

Clough, G. W., and Duncan, J. M. (1971). Finite element analyses of retaining wall behavior. ASCE Journal of the Soil Mechanics and Foundations Division, 97(SM12): 1657-1672.

Cole, R.T. (2003). Full-scale effects of passive earth pressure on the lateral resistance of pile caps. Doctor of Philosophy Dissertation, Brigham Young University, Department of Civil and Environmental Engineering, Provo, Utah.

COM624 (1993). Laterally loaded pile analysis program for the microcomputer. FHWASA-91-048, Computer program documentation, by S. T. Wang and L. C. Reese.

Davis, R. O. and Selvadurai, A. P. S. (1996). Elasticity and geomechanics. Cambridge University Press. 201 pp. ISBN 0-521-49506-7

Dean, E. T. R., James, R. G., Schofield, A. N., Tan, F. S. C. and Tsukamoto, Y. (1992). The bearing capacity of conical footing on sand in relation to the behaviour of spudcan footing of jack-ups. Predictive Soil Mechanics − *In* Proceedings of the Wroth Memorial Symposium, Oxford, UK, pp. 230–253.

Doherty, J.P., Deeks, A.J. (2003). Elastic response of circular footings embedded in a non-homogeneous half-space. Geotechnique, 53 (8): 703-714.

Doherty, J.P., Houlsby, G.T., Deeks, A.J. (2005). Stiffness of flexible caisson foundations embedded in nonhomogeneous elastic soil. Journal of Geotechnical and Geoenvironmental Engineering, 131(12): 1498-1508.

Duncan, J. M., Evans, L. T., and Ooi, P. S. (1994). Lateral load analysis of single piles and drilled shafts. ASCE Journal of Geotechnical Engineering, 120(6): 1018-1033.

Fleming, W. G. K., Weltman, A. J., Randolph, M. F., and Elson, W. K. (1992). Piling engineering. Surrey University Press, London.

Gadre, A. and Dobry, R. (1998). Lateral cyclic loading centrifuge tests on square embedded footing, ASCE Journal of Geotechnical and Geoenvironmental Engineering, 124(11): 1128-1138.

Georgiadis, M., and Butterfield, R. (1988). Displacements of footings on sand under eccentric and inclined loads. Canadian Geotechnical Journal. 25(2): 199-212.

Gill, H. L. and Demars, K. R. (1970). Displacement of Laterally Loaded Structures in Nonlinearly Responsive Soil. Technical Report R-670, U.S. Naval Civil Engineering Laboratory, California.

Gottardi, G. & Houlsby, G. T. (1995). Model tests of circular footings on sand subjected to combined loads. Report No. OUEL 2071/95. Oxford: University of Oxford.

Gottardi, G., Houlsby, G. T. & Butterfield, R. (1999). Plastic response of circular footings on sand under general planar loading, Geotechnique, 49(4): 453-469.

Gourvenec, S. and Randolph, M. F. (2003). Effect of strength nonhomogeneity on the shape and failure envelopes for combined loading of strip and circular foundations on clay. Geotechnique, 53(6): 575-586.

Gourvenec, S. (2007). Shape effects on the capacity of rectangular footings under general loading Geotechnique, 57(8): 637-646.

Gourvenec, S. (2008). Effect of embedment on the undrained capacity of shallow foundations under general loading. Geotechnique, 58(3): 177-185.

Green, A.P. (1954). The Plastic Yielding of Metal Junctions Due to Combined Shear and Pressure. Journal of Mechanics and Physics of Solids, Vol. 2, 197-211.

Hambly, E.C., Imm, G.R., and Stahl, B. (1990). Jackup performance and foundation fixity under developing storm conditions. Paper OTC 6466, Offshore Technology Conference

Hansen, J. B. (1963). Discussion on hyperbolic stress-strain response Cohesive soils. ASCE Journal for Soil Mechanics and Foundation Engineering, 89(SM4): 241 - 242.

Hansen, J. B. (1970). A Revised and Extended Formula for Bearing Capacity. *In* Danish Geotechnical Institute, Copenhagen, Bul. No. 28, 21 pp. (successor to Bul. No. 11).

Hetenyi, M. (1946). Beams on Elastic Foundation. Ann Arbor, The University of Michigan Press.

Horvath, J. S. (1984). Simplified elastic continuum applied to the laterally loaded pile problem - part 1: theory. Laterally Loaded Deep Foundations: Analysis and Performance, American Society for Testing and Materials, 112-121.

Horvath, J.S. (1991), Effect of footing shape on behaviour of cantilever retaining wall. ASCE Journal of Geotechnical Engineering, 117(6): 973-978.

Houlsby, G.T. & Martin, C.M. (1992). Modelling of the behaviour of foundations of jack-up units on clay. *In* Proceedings of the Wroth Memorial Symposium., "Predictive Soil Mechanics", Oxford, pp 339-358.

Houlsby, G. T. (1997). The work input to an unsaturated granular material. Géotechnique, 47(1), 193-196.

Houlsby, G. T. and Puzrin, A. M. (1999). The closed-form solutions for the bearing capacity of strip footing under combined loadings. *In* Proceedings of the Royal Society Conference, London, UK, pp. 893-916.

Houlsby, G. T. and Cassidy, M. J. (2002). A plasticity model for the behaviour of footing on sand under combined loading. Geotechnique 52(2): 117–129.

Houlsby, G. T. (2003). Modelling of Shallow Foundations for Offshore Structures. Invited Keynote Lecture at International Conference on Foundations, Dundee, 4 September.

Jamiolkowski, M., and Garassino, A.(1977). Soil modulus for laterally loaded piles. *In* Proceedings of the 9th International Conference of Soil Mechanics and Foundation Engineering, Tokyo, 87‒92.

Kim J.B. and Brungraber R.J. (1976). Full-Scale Lateral Load Tests of Pile Groups. ASCE Journal of Geotechnical Engineering, 102 (GT1): 87-105.

Kim, J. B., and Singh, L. P. (1974). Effect of pile cap - soil interaction on lateral capacity of pile groups. Master of Science Thesis, Bucknell University, Lewisburg, PA.

Kim, J. B., Singh, L. P., and Brungraber, R. J. (1979). Pile cap soil interaction from full scale lateral load tests. ASCE Journal of Geotechnical Engineering, 105(5): 643-653.

Klar, A. and Randolph, M.F. (2008). 3D upper-bound and load-displacement solutions for laterally loaded piles in clays based on energy minimization. Geotechnique, 58(10): 815-820.

Lam, P.L.,Martin, G.R., and Imbsen, R. (1991). Modeling bridge foundations for seismic design and retrofitting. Transportation Research Record, 1290: 113-126.

Lambe, T. W. and Whitman, R. V. (1969). Soil mechanics. John Wiley and Sons, Inc., New York.

LPILE (1997). A program for the analysis of piles and drilled shafts under lateral loads. by Lymon Reese, Shin Tower Wang, Jose A. Arrellaga, and Joe Hendrix, ENSOFT, Inc., Houston, TX.

Maharaj, D.K. (2003). Load-Deflection Response of Laterally Loaded Single Pile by Nonlinear Finite Element Analysis. EJEG .

Malhotra, S. (2007). Design and Construction Considerations for Offshore Wind Turbine Foundations. In proceedings of the 26th International Conference on Offshore Mechanics and Arctic Engineering, San Diego, California.

Martin, C. M. (1994). Physical and numerical modelling of offshore foundations under combined loads. DPhil thesis, University of Oxford, Oxford.

Martin, C.M. and Houlsby, G.T. (2001). Combined loading of spudcan foundations on clay: numerical modelling. Geotechnique, 51(8): 687-699.

Martin, C.M. & Randolph, M.F. (2006). Upper bound analysis of lateral pile capacity in cohesive soil. Géotechnique, 56(2), pp 141-145.

Matlock, H. (1970). Correlations for Design of Laterally Loaded Piles in Soft Clay. *In* Proceedings of the 2nd Annual Offshore Technology Conference, Paper No. OTC 1204,

Houston, TX, pp 577-594.

Matlock, H., and Reese, L. C. (1960). Generalized solutions for laterally loaded piles. ASCE Journal of Soil Mechanics and Foundations Division, 86(SM5), 63-91.

Matlock, H., and Reese, L. C. (1961). Foundation Analysis of Offshore Pile Supported Structures. *In* proceedings of the 5th International Conference of Soil Mechanics and Foundation Engineering, Vol. 2, pp. 91-97.

McClelland, B., and Focht, J. A. (1956). Soil Modulus for laterally loaded piles. Journal of the Soil Mechanics and Foundation Division, Proceedings Paper (101), 1049- 1063.

Meyerhof, GG (1951). The ultimate bearing capacity of foundations. Geotechnique, 2(4): 301-331.

Meyerhof, G. G. (1953). The bearing capacity of foundation under eccentric and inclined loads. *In* Proceedings of the 3rd International Conference on Soil Mechanics and Foundations Engineering, 1, pp. 440-445.

Mokwa, R.L. (1999). Investigation of the Resistance of Pile Caps to Lateral Loading. Ph.D Thesis, Virginia Polytechnic Institute, Blacksburg, Virginia.

Mokwa, R.L., and Duncan, J.M. (2001). Experimental evaluation of lateral-load resistance of pile caps, ASCE Journal of Geotechnical and Geoenvironmental Engineering, 127(2): 185 -192.

Mokwa, R.L., and Duncan, J.M. (2003). Rotational restraint of pile caps during lateral loading, ASCE Journal of Geotechnical and Geoenvironmental Engineering, 129(9): 829-837.

Murff J.D., and Hamilton J.M. (1993). P-Ultimate for undrained analysis of laterally loaded piles. ASCE Journal of Geotechnical Engineering, 119 (1): 91-107.

Ngo-Tran C.L. (1996). The Analysis of Offshore Foundations Subjected to Combined Loading. Doctor of Philosophy, Brasenose College, University of Oxford.

Nova, R. and Montrasio, L. (1991). Settlements of shallow foundations on sand. Geotechnique, 41(2): 243-256.

Prakash, S., and Sharma, H. D. (1990). Pile Foundations in Engineering Practice, John Wiley and Sons, New York.

Prandtl, L. (1921). Uber die Eindringungsfestigkeit (Harte) plastischer Baustoffe und die Festigkeit von Schneiden, Zeitschrift fur angewandte Mathematik und Mechanik, 1(1): 15–20.

Poulos, H. G. (1971a). Behavior of laterally loaded piles: Part I-single piles. ASCE Journal of the Soil Mechanics and Foundations Division, 97(SM5), 711-731.

Poulos, H. G. (1971b). Behavior of laterally loaded piles: Part II - group piles. ASCE Journal of the Soil Mechanics and Foundations Division, 97(SM5), 733-751.

Poulos, H. G. (1980). Comparisons between theoretical and observed behaviour of pile foundations. Australia-New Zealand Conference on Geomechanics, 95-104.

Poulos, H.G. and Davis, E.H., (1974). Elastic Solutions for Soil and Rock Mechanics. John Wiley and Sons, New York.

Poulos, H.G. and Davis, E.H., (1980). Pile Foundation Analysis and Design. John Wiley and Sons, New York.

Poulos, H.G and Randolph, M.F. (1983.) Pile group analysis: a study of two methods. ASCE Journal of Geotechnical Engineering, 109(3): 355-372.

Poulos, H.G. (1988). Marine Geotechnics. Unwin Hyman, London.

Powrie, W. and Daly, M.P. (2007). Centrifuge modeling of embedded retaining wall with stabilizing bases. Geotechnique, 57(6), 485-497.

Randolph, M. F. (1981). The response of flexible piles to lateral loading. Géotechnique, 31(2): 247-259.

Randolph, M.F. and Houlsby, G.T (1984). The Limiting Pressure on a Circular Pile Loaded Laterally in Cohesive Soil. Geotechnique, 34(4): 613-623.

Reddy, J. N. (1993). An Introduction to the Finite Element Method. 2nd edition, McGraw-Hill. Inc., NY.

Reese, L. C., Cox, W. R., and Koop, F. D. (1974). Analysis of laterally loaded piles in sand. *In* Proceedings of the Offshore Technology Conference, Vol. II, Paper No. 2080, Houston, Texas, 473-484.

Reese, L. C., and Welch, R. C. (1975). Lateral loading of deep foundations in stiff clay. ASCE Journal of the Geotechnical Engineering Division, 101(GT7): 633-649.

Reese, L. C. (1977). Laterally loaded piles: program documentation. ASCE Journal of Geotechnical Engineering, 103(GT4): 287-305.

Reese, L. C. (1984). Handbook on Design of Piles and Drilled Shafts under Lateral Loads. US Department of Transportation, Federal highway Administration.

Rollins, M., K., Weaver, T. J., and Peterson, K. T. (1997). Statnamic lateral load testing of a full-scale fixed-head pile group. Report, UDOT, FHWA.

Rollins, K.M., and A. Sparks (2002). Lateral resistance of full-scale pile cap with gravel backfill. ASCE Journal of Geotechnical and Geoenvironmental Engineering, 128(9): 711–723.

Roscoe, K.H. and Schofield, A.N. (1957). The stability of short pier foundations on sand, discussion. British Welding Journal, January, pp. 12-18.

Stone, K., Newson, T. and Sandon, J. (2007). An Investigation of the Performance of a 'Hybrid' Monopile-Footing Foundation for Offshore Structures. *In* Proceedings of the 6th International Offshore Site Investigation and Geotechnics Conference, London, UK, 391-396.

Tan, F. S. C. (1990). Centrifuge and theoretical modelling of conical footings on sand. Ph.D. thesis, University of Cambridge, London, UK.

Terzaghi, K. (1943). Theoretical Soil Mechanics. John Wiley, New York.

Ticof, J. (1977). Surface footings on sand under general planar loads. PhD. Thesis, University of Southampton.

Thompson, R. S. G. (1996). Development of non-linear numerical models appropriate for the analysis of jackup units. DPhil thesis, University of Oxford.

Vesic, A. (1973). Analysis of ultimate loads of shallow foundations. Journal of the Soil Mechanics and Foundations Division, 99(1): 45-73.

Vesic, A. S. (1975). Bearing capacity of shallow foundations, Chapter 3. *In* Foundation Engineering Handbook. *Edited by* H. F. Winterkorn and H.-Y. Fang. Van Nostrand Reinhold Co., New York, N.Y., U.S.A., pp. 121-147.

Welch, R. C., and Reese, L. C. (1972). Laterally Loaded Behaviour of Drilled Shafts. Research Report No. 3-5-65-89, Center for Highway Research, University of Texas at Austin, Austin, TX.

Zaaijer, M.B. (2003). Comparison of monopile, tripod, suction bucket and gravity base design for a 6 MW turbine. *In* Proceedings of the European Seminar on Offshore Wind energy in Mediterranean and Other European Seas, OWEMES-2003, Naples, Italy.

Zafir, Z., and Vanderpool, W. E. (1998). Lateral response of large diameter drilled shafts: I-15/US 95 load test program. *In* Proceedings of the 33rd Engineering Geology and Geotechnical Engineering Symposium, University of Nevada, Reno, 161-176.

Zhang, L., Silva, F. and R Grismala, R. (2005). Ultimate Lateral Resistance to Piles in Cohesionless Soils. Journal of Geotechnical and Geoenvironmental Engineering, 131(1): 78–83.

Chapter 3

3 Numerical Investigation of Hybrid Monopile-Footing Foundation Systems under Drained Loading Conditions

Laterally loaded structures such as wind turbines, earth retaining structures, bridge abutments and offshore structures impose complex loading combinations on their supporting foundations. These foundations are typically subjected to a combination of vertical, horizontal and moment loadings as a result of the vertical self-weights of the foundation system, superstructure, soil fill and surface surcharge, in addition to lateral loads and moments due to horizontal soil pressures, and in the case of water front structures and offshore wind turbines, wind, waves and currents loads.

There are several types of foundation systems that are capable of supporting laterally loaded structures. The selection of a suitable foundation system is a crucial factor in determining the economic viability of the design and depends on the nature of the applied loads in addition to specific soil characteristics. In the case of relatively small loads and firm supporting soils, a shallow foundation would represent the most economical solution, especially when the foundation level is above the ground water table. The weight and dimensions of the foundation must be sufficient to resist the tilting and sliding, while at the same time preventing the failure of the subsoil and satisfying serviceability conditions. This target can be achieved by properly sizing the width and thickness of the shallow foundation. However, for large loads and/or small soil bearing capacity it is essential to use large and thick footings, which can be a major construction challenge especially in locations with limited areal dimensions. Additionally, in the case of offshore foundations the presence of large gravity bases has a large influence on the currents and the movement of surrounding water, which can generate significant heave forces (Zaaijer, 2003).

Several studies have examined the response of shallow footings under complex vertical, horizontal and moment V-H-M load combinations considering various analytical and technological approaches (e.g. Bransby and Randolph, 1998; Houlsby and Puzrin, 1999;

Gourvenec and Randolph, 2003). Gottardi *et al.* (1999) proposed a plastic model to describe the behavior of circular footings on sand under general planar loading conditions. Martin and Houlsby (2000) conducted a series of laboratory tests on spudcan foundations on clay under general planar loadings, and Martin and Houlsby (2001) extended their work to cover a full numerical analysis for the same problem. Further studies have investigated support structures for offshore wind turbines (eg. Byrne and Houlsby, 2002 and 2003; Stone *et al.,* 2007). Numerical modeling by Gourvenec and Randolph (2003) developed design aids for circular footings under combined loading. Horvath (1991) discussed the effect of shear keys on the resistance of shallow footings to sliding.

In this study, an efficient and economical hybrid foundation system is proposed. The idea is to strengthen the footing plate with a central, short monopile to create a 'hybrid' monopiled-footing arrangement.

3.1   Objectives and Scope of Work

The geometry and assumed loading state for the proposed innovative foundation system are shown in Figure 3-1, where a single central pile is employed. The pile diameter and length are (D) and (L) respectively, and the footing width is (W). The objectives of this study are twofold: (1) to examine the behavior of this foundation system under various combinations of vertical, horizontal and moment loading and (2) to generate detailed information about the failure envelopes in the three-dimensional *V-H-M* load space.

An extensive numerical modeling investigation using the finite element program PLAXIS 2D V8 has been conducted to study the behavior of the system under various combinations of vertical, horizontal and moment *V-H-M* loading. In the finite element models, the width of the footing and the diameter of the pile are kept unchanged with values of 5.0 and 0.5 m, respectively, while the pile length to footing width ratio is increased from 0.0 to 1.0. The results from the parametric study are used to illustrate the failure mechanism and to generate information regarding the failure envelopes in three-dimensional *V-H-M* load space. Further 3D finite element analysis will be discussed later in this chapter.
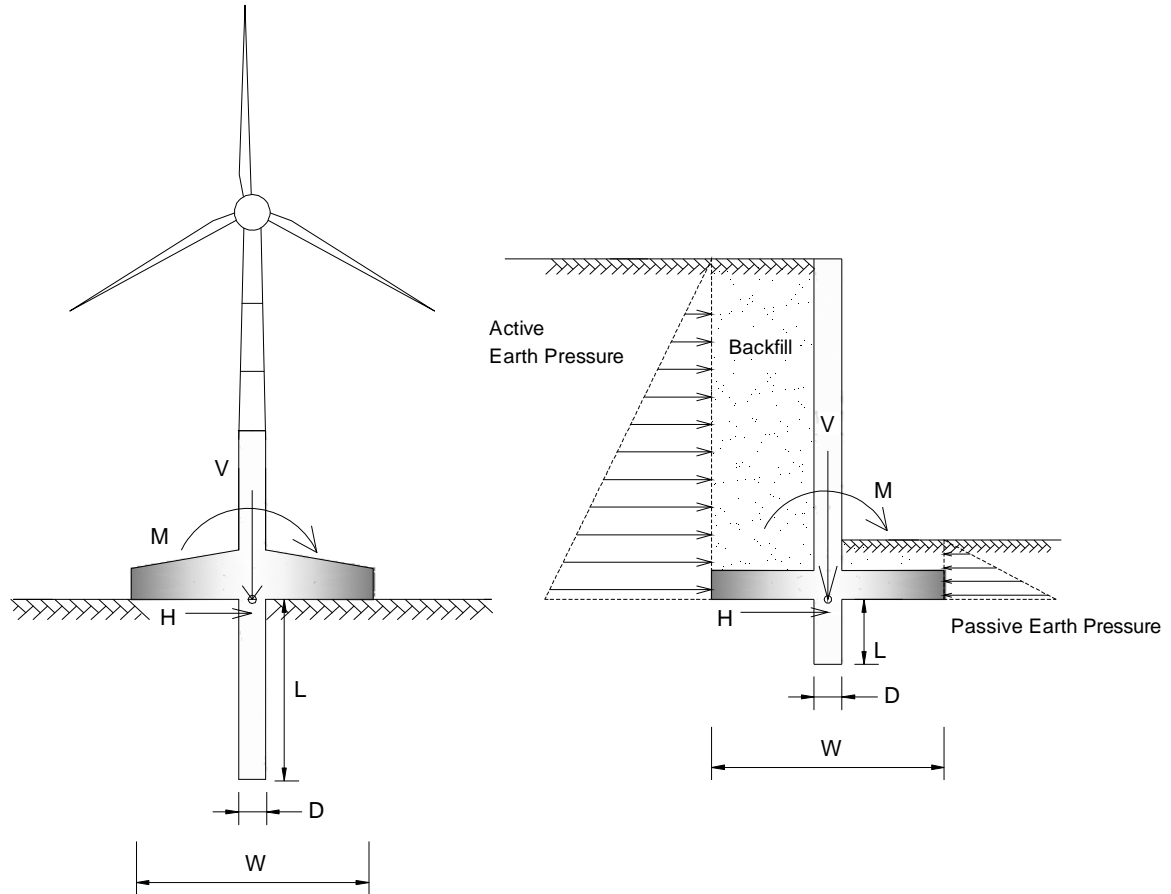
Figure 3-1 Examples of laterally loaded structures supported on the proposed hybrid system

3.2   2-D Numerical Modeling

An extensive finite element investigation was performed using the finite element code PLAXIS 2D V8 (Brinkgreve, 2002). The objective of this numerical modeling study is to better understand the role of the individual components of the hybrid system and consequently provide guidance for choosing their optimal dimensions. This simplified analysis of the numerical modeling results has provided the basis for developing the relationships between the applied vertical, horizontal and moment loads in the form of a complete failure surface in V-H-M space. Consequently, the ultimate bearing capacity of the hybrid system under general combinations of V-H-M loadings has been established.

Whilst in practice these hybrid systems are envisioned to be close to circular in plan (with the exception of foundations supporting long retaining walls), an essential precursor to the understanding of the behavior of circular hybrid systems is the study of the simple 2D plane strain problem of a long, rigid strip footing resting on a continuous rigid wall. Given the complexities and time involved for a full parametric study of the 3D problem, this provided a significant initial step in the development of this foundation form. Hence, the numerical models used in this study represent the 2D plane strain problem and this should still capture the main features required to understand the characteristics of the new hybrid system and are used to validate and broader the 3D analyses conducted and described later in the chapter.

3.2.1   Finite Element Model

All structural elements and soils are modeled in this study using unstructured meshes with 15-noded plane strain triangular elements with 12 Gaussian points. The hybrid structural system material is modeled as very stiff, linear elastic, non-porous material with unit weight, $\gamma = 25$ kN/m^3, modulus of elasticity, $E = 10^7$ times the soil's elastic modulus, and Poisson's ratio, $v = 0.15$. The soil bed has been modeled as loose to medium dense sand simulated by a Mohr-Coulomb, elastic-perfectly plastic constitutive model. The default soil parameters used in the analysis are summarized in Table 3-1 below. Note that this assumes a non-associated flow condition with friction angle (ϕ') of 30° and a dilation angle (ψ') of 7°, representing a more realistic case than associated flow.

Table 3-1 Sand Properties, Mohr-Coulomb model

Properties	Value	Unit
Saturated Unit Weight	17.8	kN/m^3
Young's Modulus, E	1E5	kN/m^2
Poisson's Ratio, v	0.35	N/A
Cohesion Stress, c	0.01	kN/m^2
Friction Angle, ϕ	30	Degree
Dilatancy Angle, ψ	7	Degree
Material Model	Mohr-Coulomb	N/A

A typical mesh discretization used in the analysis is shown in Figure 3-2. The model boundaries are simulated using the standard fixities in PLAXIS, which are imposed to constrain lateral displacements at the mesh sides and provide total fixity at the bottom.

The location of the outer mesh boundaries was chosen to provide a sufficient distance from the foundation to eliminate any possible boundary effects, especially during the early stages of loading, before the onset of strain localizations associated with failure conditions. During the analysis, variable mesh density was employed to achieve acceptable accuracy while maintaining the computational efficiency of the solution. As shown in Figure 3-2, local refinements are assigned to areas where large stress concentrations or large deformation gradients are expected. These include the anticipated location of failure planes underneath and surrounding the strip footing and the continuous wall.
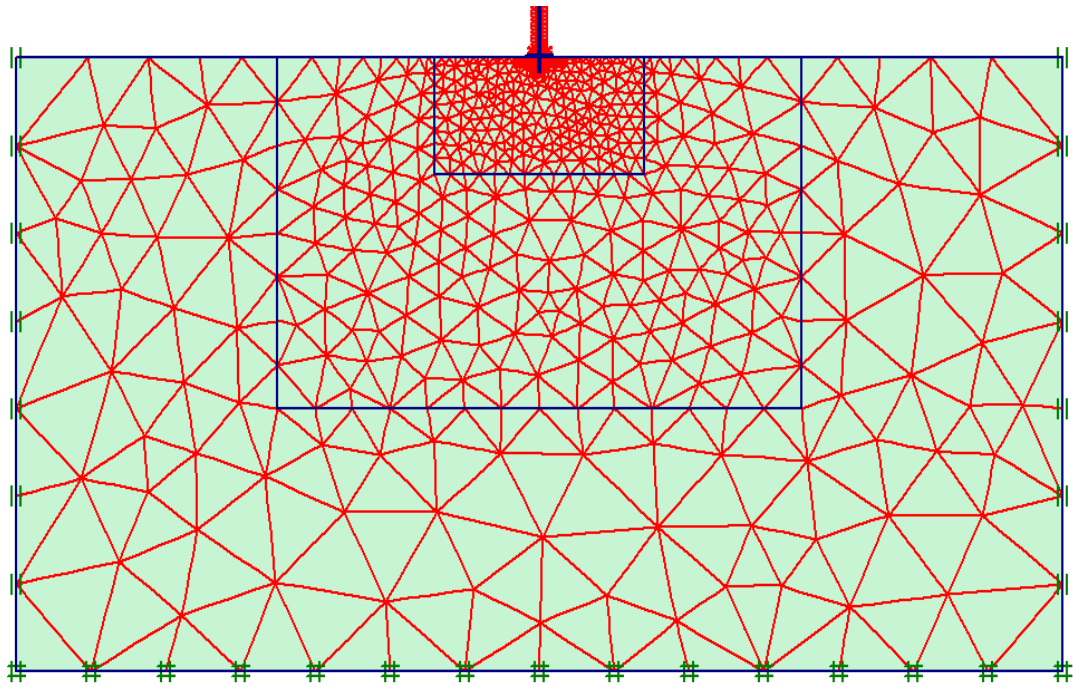
Figure 3-2 Typical mesh discretization in the finite element analysis

As previously noted by Frydman and Burd (1997), an important challenge in the analysis of this problem is associated with the high stress gradients developed at the singularity points at the foundation edges. Below the footing, the major principal stress acts

vertically in the case of the smooth footing and at a variable inclination to the vertical in the rough footing case. However, the vertical stress at the soil surface just outside the footing edge is zero and thus the shear strength of the sand, and all other stresses, are zero. Close to the soil surface, the major principal stress acts horizontally. This abrupt transformation in the principal directions at the edge of the footing creates computational difficulties. This problem was addressed by using 10-noded interface elements that extend a little farther than the footing edges together with a concentration of small elements in the region of the footing edge (Frydman and Burd, 1997). Furthermore, the interface aided the modeling of the interaction between the hybrid system and the soil, which is intermediate between smooth and rough. The roughness of the interface was modeled using a strength reduction factor (R_{inter}) of 0.67. This factor relates the interface strength to the soil strength (i.e. $c'_{inter} = R_{inter} \times c'$ and $\tan \phi'_{inter} = R_{inter} \times \tan \phi'$).

3.2.2   Sign Convention and Notations

This study follows the sign convention for displacements and loads proposed by Butterfield et al. (1997), as demonstrated in Figure 3-1. The position of the reference point for loads and moments, which is positioned at the middle of the foundation at the ground level, is also shown in Figure 3-1.

For the ultimate resistance for pure loadings, V_{max}, M_{max} and H_{max} represent the vertical ultimate bearing capacity (V_{max}, at $H = M = 0$), the horizontal ultimate bearing capacity (H_{max}, at $V = M = 0$) and the ultimate moment capacity (M_{max}, at $V = H = 0$), respectively.

3.2.3   Load Paths

For laterally loaded structures mounted on a shallow foundation, a piled foundation or the proposed hybrid system, the vertical loading on the foundation is nearly constant over the life of the structure and is equal to the combined weights of the structure and foundation system and any soil surcharge. On the other hand, the lateral loads may vary temporally depending on their source, whether due to soil pressures only or combinations of loads imposed by wind, waves and currents. The presence of a lateral loading component that acts at a certain distance above the foundation level typically adds a complex

combination of lateral load accompanied by a moment component to the vertical weights. In most cases, the load combination will occur in one plane of *V-H-M* space with a fixed ratio of V/V_{max}. In this situation, both the horizontal and moment load components acting on the foundation will act in the same direction so that this quadrant of the yield locus will be critical for the foundation design.

The numerical investigation involved two sets of analyses, namely: loading probes and swipe tests. In the load probes, each analysis consisted of two main loading stages. In the first loading stage, a prescribed vertical load, selected as a percentage of the ultimate vertical capacity of the shallow footing alone, was applied on the hybrid system. In the second loading stage, the vertical load was maintained constant, and a horizontal load was applied at a specified vertical elevation from ground level. Both the horizontal load and the associated moment were gradually increased until failure was reached.

The second method adopted in the finite element investigation consisted of using swipe tests to produce *V-H* or *V-M* failure envelopes. Tan (1990) introduced the swipe test, which was consequently used by many researchers (*e.g.*: Bransby and Randolph, 1998; Gourvenec & Randolph, 2003; Bienen *et al.* 2006). In theory, a single swipe test would be sufficient to determine a complete failure envelope in any two-dimensional loading plane. The swipe test typically consists of two loading stages. In the first stage, a prescribed displacement (typically vertical) is applied to the foundation until reaching the ultimate vertical load bearing capacity. Subsequently, the footing is swiped laterally (or rotated) while the vertical displacement is kept constant. The measured loads during the second phase generate a load path falling slightly within the true failure envelope, as reported by Gourvenec and Randolph, (2003).

3.3 Resistance to Vertical Loading

When the hybrid system is loaded vertically and the system settles, the pile starts to mobilize the skin friction over its shaft. As the applied pressure increases, a failure zone is initialized at the edges of the footing and gradually extends downward and outward. The same behavior takes place below the pile toe.

Previous studies by Stone *et al.* (2007) proposed that the vertical capacity of the hybrid system can be taken to be the sum of the capacities of its individual components (pile and footing). This assumption may be acceptable in the case of long and slender pile connected to a relatively narrow footing (*L/W* ratio = 3 or more), where the resistance of the pile is dominating the behavior of the hybrid system. On the other hand, in the case of short piles or a continuous wall connected to a wide footing, the vertical capacity of the system is expected to fall below the sum of the resistances of the individual components of the system. This is because the stressed soil zones beneath the foundation tend to overlap, eliminating the development of the full capacity of the individual structural elements of the hybrid system. Furthermore, at *L/W* = 0.25 the presence of the short central pile has lowered the vertical capacity of the hybrid system below that of the shallow footing. This can be attributed to the formation of an overstressed zone below the short pile that limits the propagation of the complete failure mechanism below the footing and results in a form of a progressive failure. White *et al.* (2008) previously observed the same phenomena in their study of vertically loaded conical footings.

Figure 3-3 shows that a hybrid system with a short pile (*L/W* = 0.5) provides little or no gain in the vertical load resistance compared to a shallow footing of the same dimensions.
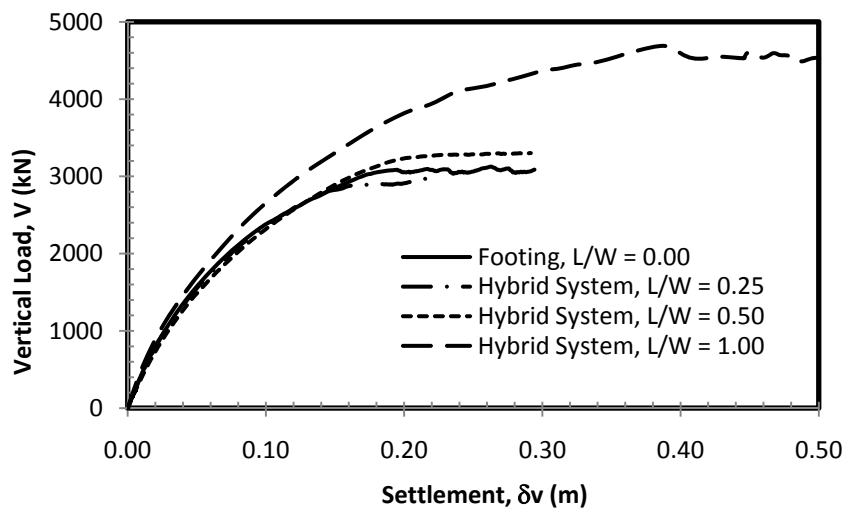
Figure 3-3 Plot of vertical load (V) versus vertical displacement (δv)

At failure, the rupture planes beneath the footing can be separated into three main zones; 1) a triangular elastic zone right underneath the footing; 2) a radial shear zone; and 3) a triangular passive resistance zone as shown in Figure 3-4a. For a hybrid system with a short pile, the pile shaft would be fully embedded in the elastic soil zone developed right below the footing as can be noted from Figure 3-4b and 4c. For a hybrid system with a medium length pile, the majority of the pile shaft falls within the elastic soil zone as shown in Figure 3-4d. In this moving soil wedge, neither significant bearing pressure nor shaft friction could be mobilized. It is safe to conclude that for a hybrid system provided with a short pile, as proposed in this study for practical considerations, the vertical capacity of the hybrid system will always fall below the sum of the capacities of its structural elements (footing and pile) as shown in Figure 3-3.

As an approximation, the vertical capacity of the hybrid system may be taken as the sum of 3 components: 1) the bearing load of the footing, which is calculated using the theoretical bearing capacity equations; 2) the end bearing of the pile; and 3) the skin friction produced along the section of the pile shaft that extends outside the failure zones of the footing. The third term may be neglected with a low margin of error.

a) Shallow footing L/W=0.0

b) Hybrid system with L/W=0.25

c) Hybrid system with L/W=0.5

d) Hybrid system with L/W=1
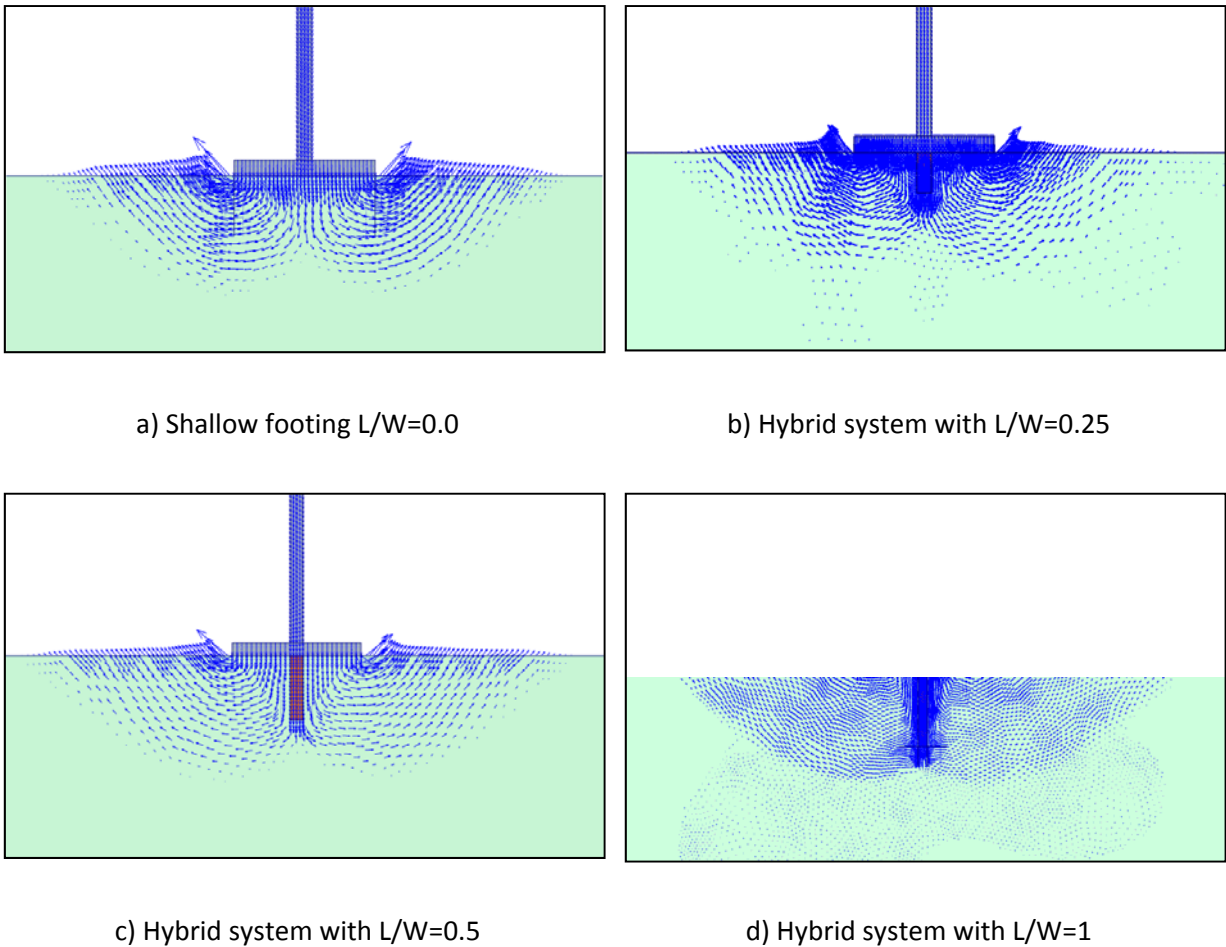
Figure 3-4 Displacement vectors at failure for: a) Shallow footing L/W=0, b) Hybrid system with L/W=0.25, c) Hybrid system with L/W=0.5 and d) Hybrid system with L/W=1

3.4   Resistance to Generalized *V-H-M* Load Combinations

The characteristics of the load combination acting on a foundation system are directly related to the function of the supported structure. For example, in case of an earth retaining structure, the foundation is subjected to a fairly large vertical load component resulting from the self-weight of the foundation system, superstructure, soil fill and surface surcharge. In addition, it is subjected to a lateral load resultant acting near the foundation level and producing an additional overturning moment at a low *M/H* ratio. On the other hand, in case of light laterally loaded structures, such as wind turbines, the

weight of the structure is relatively low when compared to the applied horizontal and moment loads derived from the wind. In addition, the lateral resultant acts at a large distance above the foundation level resulting in a large M/H ratio. The purpose of the analysis reported here is to explore the capability of the hybrid foundation system to efficiently support a wide variety of laterally loaded structures and resist general planar loading in V, H and M space.

The feasibility of implementing the hybrid system to improve the lateral resistance over that of traditional shallow foundations is investigated. A finite element analysis consisting of two main loading stages was employed to accomplish this task. In the first loading stage, a vertical load, selected based on a percentage (50%) of the ultimate vertical capacity of the shallow footing alone, is applied to the hybrid system. In the second loading stage, the vertical load is maintained constant, and a horizontal load is applied at a specified vertical distance above the ground level, $e = M/H = 0.5$ and 3.0 m. Both the horizontal load and the associated moment are gradually increased until reaching failure. The results of the finite element models are expressed in Figure 3-5 as plots of the lateral load (H) versus lateral displacement (δu). In Figure 3-5, the lateral stiffness (initial slope of the load displacement curve) of the hybrid system and its capacity increased as the ratio L/W increased (i.e. pile length increased).
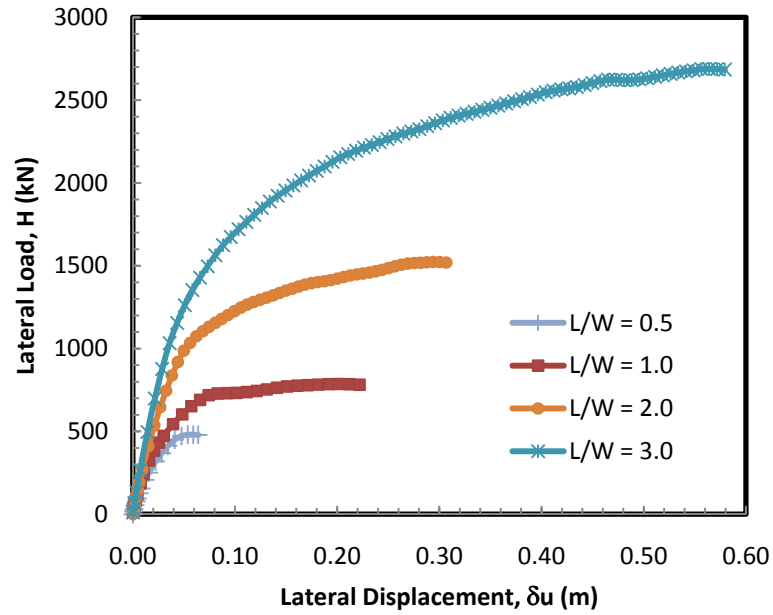
a) M/H = 0.5 m
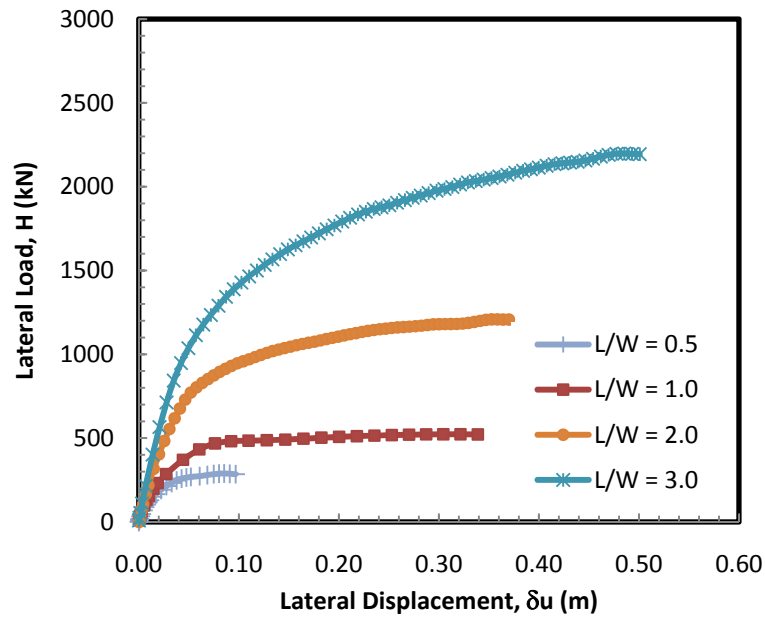
b) M/H = 3.0 m

Figure 3-5 Effect of L/W ratio on the lateral resistance of the hybrid system (for W/D=10) for: a) e = 0.5 m and b) 3.0 m

3.5 Analytical Solution to Estimate the Lateral Capacity of the Hybrid Foundation System

To provide a relatively simple analytical method for predicting the lateral capacity of this system, the limit equilibrium method has been used. The 2D plane strain finite element analysis of the laterally loaded hybrid system will be used for comparison. The problem in the 2D plane is analogous to the analysis of an embedded continuous wall with a stabilizing base previously proposed by Powrie and Daly (2007). The limit equilibrium approach is based on the classical solution of cantilever sheet pile walls, which assumes the presence of a virtual point of rotation lying in the plane of the wall at some point between formation level and the toe (Figure 3-6).
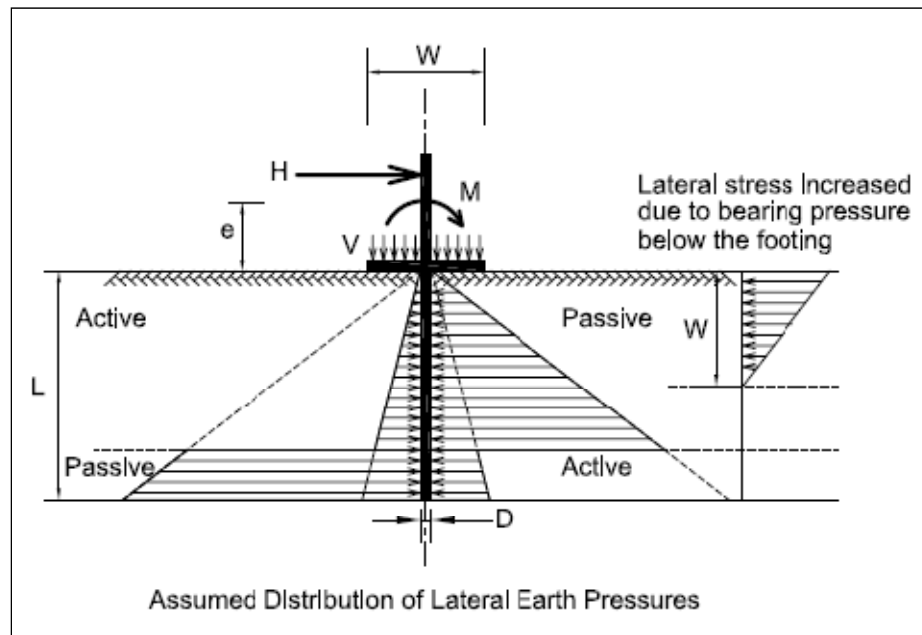
Figure 3-6 Geometry and definition of the studied problem

The analysis assumes the development of the failure mechanism by rigid body rotation about that point (this failure mechanism is straightforwardly observed from the finite element analysis shown in Figure 3-7. Figure 3-8 shows the proposed limit equilibrium stress distribution adopted in the analytical solution.
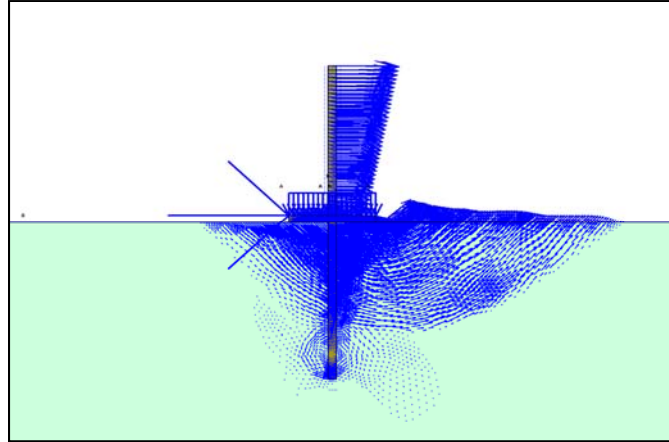
Figure 3-7 Failure mechanism, (L/W=2, W/D=10)

When lateral loads are applied to the hybrid system, the footing is subjected to compressive stresses on one side and tensile stresses on the other. Inspection of the studied cases, the deformed meshes and the stress distributions below the footing provided evidence of the development of a gap separating the soil from the tensioned side of the footing (as in Figure 3-8). Based on these observations, we proposed in the analysis the assumption of zero bearing pressures beneath the footing side subjected to tension stresses. Beneath the compressed portion, the bearing stresses are assumed to be uniformly distributed with a value equal to the ultimate bearing capacity of a strip footing with half the total footing width.

To accommodate the presence of the compressive portion of the footing in the limit equilibrium analysis, the following assumptions are made in the analysis: a) a restoring moment resulting from the concentration of the bearing stresses below the footing is introduced; b) bearing stresses are assumed to act as uniform surface surcharge acting on a strip area. As a result, additional lateral stresses at the wall side are calculated based on the theory of elasticity (Figure 3-9). Figure 3-10 shows the calculated lateral stress distribution beneath the edge of the strip adjacent to the embedded wall. In Figure 3-10, the lateral stress ratio represents the value of the lateral stress at any depth normalized by the initial lateral stress value right underneath the strip edge. The depth is normalized by the total footing width (twice the width of the loaded strip). Figure 3-10 shows that the lateral stresses tend to diminish with depth and there is no need to consider the lateral

stresses below a depth equal to the total footing width. In the proposed analysis, we replaced the calculated distribution by a simplified linear equivalent distribution starting at the ground surface from the initial lateral stress value right underneath the strip edge and reaching a zero value at depth equal to the total footing width.
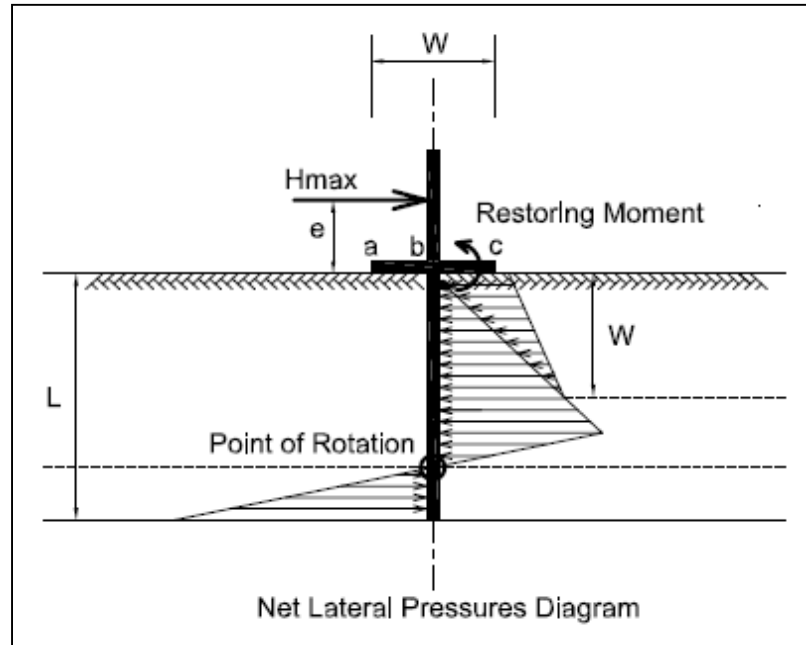
Figure 3-8 Net lateral pressure distribution applied in the limit equilibrium analysis
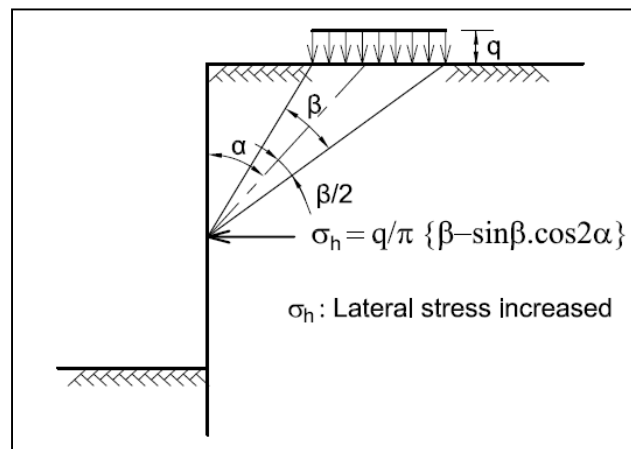
Figure 3-9 Lateral stress increased due to uniform surface surcharge (after NAVFAC Engineering Manual EM 1110-2-2504)

Shear stresses below the footing are neglected in the analysis. The coefficients of lateral earth pressure are determined from Coulombs equations, with respect to the effective angle of shear resistance ϕ' and soil-structure friction angle δ. Based on the net lateral stress distribution shown in Figure 3-8, the conditions of horizontal forces and moment equilibrium are used to calculate the position of the rotation point as well as the maximum lateral load value to be resisted by the hybrid system.
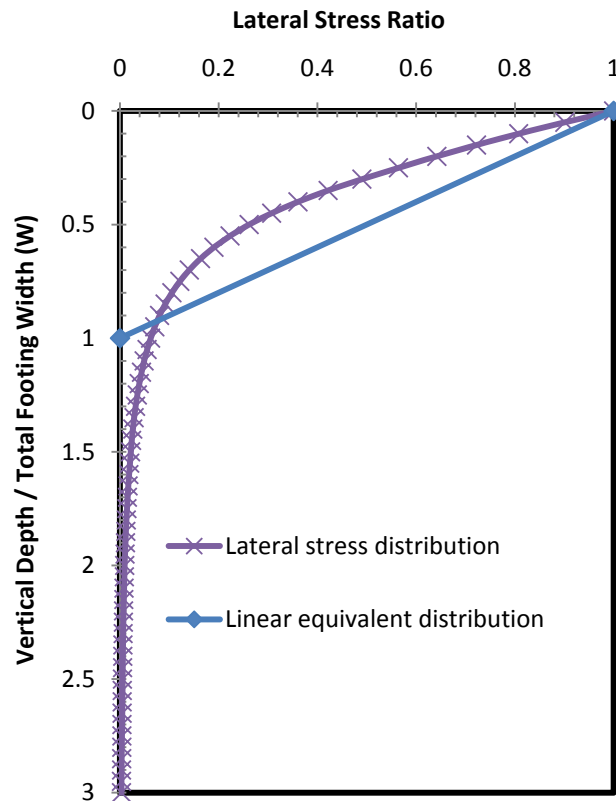
Figure 3-10 Lateral stresses distribution beneath the edge of uniformly loaded strip area
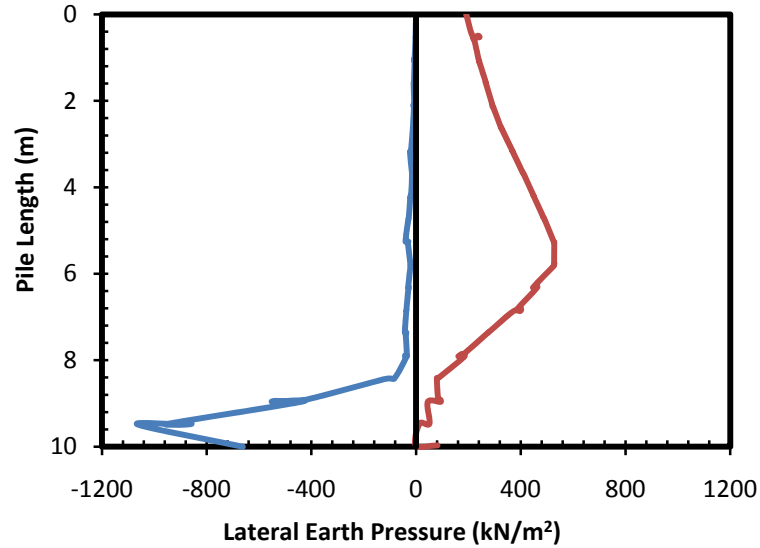
Figure 3-11 Distribution of lateral pressures as generated from the finite element analysis (for W/L=0.5, W/D=10)

The net lateral stress distribution generated from the finite element analysis is shown in Figure 3-12. This distribution shows excellent correspondence to the net stress distribution presumed in the limit equilibrium analysis and shown in Figure 3-8, and creates confidence in the results.
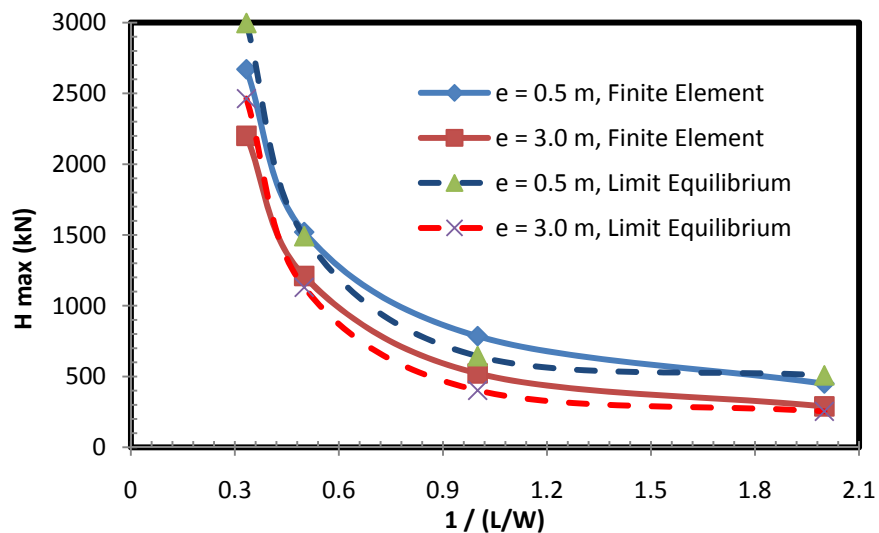
Figure 3-12 Comparison between the finite element and the limit equilibrium solutions for various L/W ratios

To evaluate the analysis methodology, the maximum lateral load resistance of the hybrid system at various L/W ratios, as calculated from both the finite element and the limit equilibrium analyses, are plotted in Figure 3-12. The plotted graphs demonstrate the accuracy of the procedure applied in the limit equilibrium analysis.

3.6 Effect of the Geometry of the Hybrid System (*W/D* and *L/W* ratios) on the Lateral Load Resistance

To study the effect of foundation width-to-pile diameter ratio, a series of loading probes was carried out at a constant wall (pile) length ratio to footing width (*L/W*=1), and at varying footing width to wall thickness ratios (*W/D*) of 1, 2, 5 and 10. The curves presented in Figure 3-13 illustrate the slight influence of the wall thickness on the lateral resistance of the hybrid system. The additional capacity gained by increasing the wall thickness is counteracted by the reduction in the rotational constraints at the wall head. The two curves demonstrate the same pattern in the response of the hybrid system for different *M/H* ratios.
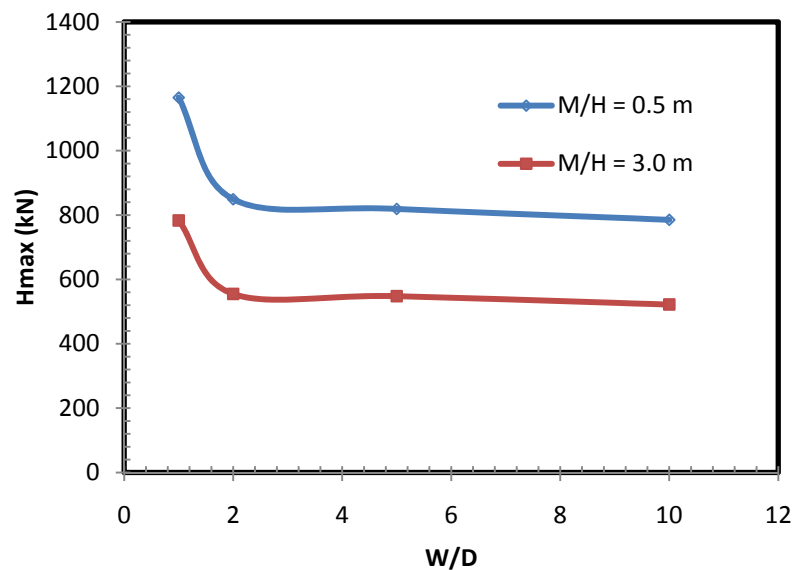
Figure 3-13 Effect of W/D ratios on the lateral resistance (for L/W = 1.0)

To study the effect of wall length to footing width ratio, another series of loading probes was carried out at a constant normalized wall thickness ratio (*W/D*=10), and a wide range

of *L/W* ratios. Figure 3-14 clearly demonstrates the impact of *L/W* ratio on the ultimate lateral resistance of the hybrid system.
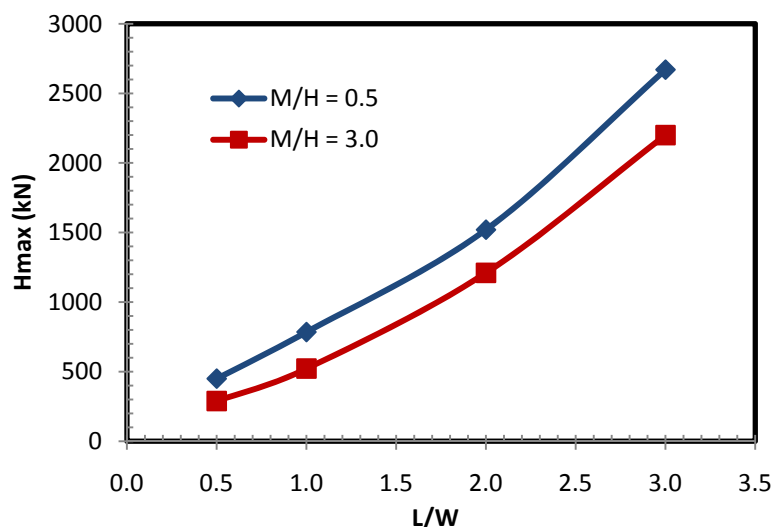
Figure 3-14 Effect of W/L ratio on the lateral resistance (for W/D = 10)

Figure 3-15 shows the *V-H* failure envelopes produced for different geometries of the hybrid system. The curves confirm that even a short central pile acting as a shear key below the footing (at *L/W = 0.25*) can significantly improve the lateral load resistance of the foundation system, especially at low *V*-load ratios. This finding is very useful when constructing foundations on weak, soft soils where it is essential to reduce the vertical loads applied to the soil. Obviously, increasing the pile length (increasing *L/W* ratio) will increase the resistance of the system. However, the lateral behaviour of piles is largely controlled by the soil resistance along the top 10 pile diameters; this suggests that pile length could be limited to 10 *d*. A better demonstration of the effect of increasing *L/W* ratio on increasing the lateral capacity of the hybrid system can be observed in Figure 3-16, which shows *V-H* failure envelopes normalized by V_{max}, the corresponding maximum vertical load resistance reached in each case.

Figure 3-15 Effect of the W/L ratio on the shape of V - H failure envelopes
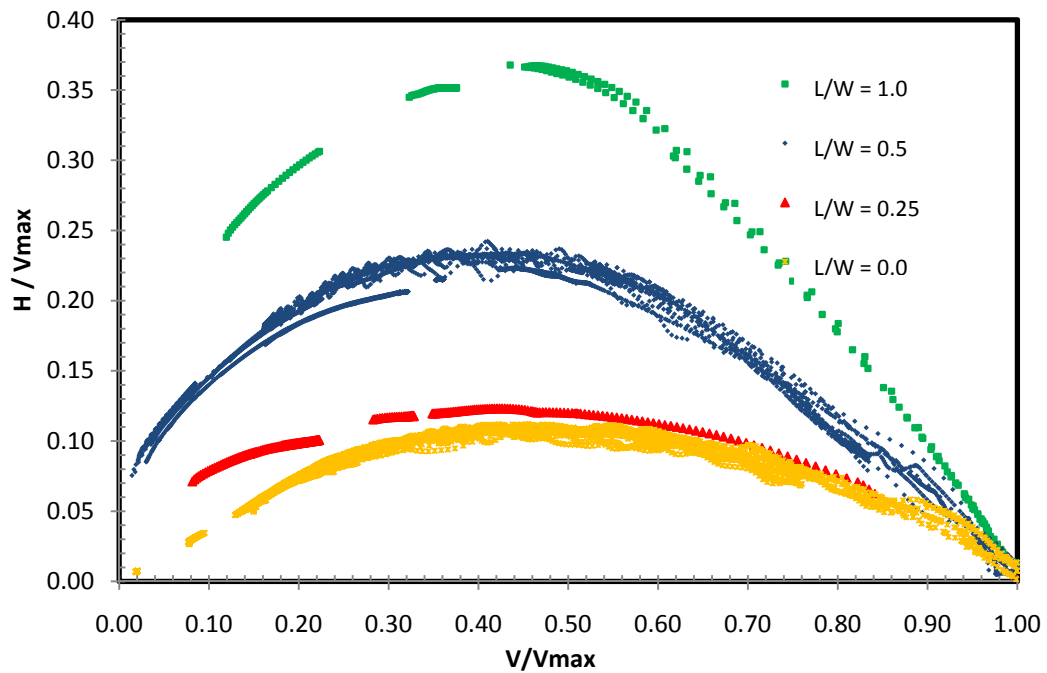
Figure 3-16 Effect of the geometry of the hybrid system on the shape of the normalized V-H failure envelops

3.7   Effect of Dilatancy on Size and Shape of *V-H* Failure Envelopes

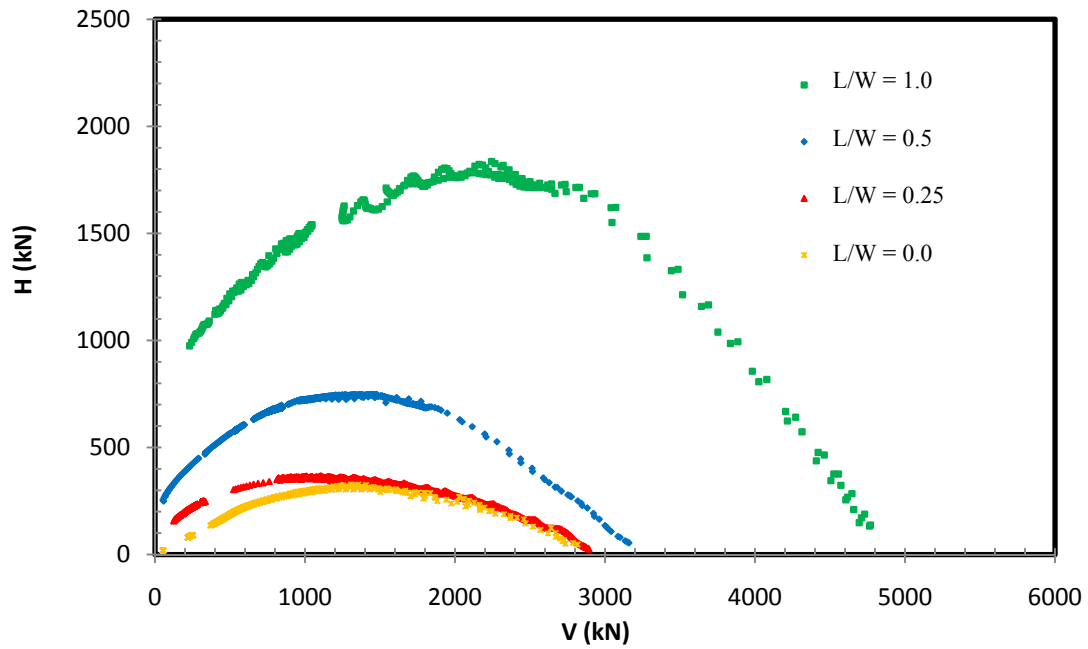In PLAXIS 2D V8, the dilation angle (ψ) is needed to model the irreversible increase in volume (as actually observed in sands), which depends on the density and the friction angle of the soil. To examine the effect of a non-associated flow rule on the size of the failure envelopes, a shallow footing and a hybrid system were analyzed considering different dilation angles (0, 7, 15 and 30°). The *V-H* failure envelopes obtained are presented in Figure 3-17. It can be proposed from this figure that increasing the dilation angle increases the size and extent of the failing soil zones underneath the footing, thus loading to a larger failure surface and consequently higher capacity of the foundation. Similar observations were made by a number of researchers (e.g. Louikidis *et al.,* 2008).

The *V-H* failure envelopes of the shallow footing are normalized by V_{max}, the corresponding maximum vertical capacity reached in each case, and the normalized envelopes are plotted in Figure 3-18a. It can be noted from this figure that, in general, the size and shape of the normalized envelopes appear to be independent of the dilation angle. The normalized curves show a maximum lateral load resistance, H_{max} = 0.10 - 0.11 *Vmax*, which occurs at V/V_{max} = 0.5. These numbers are in agreement with the results of previous experimental and numerical studies of shallow footings (Louikidis et al., 2008; Gottardi and Butterfield 1993; Georgiadis and Butterfield 1988). Similar observations are made in the case of the normalized *V-H* failure envelopes of the hybrid system (L/W = 0.5). Figure 3-18b shows that for the hybrid foundation system with L/W = 0.5, the maximum lateral load resistance, H_{max} = 0.22 - 0.23 V_{max}, which occurs at V/V_{max} = 0.4. This represents twice the resistance of the shallow footing with the same vertical load capacity. Moreover, the hybrid system generated an initial lateral resistance of 0.08 V_{max} at a very low vertical loading ratio, while the shallow footing has zero resistance. Since in many cases the sliding resistance is the governing factor in the design of the foundations supporting earth retaining structures, the use of the hybrid system can dramatically reduce the installation costs and foundation size.
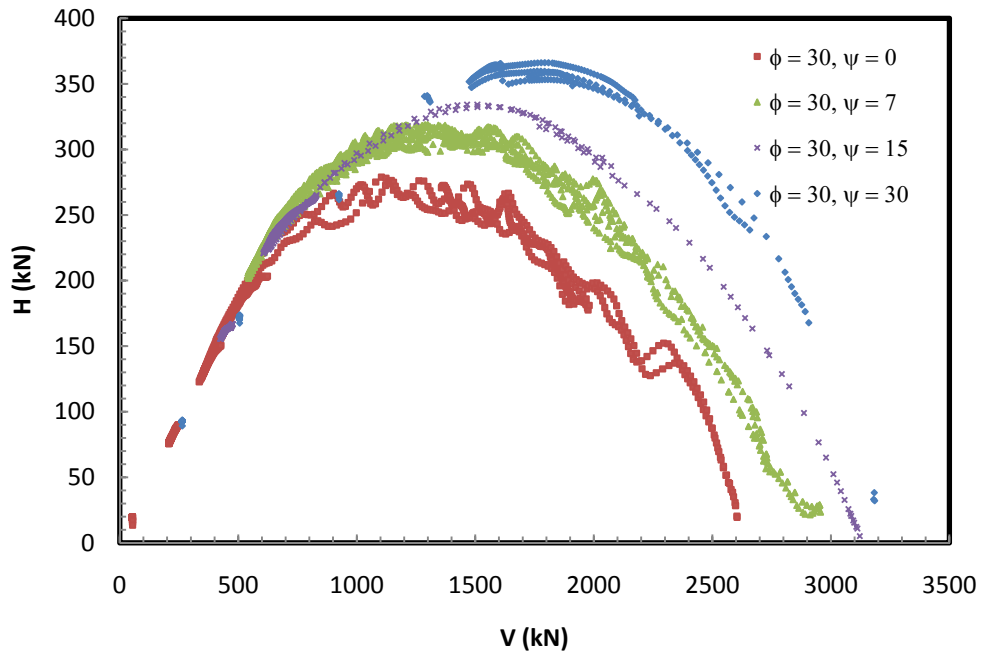
a) shallow footing
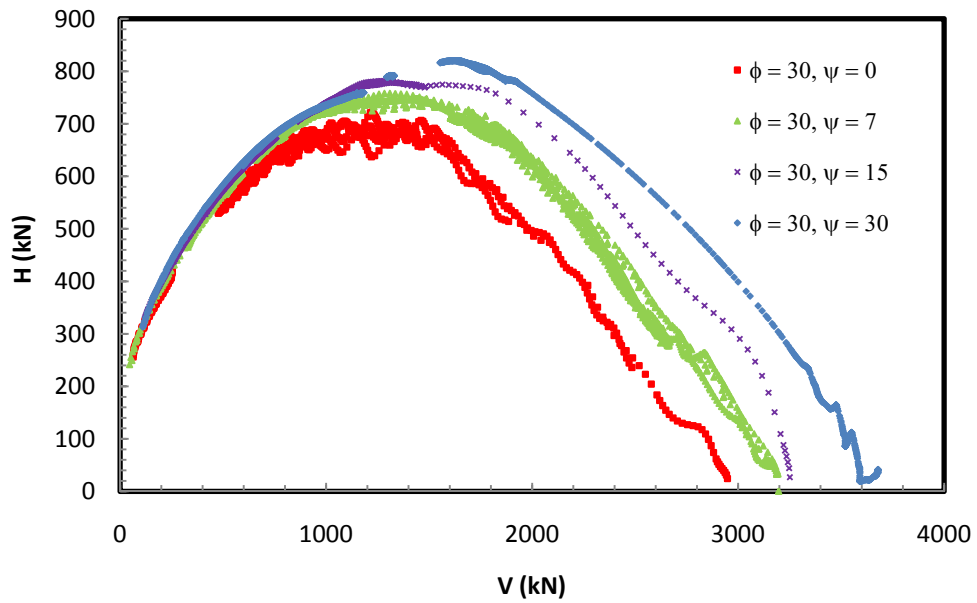
b) hybrid system at L/W = 0.5

Figure 3-17 Effect of the angle of dilation of cohesionless soil on the shape of the V-H failure envelopes for: a) shallow footing and b) hybrid system at L/W = 0.5
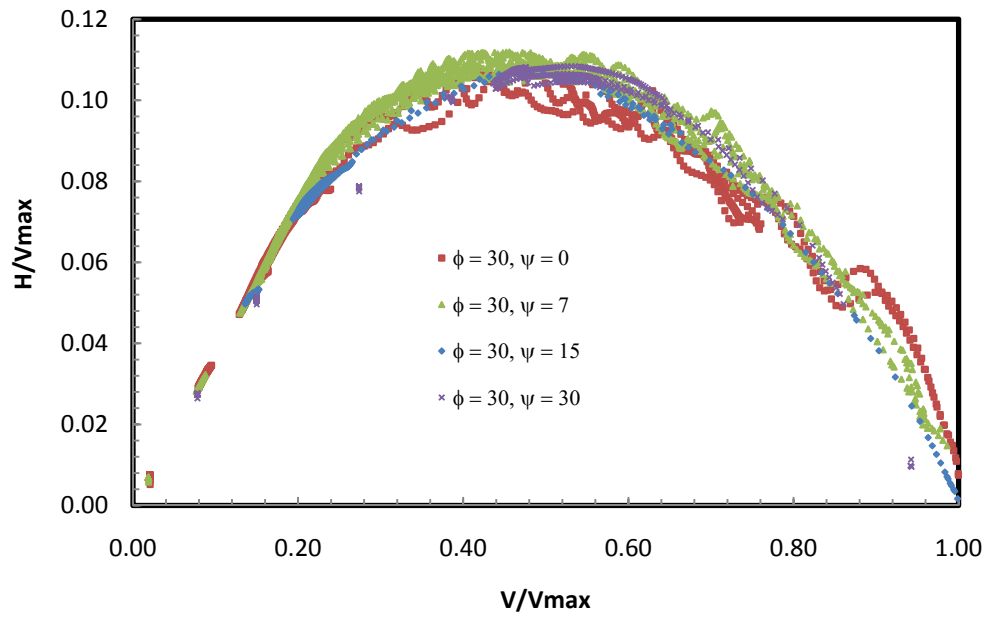
a) shallow footing
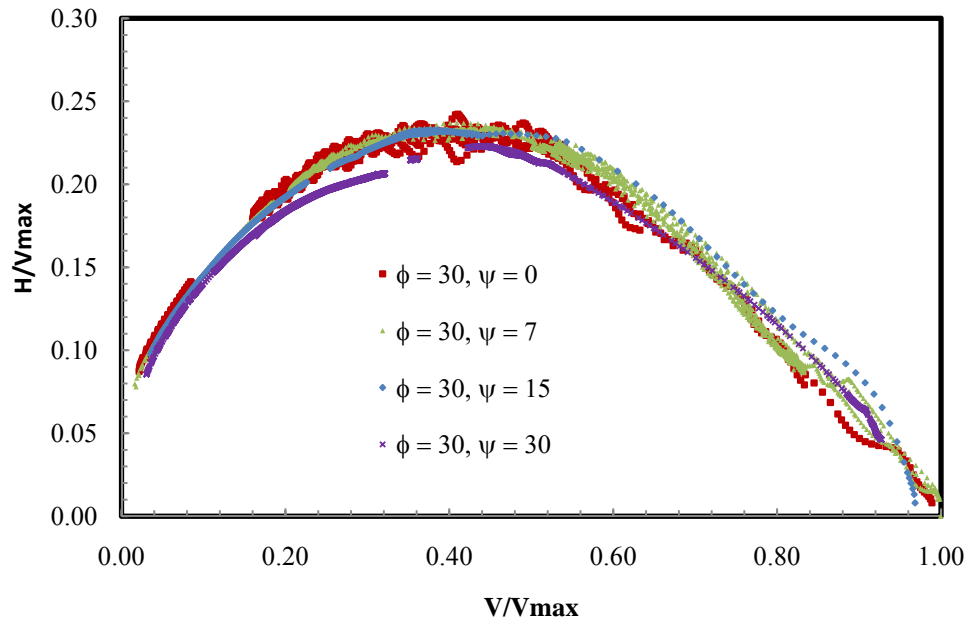
b) hybrid system at L/W = 0.5

Figure 3-18 Normalized V-H failure envelopes for: a) shallow footing and b) hybrid system at L/W = 0.5

3.8 Closed Form Expressions for the V-H Failure Envelopes

Several researchers have proposed equations that describe the shape of the V-H failure envelope of a strip footing (e.g. Gottardi and Butterfield, 1993; Loukidis et al., 2008). For example, Gottardi and Butterfield (1993) proposed that the V-H failure envelopes of strip footings is best fitted with a function similar to the following:

$$H = \beta_1.V\left[1 - \left(\frac{V}{V_{max}}\right)^{\beta_2}\right] \tag{3-1}$$

$$H = \beta_1.V\left(1 - \frac{V}{V_{max}}\right)^{\beta_3} \tag{3-2}$$

Where, β_1 is a parameter used to represent the initial slope of the parabola and depends on the friction angle of the footing – soil interface, while β_2 and β_3 control the position and value of the peak point. Similarly, the classical general bearing capacity equation can be used to derive the following equations to describe the V-H failure envelope:

$$H = 1.4286\,\frac{V}{V_{max}}\left[1 - \left(\frac{V}{V_{max}}\right)^{0.2}\right] \qquad \text{(based on Hansen, 1970)} \tag{3-3}$$

$$H = \frac{V}{V_{max}}\left[1 - \left(\frac{V}{V_{max}}\right)^{0.33}\right] \qquad \text{(based on Vesic, 1975)} \tag{3-4}$$

Equations 3-1 and 3-2 can be much simplified by setting β_2 and β_3 to equal 1. In this case, the equation of the V-H failure envelope simplifies to a simple second-order parabola, i.e.

$$H = \beta_1.V\left(1 - \frac{V}{V_{max}}\right) \tag{3-5}$$

Gottardi and Butterfield (1993) suggested a value of 0.48 for β_1, which produced a maximum lateral resistance, $H_{max} = 0.12\ V_{max}$. The results of the current finite element study suggest that β_1 could be reduced slightly to 0.44 and $H_{max} = 0.11\ V_{max}$. These values

achieve the best fitting curves for the normalized *V-H* envelopes. Substituting these
values into Equation 3-5 yields:

$$\frac{H}{V_{max}} = 0.48 \; \frac{V}{V_{max}}\left(1 - \frac{V}{V_{max}}\right) \qquad \text{(based on Gottardi and Butterfield, 1993)} \qquad (3\text{-}6)$$

$$\frac{H}{V_{max}} = 0.44 \; \frac{V}{V_{max}}\left(1 - \frac{V}{V_{max}}\right) \qquad \text{(based on the current study)} \qquad (3\text{-}7)$$

Figure 3-19 compares the different equations that describe the *V-H* failure envelope of a
from Figure 3-19 that all of the failure envelopes display the same form and have similar
values.
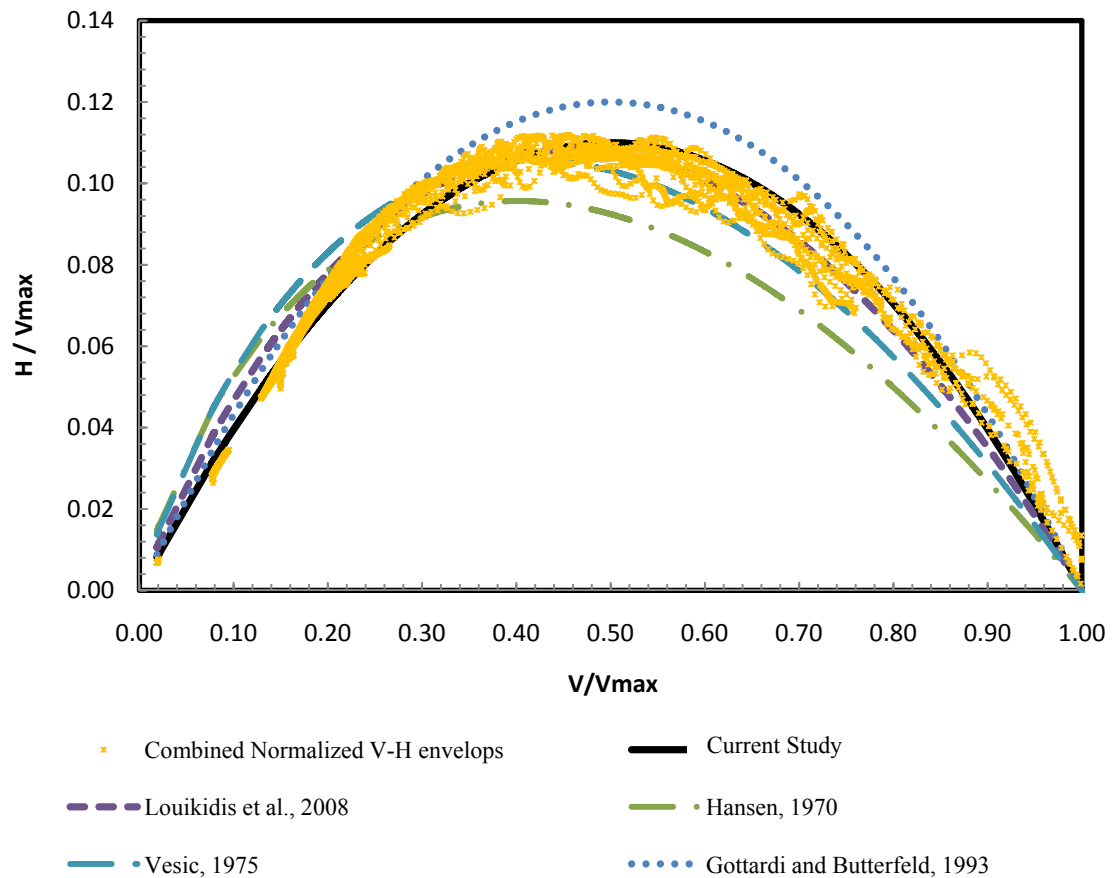
Figure 3-19 Best fitting equations for the normalized V-H failure envelopes of a
shallow footing

The results of the numerical modeling investigation reported herein can be employed to establish an equation to describe the shape of the *V-H* failure envelopes of the proposed hybrid system. Adopting the same form of the failure envelope of the shallow footing and curve fitting the normalized *V-H* envelopes of the hybrid system, the following equation is proposed:

$$\frac{H}{V_{max}} = \beta_1 \left(\frac{V}{V_{max}}\right)^{\beta_2} \left[1 - \left(\frac{V}{V_{max}}\right)^{1+\beta_2}\right] \tag{3-8}$$

Where the parameter β_2 is a constant obtained from curve fitting equal to 0.5. Whereas the parameter β_1 defines the size of the normalized *V-H* failure envelope and varies depending on the *L/W* ratio of the hybrid system according to the following equation:

$$\beta_1 = 0.0532 \left(\frac{W}{L}\right)^2 - 0.4325 \left(\frac{W}{L}\right) + 1.1323 \tag{3-9}$$

The parameter β_1 is obtained from curve fitting as 0.75, 0.48 and 0.25 for *L/W* = 1, 0.5, and 0.25, respectively. Substituting these values into Equation 3-8, the following equations are obtained for the hybrid system with *L/W* = 0.25, 0.5 and 1:

$$\frac{H}{V_{max}} = 0.25 \left(\frac{V}{V_{max}}\right)^{0.5} \left[1 - \left(\frac{V}{V_{max}}\right)^{1.5}\right] \tag{3-10}$$

$$\frac{H}{V_{max}} = 0.48 \left(\frac{V}{V_{max}}\right)^{0.5} \left[1 - \left(\frac{V}{V_{max}}\right)^{1.5}\right] \tag{3-11}$$

$$\frac{H}{V_{max}} = 0.75 \left(\frac{V}{V_{max}}\right)^{0.5} \left[1 - \left(\frac{V}{V_{max}}\right)^{1.5}\right]$$

$$\tag{3-12}$$

The normalized *V-H* failure envelopes are plotted in Figure 3-20 along with the curves produced from Equations 3-10 to 3-12.
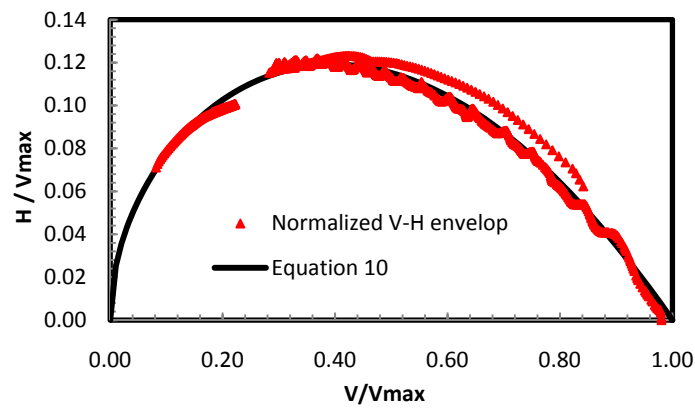
a) Hybrid system with L/W = 0.25
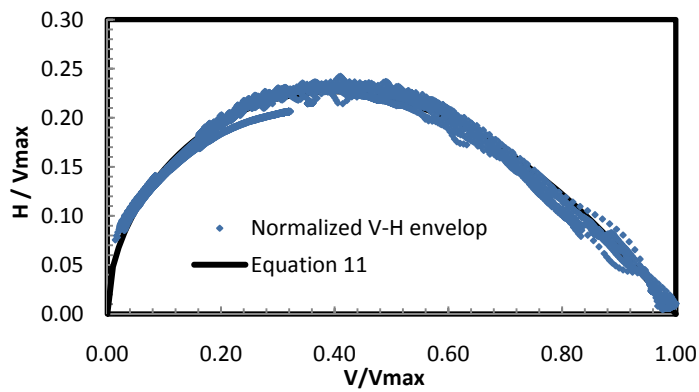
b) Hybrid system with L/W = 0.5
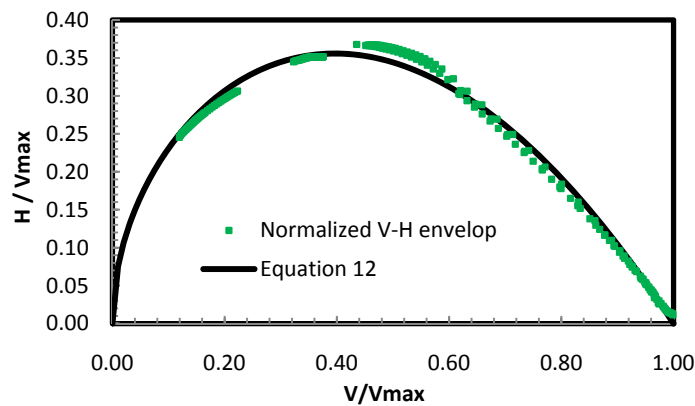
c) Hybrid system with L/W = 1

Figure 3-20 Normalized V-H failure envelopes for hybrid systems with: a) L/W = 0.25, b) L/W = 0.5 and c) L/W = 1

3.9 Effect of Geometry of Hybrid System (*L/W* ratio) on Its Rocking Resistance

Figure 3-21 shows the normalized *V-M* failure envelopes produced for different geometries of the hybrid system. The curves show that the gain in the rocking resistance of the hybrid system can be achieved when the pile length is more than half the footing width (*L/W>0.5*). At *L/W=0.25*, the presence of the short pile reduced the size of the *V-M* failure envelope below that of the shallow footing. This can be attributed to the effect of the short pile on reducing the maximum vertical capacity of the hybrid system due to the formation of an overstressed zone below the short pile that limits the propagation of the complete mechanism below the footing. Despite the finding that the hybrid system at *L/W*=0.5 has a slightly lowered maximum rocking resistance than the shallow footing, the hybrid system gained a superior initial rocking resistance at low *V/V$_{max}$* values.
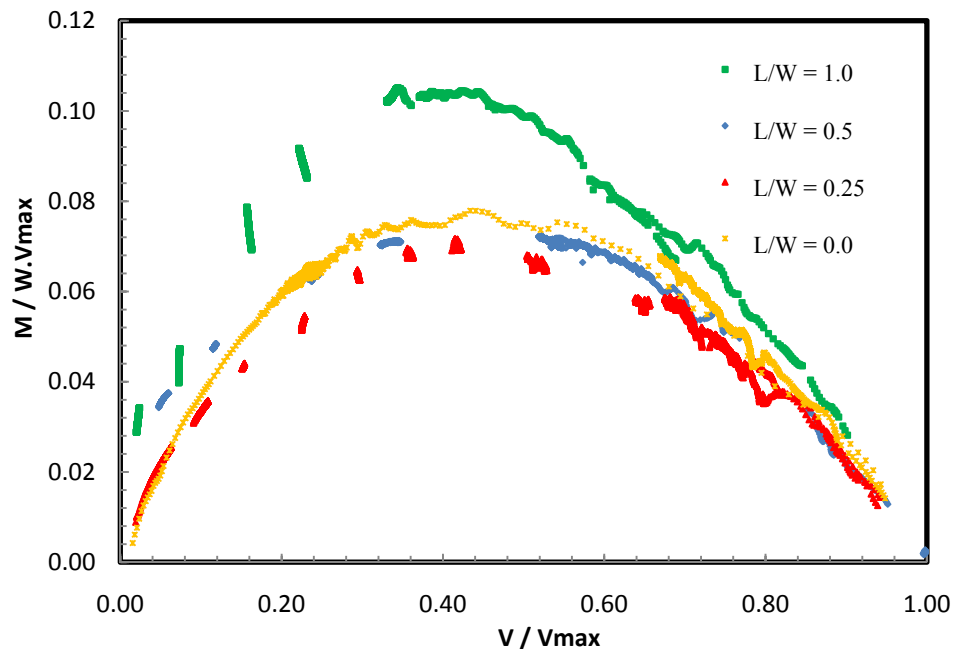
Figure 3-21 Effect of the L/W ratio on the shape of the normalized V-M failure envelopes

3.10 Effect of Dilatancy on Size and Shape of the V-M Failure Envelopes

The normalized failure envelopes of the shallow footing and hybrid foundation system at *L/W* = 0.5 are plotted in Figure 3-22 for different dilation angles.
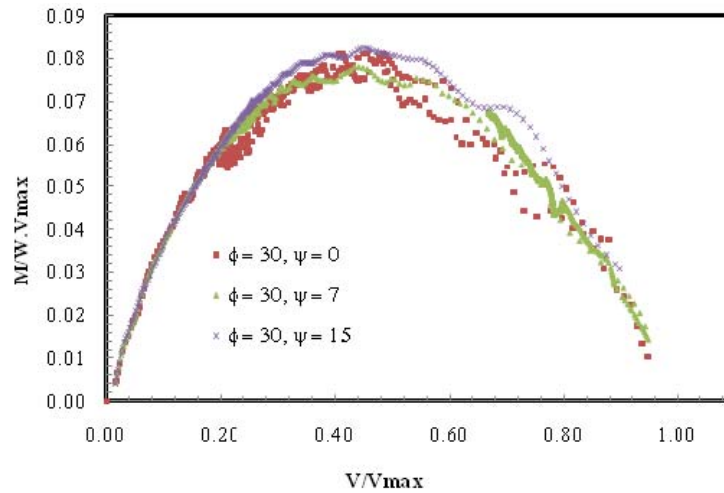
a) shallow footing
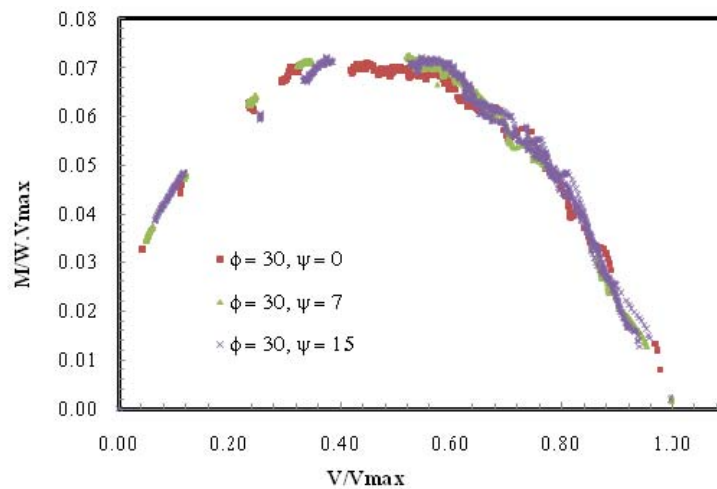
b) hybrid system at L/W = 0.5

Figure 3-22 Normalized V-M failure envelopes for: a) shallow footing and b) hybrid system at L/W = 0.5

Similar to the observations made for the *V-H* envelopes, the shape and size of the normalized failure envelops are still independent of the dilation angle in the *V-M* plane. This suggests that there should be a unique normalized *V-H-M* failure surface with no regard to the adopted angle of dilation.

3.11 Closed Form Expressions for the V-M Failure Envelopes

Figure 3-23 displays the normalized *V-M* failure envelopes of a shallow footing resting on soils with different dilation angles. *V* is normalized by V_{max} and *M* is normalized by $W.V_{max}$. It is noted that the normalized *V-M* failure envelopes display a maximum rocking resistance, $M_{max} = 0.075 - 0.080$ $W.V_{max}$. This maximum rocking resistance occurs at $V/V_{max} = 0.46 - 0.48$. Again, these results agree with the failure envelopes proposed by other researchers for shallow foundations and given by Equations 3-13 to 3-15 (Louikidis *et al.,* 2008; Gotardi and Butterfield 1993; Georgiadis and Butterfield 1988). Equation 16 represents the failure envelope based on the numerical results obtained in the current study.

$$\frac{M}{W.V_{max}} = 0.5 \frac{V}{V_{max}} \left[1 - \left(\frac{V}{V_{max}}\right)^{0.5}\right]$$
(based on Hansen, 1970)   (3-13)

$$\frac{M}{W.V_{max}} = 0.44 \frac{V}{V_{max}} \left[1 - \left(\frac{V}{V_{max}}\right)^{0.625}\right]$$
(based on Louikidis *et al.,* 2008)   (3-14)

$$\frac{M}{W.V_{max}} = 0.36 \frac{V}{V_{max}} \left[1 - \left(\frac{V}{V_{max}}\right)\right]$$
(based on Gottardi and Butterfield, 1993) (3-15)

$$\frac{M}{W.V_{max}} = 0.53 \frac{V}{V_{max}} \left[1 - \left(\frac{V}{V_{max}}\right)^{0.5}\right]$$
(based on the current study) (3-16)
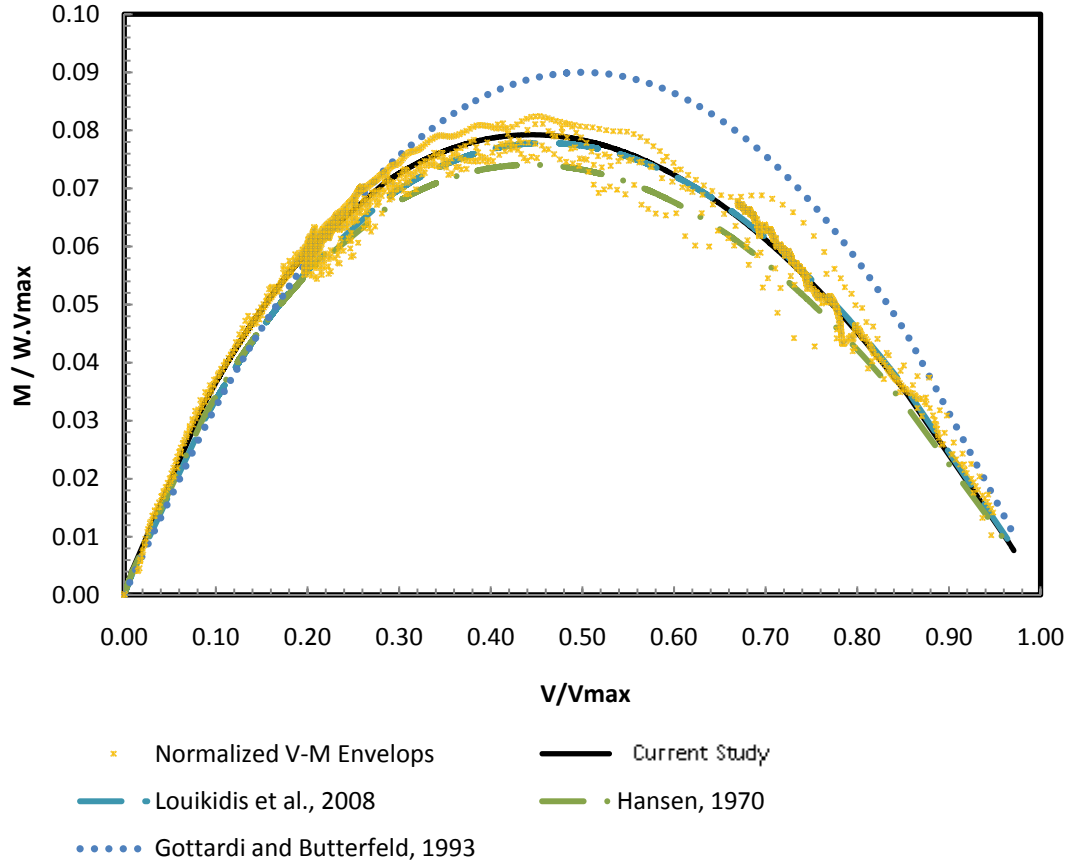
Figure 3-23 A comparison of the best fitting equations for the normalized V-M failure envelope of a shallow footing

The results of the numerical modeling investigation reported herein were employed to establish the following equation to describe the shape of the *V-M* failure envelopes of the proposed hybrid system:

$$\frac{M}{W.V_{max}} = \beta_1 \left(\frac{V}{V_{max}}\right)^{\beta_2} \left[1 - \left(\frac{V}{V_{max}}\right)^{\beta_3}\right] \tag{3-17}$$

The following equations describe the *V-M* envelopes of the hybrid systems with *L/W* = 0.25, 0.5 and 1 respectively:

$$\frac{M}{W.V_{max}} = 0.473 \left(\frac{V}{V_{max}}\right) \left[1 - \left(\frac{V}{V_{max}}\right)^{0.5}\right] \qquad \text{(at } L/W\text{=0.25)} \tag{3-18}$$

$$\frac{M}{W.V_{max}} = 0.137 \left(\frac{V}{V_{max}}\right)^{0.5} \left[1 - \left(\frac{V}{V_{max}}\right)^{2}\right] \qquad \text{(at } L/W{=}0.5\text{)} \qquad \text{(3-19)}$$

$$\frac{M}{W.V_{max}} = 0.217 \left(\frac{V}{V_{max}}\right)^{0.5} \left[1 - \left(\frac{V}{V_{max}}\right)^{1.5}\right] \qquad \text{(at } L/W{=}1\text{)} \qquad \text{(3-20)}$$

The fitted equation of the hybrid system at $L/W{=}0.25$ has exactly the same form as the shallow footing with reduced parameters, which supports the thesis that at this geometrical configuration, the rocking resistance is governed solely by the footing. The plots of the best fit equations 3-18 to 3-20 are shown in Figure 3-24 below.
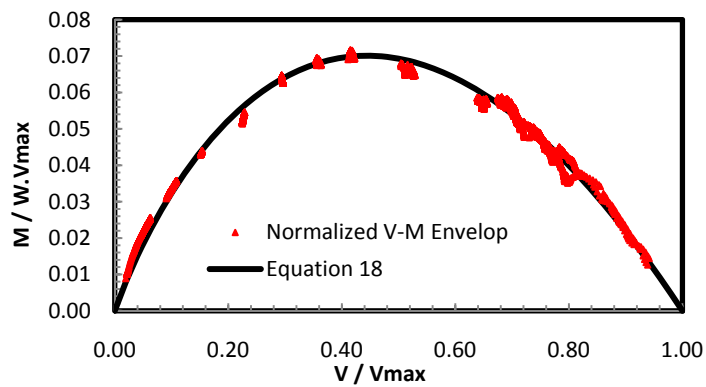
a) Hybrid system with L/W = 0.25
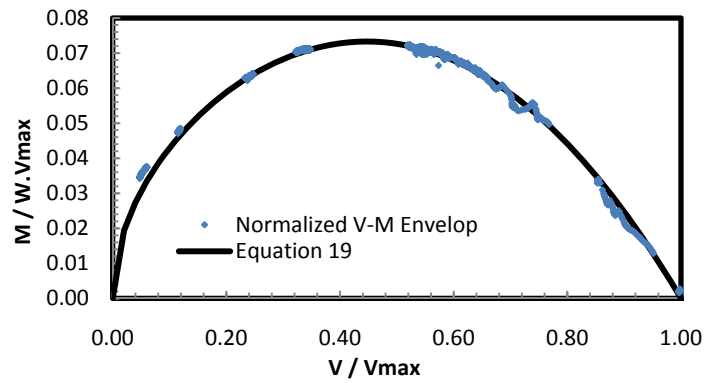
b) Hybrid system with L/W = 0.5
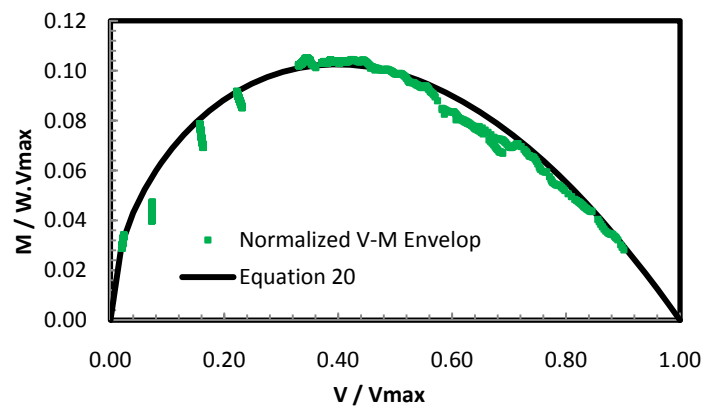
c) Hybrid system with L/W = 1

Figure 3-24 Normalized V-M failure envelopes for hybrid systems with: a) L/W = 0.25, b) L/W = 0.5 and c) L/W = 1

3.12 Failure Mechanisms

The soil failure mechanisms have been visualised for V-H and V-M loading for the default analysis (ϕ=30° and ψ=7°) for different L/W ratios. The combined V-H loading acting on the foundation results in complex asymmetrical failure mechanisms. As displayed in Figure 3-25 to Figure 3-30, these failure mechanisms vary from shallow sliding wedges at low V-load ratios ($V/V_{max} > 0.1$), to deeper and wider combined wedge and scoop mechanisms as the V-load ratio is increased. The presence of the monopile significantly modified the failure mode. Increasing the pile length tends to create a deeper and wider failure mechanism, thus increasing the load capacity of the foundation system under V-H loading. It should be noted that the wide variations of the failure modes for different V-H load combinations and geometry configurations (L/W ratios) would make it difficult to produce a general upper bound solution based on a single kinematically admissible failure mechanism (Houlsby and Puzrin, 1999). The failure mechanisms displayed in Figures 21 to 23 show the failure mechanisms for the case of V-M loading. These plots show a similar progression of increasing soil volumes and more complex scoop failures with increased V/V_{max} and L/W ratios.
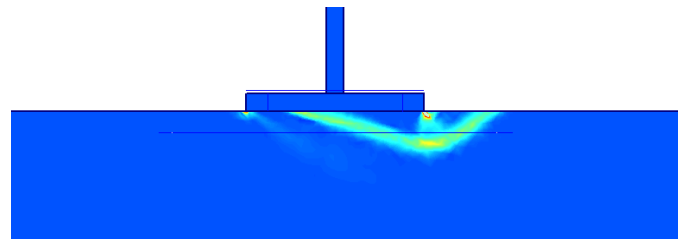
a) Shallow footing
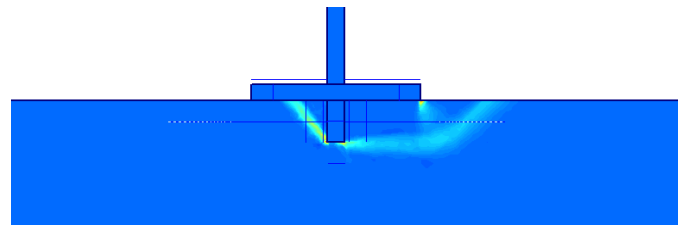
b) Hybrid system with L/W=0.25
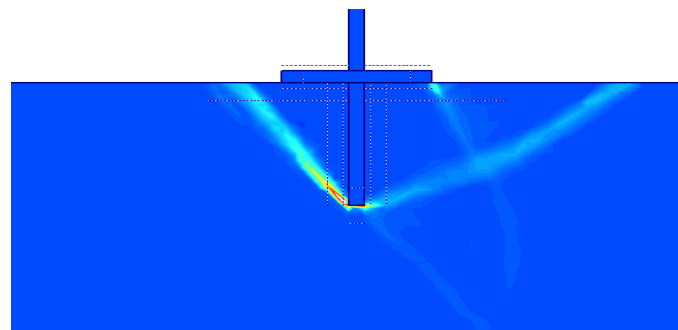
c) Hybrid system with L/W=1

Figure 3-25 Failure mechanisms under combined V-H loading at V/Vmax < 0.1, for: a) Shallow footing, b) Hybrid system with L/W=0.25 and c) Hybrid system with L/W=1
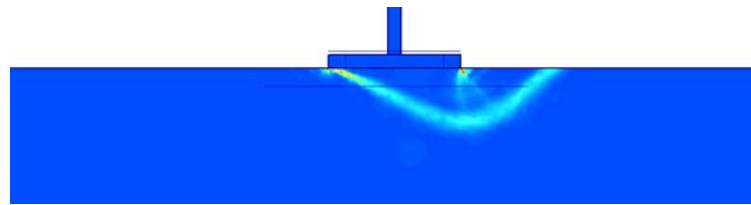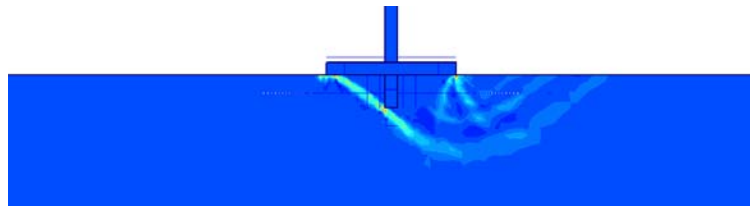
a) Shallow footing

b) Hybrid system with L/W=0.25
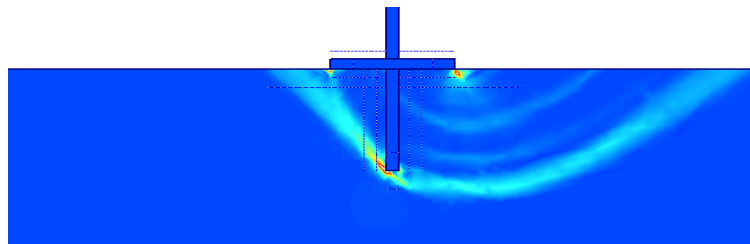
c) Hybrid system with L/W=1

Figure 3-26 Failure mechanisms under combined V-H loading at V/V$_{max}$ ~ 0.5, for: a) Shallow footing, b) Hybrid system with L/W=0.25 and c) Hybrid system with L/W=1
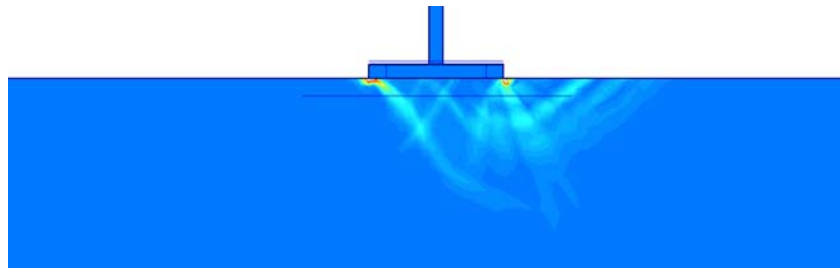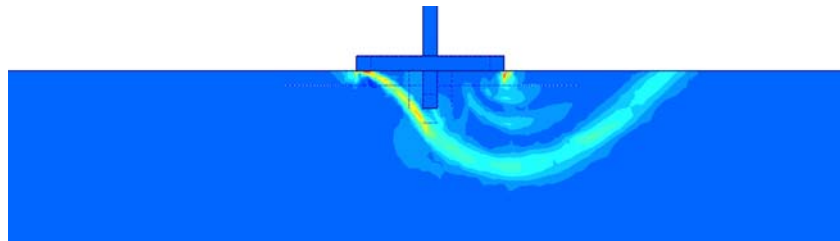
a) Shallow footing

b) Hybrid system with L/W=0.25
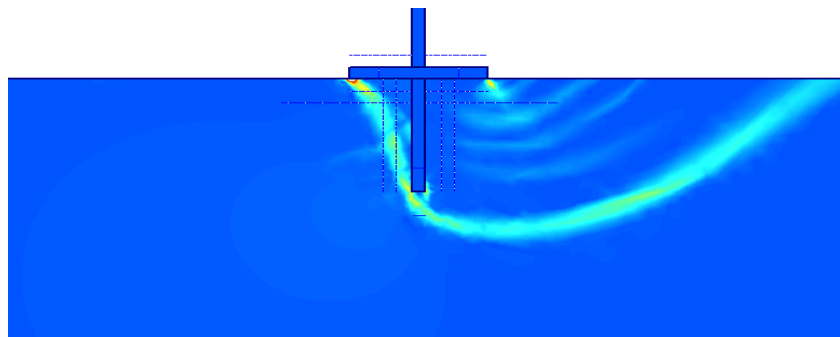
c) Hybrid system with L/W=1

Figure 3-27 Failure mechanisms under combined V-H loading at V/V$_{max}$ > 0.9, for: a) Shallow footing, b) Hybrid system with L/W=0.25 and c) Hybrid system with L/W=1
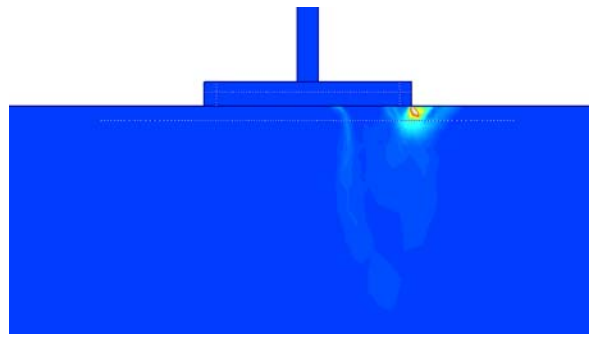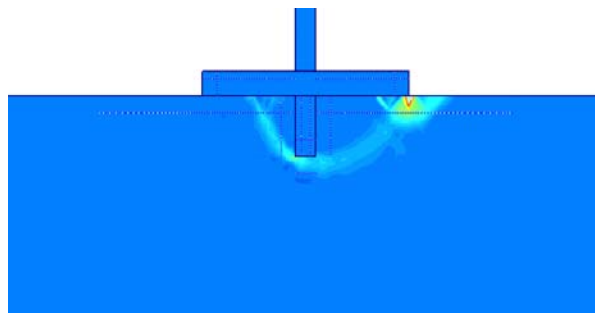
a) Shallow footing

b) Hybrid system with L/W=0.25
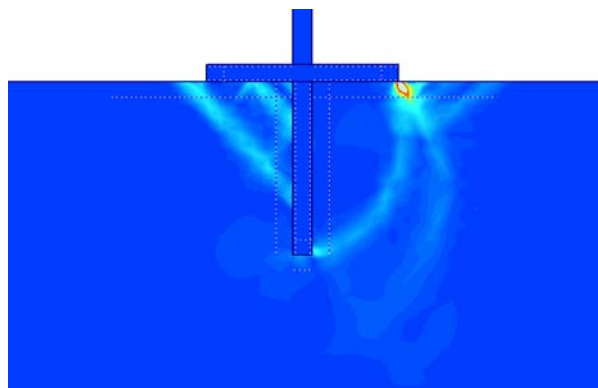
c) Hybrid system with L/W=1

Figure 3-28 Failure mechanisms under combined V-M loading at V/V$_{max}$ < 0.1, for: a) Shallow footing, b) Hybrid system with L/W=0.25 and c) Hybrid system with L/W=1
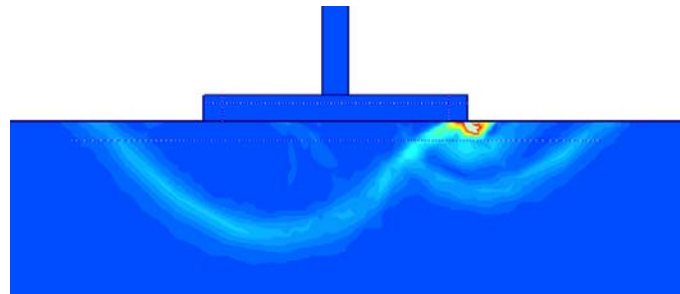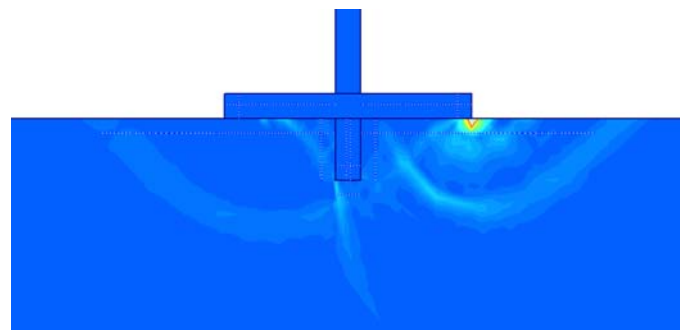
a) Shallow footing

b) Hybrid system with L/W=0.25
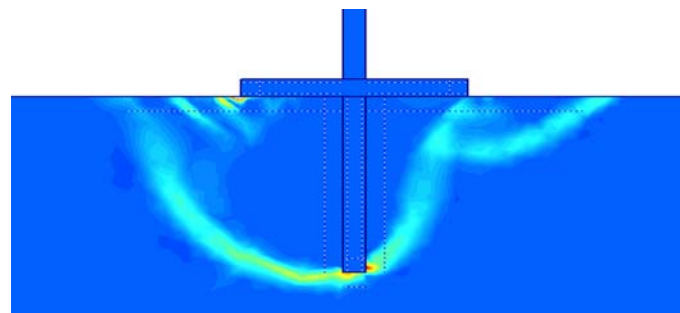
c) Hybrid system with L/W=1

Figure 3-29 Failure mechanisms under combined V-M loading at V/V$_{max}$ ~ 0.5, for:
a) Shallow footing, b) Hybrid system with W/L=4 and c) Hybrid system with W/L=1
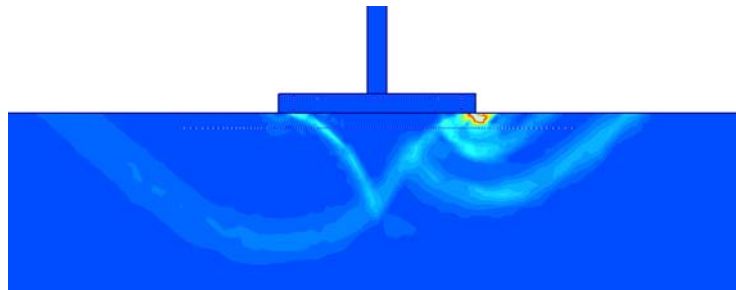
a) Shallow footing
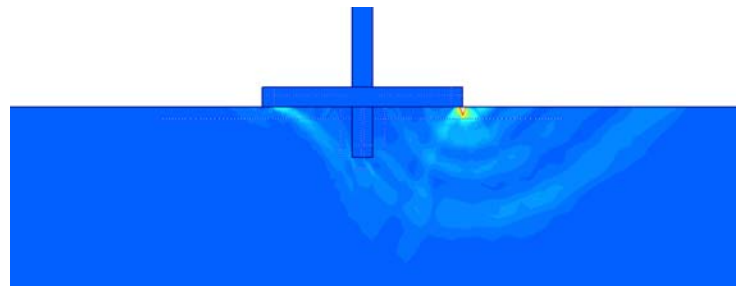
b) Hybrid system with L/W=0.25
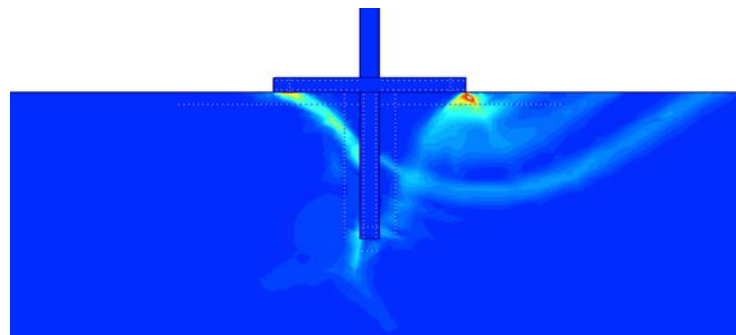
c) Hybrid system with L/W=1

Figure 3-30 Failure mechanisms under combined V-M loading at V/V$_{max}$ > 0.9, for: a) Shallow footing, b) Hybrid system with L/W=0.25 and c) Hybrid system with L/W=1

3.13 2D versus 3D Modeling of Monopiled-Footing Hybrid Systems

In practice, the proposed monopiled-footing hybrid foundation system is expected to be close to circular in plan. Whilst the simple 2-D plane strain problem presented an essential precursor to the understanding of the governing parameters affecting the behaviour of circular hybrid systems, an advanced 3D numerical study is required to verify the outcomes of the 2D parametric study.

3.13.1 3D Numerical Modeling

The 3D finite element study was carried out using PLAXIS 3D-Foundations V2.2 on three geometrical configurations, namely; a shallow footing (no pile) and two hybrid systems with L/W ratios of 0.5 and 1.0. In all 3D models, constant diameters of 5.0m and 0.5m were assigned to the footing and pile, respectively, whilst the L/W ratio was varied as required. The typical mesh used in the analysis is shown in Figure 3.24. The shallow footing was modeled by removing the embedded portion of the pile while retaining the footing.

The 3D finite element mesh was modeled using 15-node wedge elements. Each element consisted of a 6-node triangle in the horizontal direction and 8-node quadrilateral in the vertical direction. The location of the exterior mesh boundaries was chosen based on the results of a sensitivity analysis to ensure sufficient distance from the foundation in order to eliminate any possible boundary effects while maintaining reasonable calculation time. A typical mesh discretization used in the analysis is shown in Figure 3-32. Again, the model boundaries were simulated using the standard fixities in PLAXIS (constrained lateral displacements at the mesh sides and total fixity at the bottom).

To simplify the comparison between the results of the 3D models and those of the 2D study, soils and foundations were assigned the same material properties in both cases. Again, the soil was modeled as loose to compact sand using a non-associated Mohr-Coulomb constitutive model. The soil parameters used in the analysis are the same as presented in Table 3-1. Also, the foundation system (footing and pile) was modeled as

very stiff, linear elastic, non-porous material with Poisson's ratio, v of 0.15 and Young's modulus, E of 10^7 times the soil's elastic modulus. This condition ensured the full rigidity of the foundation in comparison to the surrounding soils.
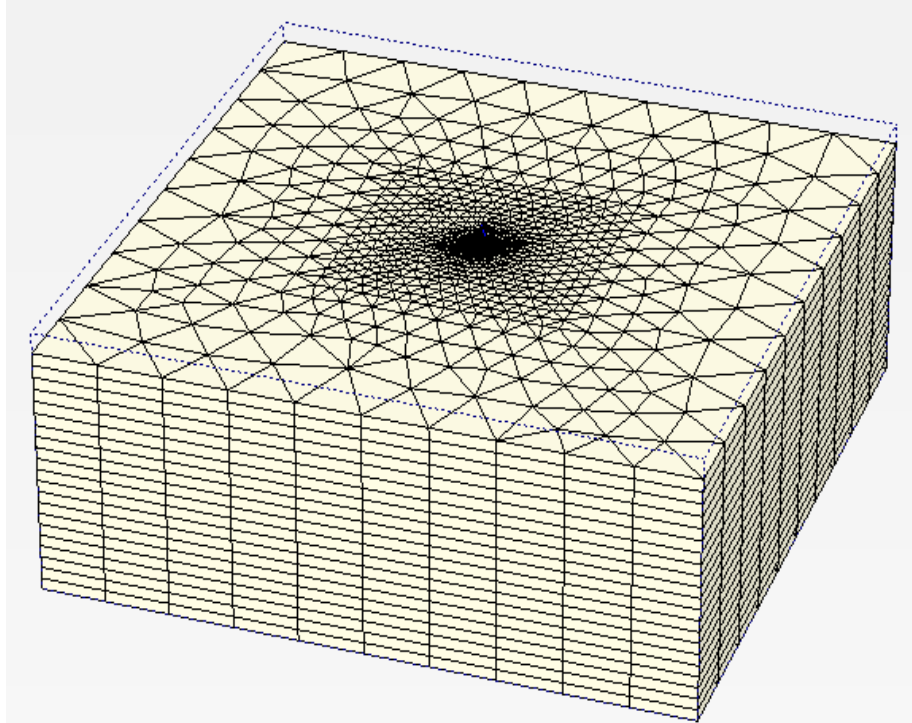
Figure 3-31 Typical mesh discretization applied in the finite element analysis

3.13.2 Load Paths

In the V-H loading space, load was applied in the form of a single inclined resultant applied at the load reference point previously described. This load resultant was gradually increased until the failure was reached and the V-load and H-load values at failure were plotted as a single point on the V-H failure envelope. The shape of the V-H failure envelope was identified by repeating this same loading procedure using different inclinations of the load resultants. The angle of inclination of the load resultants varied from 0.0 angle to the vertical axis (i.e. purely vertical load) to 90.0 degrees (i.e. purely lateral load).

 In the V-M loading space, load was applied in the form of a single vertical eccentric resultant. The load eccentricity $e = M/V$, was increased from 0.0 (for the case of purely

vertical loading) to 2.25. In each loading case, the vertical eccentric load was gradually increased until reaching failure and the vertical load and associated moment were plotted as a single point on the *V-M* failure envelope.

In the 3D numerical models, failure load was taken as the maximum load reached in the plot on the load - displacement curves.

3.13.3 Effect of the Geometry of the Hybrid System (*L/W* ratio) on the Lateral Load and Rocking Resistances

The plots of *V-H* and *V-M* failure envelopes displayed in Figure 3-32 and 3-33 and the normalized envelopes in Figure 3-34 and 3-35 confirm the previous findings of the 2D models in that the vertical capacity of the hybrid system is expected to fall below the sum of the resistances of its individual components (i.e. monopile and footing plate).

On the other hand, the normalized envelopes displayed in Figure 3-34 and 3-35 reveal an important observation. In a 2D plane strain condition, such as a shear key in a wall foundation, the presence of the shear key would have a significant effect on the lateral capacity of the system as a whole. In the 3D case such as the hybrid foundation, where the diameter of the pile is 1/10 the footing width; the action of the shallow foundation will dominate the behavior of the hybrid system especially in the case where a relatively short monopile (*L/W < 0.5*) is used.
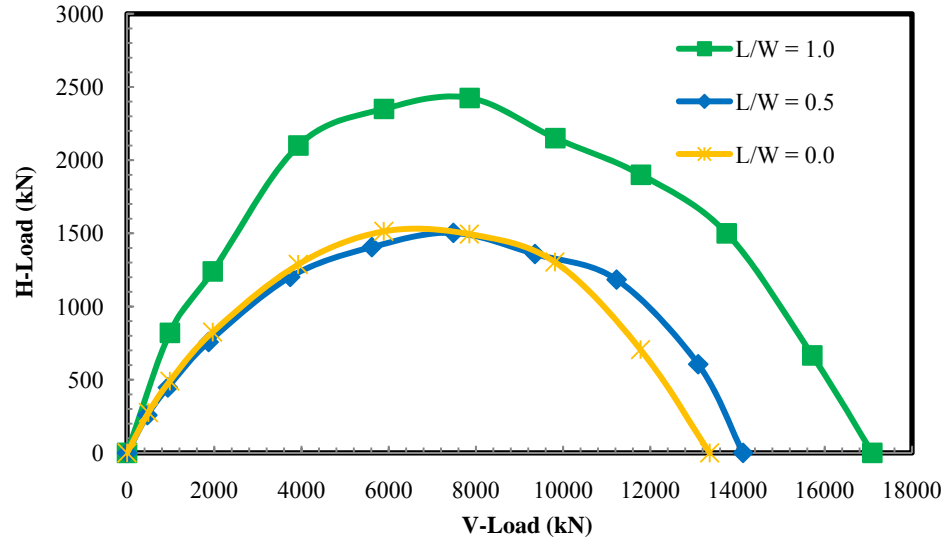
Figure 3-32 Effect of the L/W ratio on the shape of the V-H failure envelopes in undrained loading
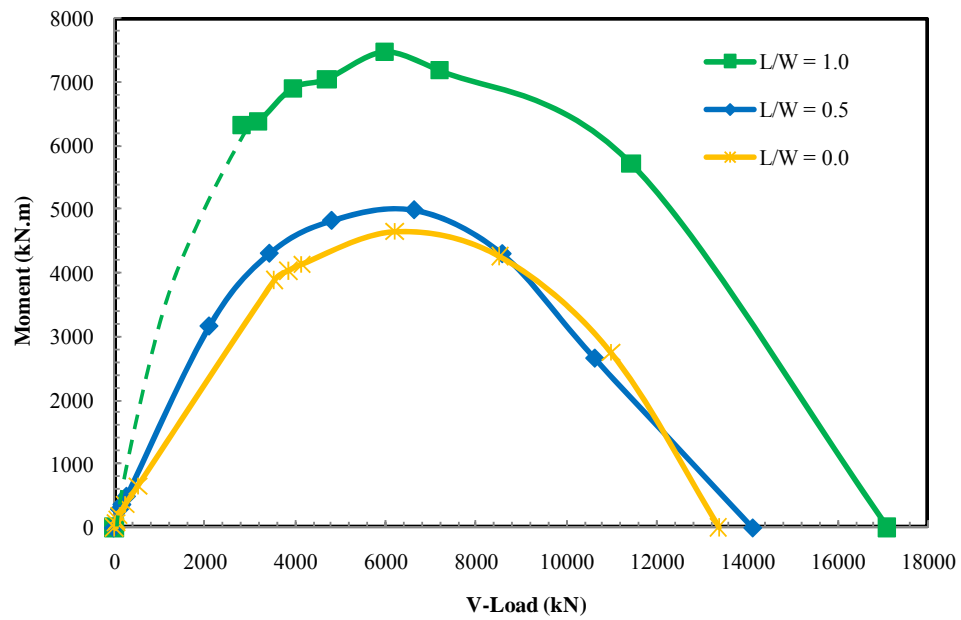
Figure 3-33 Effect of the L/W ratio on the shape of the V-M failure envelopes in drained loading
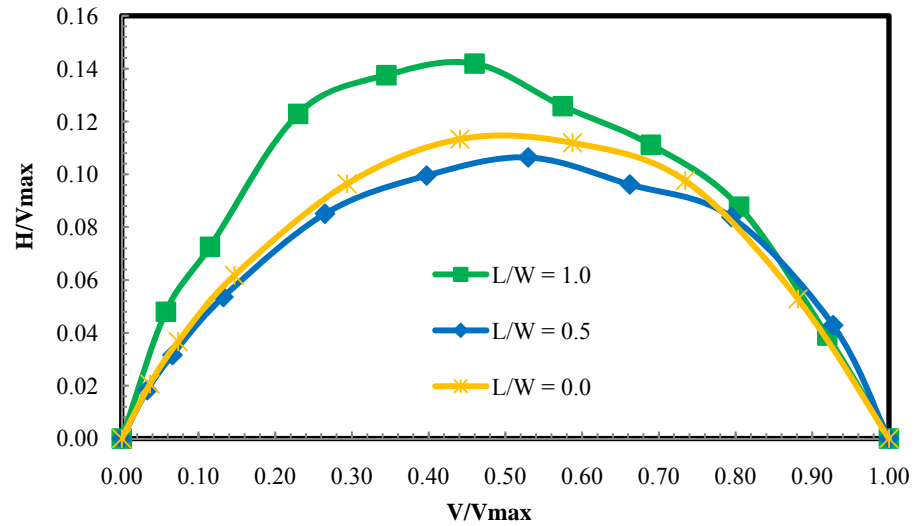
Figure 3-34 Effect of the L/W ratio on the shape of the normalized V-H failure envelopes in undrained loading
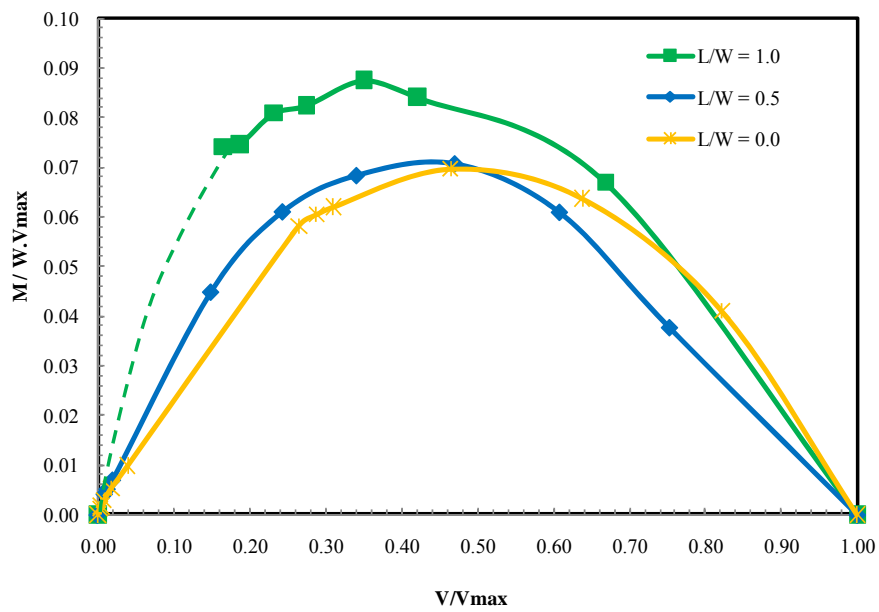
Figure 3-35 Effect of the L/W ratio on the shape of the normalized V-M failure envelopes in drained loading

3.13.4 Closed Form Expressions for the V-H Failure Envelopes

The curve fitting of the normalized *V-H* envelope of the circular footing analysed in the 3D study suggests that the same function proposed in Equation 3-5 to describe the envelope of the strip footing is still applicable for the 3D condition. A similar observation was reported by Gourvenec and Randolph (2003) found out that in the *V-H* plane, with *M* = 0, the shape of the failure envelope was essentially independent of the foundation geometry, or the degree of non-homogeneity. The constant β_1 obtained from the curve fitting was slightly increased to 0.47. Substituting this value into Equation 3-5 yields:

$$\frac{H}{V_{max}} = 0.47 \; \frac{V}{V_{max}} \left(1 - \frac{V}{V_{max}}\right) \qquad\qquad \text{(Circular footing, } L/W = 0.0) \text{ (3-21)}$$

The curve fitting for the normalized *V-H* envelope of the short hybrid foundation system (*L/W= 0.5*) supports the previous observation, which concluded that the action of the footing is expected to dominate the behavior of short hybrid systems. Equation 3-22 produced the best fitting curve for the normalized *V-H* envelope of the short system at a β_1 value of 0.43, as obtained from the curve fitting. This suggests that the presence of a short pile (*L/W < 0.5*) has a negligible effect on improving the lateral capacity of circular hybrid systems, as opposed to 2D plane strain conditions. Substituting this value into Equation 3-5 yields:

$$\frac{H}{V_{max}} = 0.43 \; \frac{V}{V_{max}} \left(1 - \frac{V}{V_{max}}\right) \qquad\qquad \text{(Hybrid System, } L/W = 0.5) \text{ (3-22)}$$

The normalized *V-H* envelopes plotted in Figure 3-34 show that for the relatively longer hybrid foundation system (*L/W = 1*), the normalized envelope has expanded with the peak shifted towards the left, which means that this hybrid system has a higher maximum lateral load capacity in addition to an improved initial capacity at low V-Load values. This follows the same trend observed for the 2D conditions. Not surprisingly, the curve fitting of the normalized *V-H* envelope of the hybrid system at *L/W=1* was better described using Equation 3-8, which was used in subsection 3.7 to describe the shape of the normalized *V-H* envelopes of the hybrid systems studied in the 2D plane strain

models. The curve fitting suggests a β_2 of 0.5, same as before, and a β_1 value of 0.28. Substituting into Equation 3-8 yields:

$$\frac{H}{V_{max}} = 0.28 \left(\frac{V}{V_{max}}\right)^{0.5} \left[1 - \left(\frac{V}{V_{max}}\right)^{1.5}\right]$$ (Hybrid System, $L/W = 1$)   (3-23)

The normalized V-H failure envelopes are plotted in Figure 3-35 along with the curves produced from Equations 3-21 to 3-23.
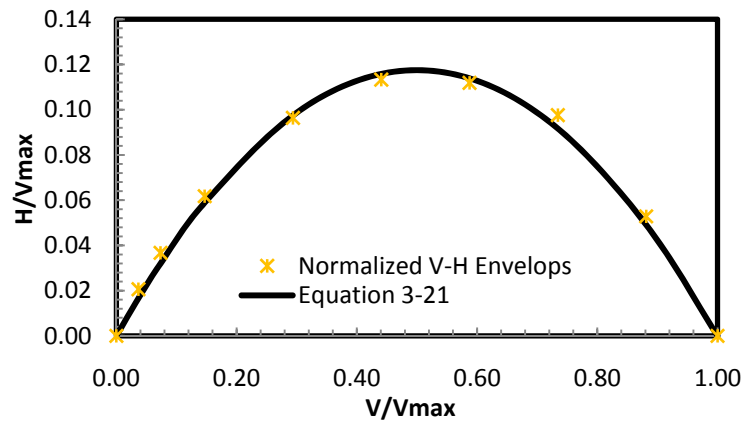
a) Shallow footing
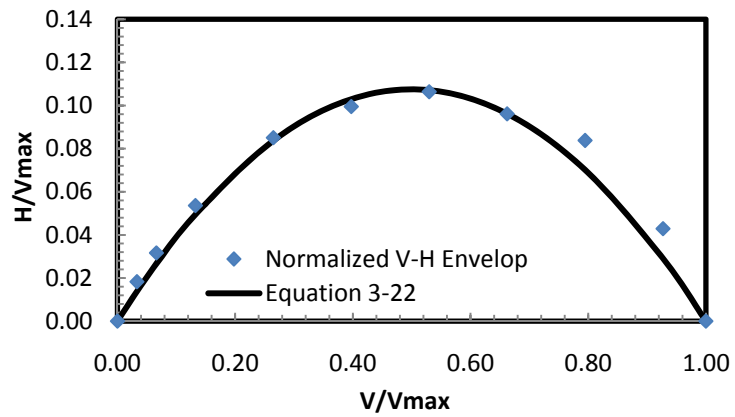
b) Hybrid system with L/W=0.5
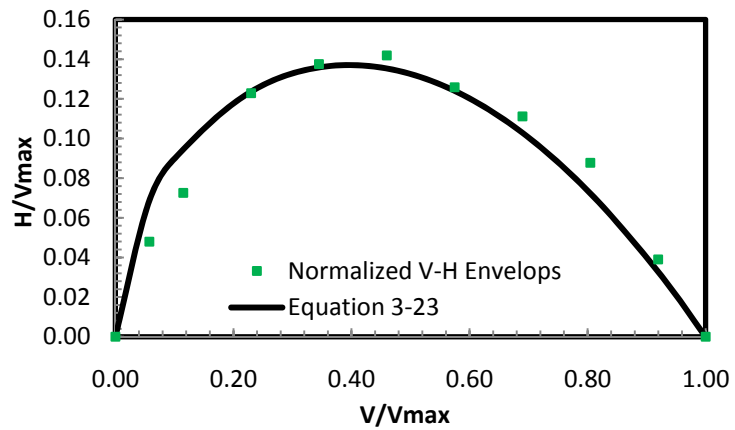
c) Hybrid system with L/W=1

Figure 3-36 Normalized V-H failure envelopes for: a) Shallow footing, b) Hybrid system with L/W=0.5 and c) Hybrid system with L/W=1

3.13.5 Closed Form Expressions for the V-M Failure Envelopes

The curve fittings of the normalized *V-M* envelopes of the 3D circular foundations produced functions of the same form as Equation 3-17, which has been previously proposed to describe the normalized *V-M* envelopes of the 2D plane strain models.

The parameter β_1 obtained from the curve fitting of the normalized *V-M* envelope of the circular footing was slightly reduced 0.457, as opposed to 0.53 for the strip footing (Equation 3-16). No changes occurred to either β_2 or β_3. Substituting these values into Equation 3-17 yields:

$$\frac{M}{W.V_{max}} = 0.457 \; \frac{V}{V_{max}} \left[1 - \left(\frac{V}{V_{max}} \right)^{0.5} \right] \qquad \text{(Circular footing, } L/W = 0.0) \; (3\text{-}24)$$

The curve fitting of the normalized V-M envelope of the short hybrid foundation system ($L/W = 0.5$) suggests a minor change in β_1, which has slightly increased to 0.478 compared to 0.457 for the circular footing (Equation 3-25 below).

$$\frac{M}{W.V_{max}} = 0.478 \; \frac{V}{V_{max}} \left[1 - \left(\frac{V}{V_{max}} \right)^{0.5} \right] \qquad \text{(Hybrid System, } L/W = 0.5) \; (3\text{-}25)$$

This observation proves that the presence of a short pile ($L/W < 0.5$) has a minor effect on improving the rocking resistance of circular hybrid systems. The same behaviour was observed for the normalized *V-M* envelope of the 2D model and was previously discussed in sub-section 3.8. On the other hand, the 2D envelopes showed that even a short hybrid system possessed a superior initial rocking resistance at low V/V_{max} values, as opposed to the strip footings. As discussed in the previous sub-sections, this behaviour is not present in a 3D condition, where the action of the footing dominates the behavior of short circular hybrid systems.

The normalized *V-M* envelopes plotted in Figure 3-35 show that for the relatively longer hybrid foundation system ($L/W = 1$), the normalized envelops has expanded and the peak value was shifted towards the left, which means that this hybrid system possess a higher maximum rocking resistance and an improved resistance at low V/V_{max} values. This

follows the same trend observed for the 2D conditions. The curve fitting of the normalized *V-M* envelope of the hybrid system at *L/W*=1 suggests a function similar to Equation 3-20, with a β_1 value of 0.186 as opposed to 0.217 for the 2D condition. Substituting in Equation 3-17 yields,

$$\frac{M}{W.V_{max}} = 0.186 \left(\frac{V}{V_{max}}\right)^{0.5} \left[1 - \left(\frac{V}{V_{max}}\right)^{1.5}\right] \qquad \text{(Hybrid System, } L/W\text{=1)} \qquad \text{(3-26)}$$

A good agreement was generally observed when comparing the results of the 3D models (circular hybrid systems) to the 2D models of the strip foundation mounted on a continuous wall/key. There was a noticeable effect of increasing the pile length (increasing *L/W* ratio) on expanding the failure envelopes and increasing the maximum lateral and rocking capacities of the hybrid system, except for the case of short hybrid system (*L/W*< 0.5). In this case, the behavior of the hybrid system is dominated by the footing behavior and the presence of the pile has a minor effect on the load resistance.

3.14 Conclusions

The study investigated a novel hybrid monpile-footing foundation system. The behavior of the hybrid system under general planar load combinations has been characterized through an extensive program of numerical modeling.

The finite element modeling showed that the vertical capacity of the hybrid system is highly dependent on the pile length - to - footing width (*L/W*) ratio. For a hybrid system with a very short pile (*L/W*= 0.25), the presence of the pile slightly reduces the vertical capacity of the hybrid system compared to that of the shallow footing, due to the formation of an overstressed zone below the short pile that produces a form of progressive failure, which eliminates the propagation of the complete failure mechanism below the footing. In general, for a hybrid system provided with a relatively short pile (as proposed in this study for practical considerations), the vertical capacity of the hybrid system will always fall below the sum of the capacities of its structural constituents (footing and pile).

The study revealed that the presence of even a short central shear key below a wall footing (at L/W = 0.25) can improve the maximum lateral load resistance of the foundation system by 27%, in addition to improving the capacity at low V-load ratios. However, this would slightly reduce the rocking resistance. This finding is very useful when constructing a laterally loaded foundation on weak bearing soil, where it becomes essential to reduce the vertical loads applied to the soil especially when sliding resistance is the governing factor in the foundation design. The interaction between the individual components of the hybrid system generates a higher lateral load resistance, greater than summing the resistance of the constituent elements. The lateral load resistance of the hybrid system appears to rely on the initial vertical load acting on the hybrid system, the mobilized frictional strength at the interface and the pile length - to - footing width (L/W) ratio. The effect of the footing width to pile diameter ratio (W/D) is less significant. On the other hand, the presence of a short pile in a circular hybrid system has a negligible effect on the load resistance of the hybrid system as a whole, since the behavior of the system will be exclusively dominated by the footing action.

In 2D plane strain loading conditions, a hybrid foundation system with L/W = 0.5 possesses a maximum lateral load resistance, H_{max} = (0.22 - 0.23) V_{max} occurring at V/V_{max} = 0.4, which is about twice the resistance of a strip footing with the same vertical load capacity. Moreover, the hybrid system generates an initial lateral resistance of 0.08 V_{max} at a very low vertical loading ratio, while the strip footing has zero resistance. At L/W = 1.0, the lateral capacity was tripled. For a circular hybrid system, it may be necessary to increase the minimum pile length-to-footing width ratio to 1.0. This provides 34% increase in the lateral resistance.

34% gain in the rocking resistance was achieved when the pile/key length was equal to the footing width (L/W = 1). At L/W = 0.5 the hybrid system had a maximum rocking resistance falling slightly below the shallow footing (2D loading condition). However, the system gained a superior initial rocking resistance at low V/V_{max} values. This initial rocking resistance is not expected for a circular hybrid system of this same L/W ratio, where the action of the footing dominates the behavior of short circular hybrid systems.

The shape and size of the normalized *V-H* and *V-M* failure envelopes are independent of the dilation angle. This means that there should be a unique normalized *V-H-M* failure surface with no regard to the adopted angle of dilation.

In a 3D situation, the action of the footing is expected to dominate the behavior of short hybrid systems (*L/W* < 0.5). This suggests that the presence of a short pile has a negligible effect on improving the lateral capacity of circular hybrid systems, as opposed to the 2D plane strain condition, where the presence of the shear key in a wall foundation can dramatically improve the lateral capacity of the system as a whole. On the other hand, for a relatively longer hybrid foundation system (*L/W* = 1), the *V-H* and *V-M* failure envelopes start to expand and the peak moves towards the left, which means that the hybrid system possesses a higher maximum lateral load capacity and an improved initial capacity at low *V*-Load values. This follows the same trend observed for the 2D conditions.

3.15 References

Bienen, B., Byrne, B. W., Houlsby, G. T. & Cassidy, M. J. (2006). Investigating six-degree-of-freedom loading of shallow foundations on sand. Geotechnique, 56 (6): 367-379.

Bransby, M. F. and Randolph, M. F. (1998). Combined loading of skirted foundations. Geotechnique, 48 (5): 637-655.

Brinkgreve, R.B.J. (2002). PLAXIS user's manual - Version 8.2. Delft University of Technology and PLAXIS b.v., The Netherlands. ISBN 9058095088.

Butterfield, R., Houlsby, G. T. and Gottardi, G. (1997). Standardized sign conventions and notation for generally loaded foundations. Geotechnique, 47(5): 1051-1054.

Byrne, B.W. and Houlsby, G.T. (2002). Investigating novel foundations for offshore wind turbines. *In* proceedings of the 21st International Conference on Offshore Mechanics and Arctic Engineering (OMAE'02), Oslo, Norway, Paper No. OMAE2002-28423.

Byrne, B.W. and Houlsby, G.T. (2003). Foundations for offshore wind turbines. *In* proceedings of the Philosophical Transactions of the Royal Society of London, Series A, 361, pp. 2909-2930.

Frydman, S. and Burd, H.J. (1997). Numerical studies of bearing capacity factor Nγ. Journal of Geotechnical and Geoenvironmental Engineering, ASCE, 123(1): 20-29.

Georgiadis, M., and Butterfield, R. (1988). Displacements of footings on sand under eccentric and inclined loads. Canadian Geotechnical Journal. 25(2): 199-212.

Gottardi, G., and Butterfield, R. (1993). On the bearing capacity of surface footings on sand under general planar load. Soils and Foundations. 33(3): 68-79.

Gottardi, G., Houlsby, G. T. & Butterfield, R. (1999). Plastic response of circular footings on sand under general planar loading, Geotechnique, 49(4): 453-469.

Gourvenec, S. and Randolph, M. F. (2003). Effect of strength nonhomogeneity on the shape and failure envelopes for combined loading of strip and circular foundations on clay. Geotechnique, 53(6): 575-586.

Hansen, J. B. (1970). A Revised and Extended Formula for Bearing Capacity. Available from the Danish Geotechnical Institute, Copenhagen, Bul. No. 28, 21 pp. (successor to Bul. No. 11).

Horvath, J.S. (1991), Effect of footing shape on behaviour of cantilever retaining wall. Journal of Geotechnical Engineering, 117(6): 973-978.

Houlsby, G. T. & Puzrin, A. M. (1999). The closed-form solutions for the bearing capacity of strip footing under combined loadings. *In* Proceedings of the Royal Society Conference, London, UK, pp. 893-916.

Loukidis, D., Chakraborty T., and Salgado R. (2008), Bearing capacity of strip footings on purely frictional soil under eccentric and inclined loads. Canadian Geotechnical Journal, 45(2): 768-787.

Martin, C.M. and Houlsby, G.T. (2000). Combined loading of spudcan foundations on clay: laboratory tests. Geotechnique, 50(4): 325-338.

Martin, C.M. and Houlsby, G.T. (2001). Combined loading of spudcan foundations on clay: numerical modelling. Geotechnique, 51(8): 687-699.

Stone, K., Newson, T. and Sandon, J. (2007). An Investigation of the Performance of a 'Hybrid' Monopile-Footing Foundation for Offshore Structures. *In* Proceedings of the 6th International Offshore Site Investigation and Geotechnics Conference, London, UK, 391-396.

Tan, F. S. C. (1990). Centrifuge and theoretical modelling of conical footings on sand. Ph.D. thesis, University of Cambridge, London, UK.

Vesic, A. S. (1975). Bearing capacity of shallow foundations, Chapter 3. *In* Foundation Engineering Handbook. *Edited by* H. F. Winterkorn and H.-Y. Fang. Van Nostrand Reinhold Co., New York, N.Y., U.S.A., pp. 121-147.

White, D. J., Teh, K. L., Leung, C. F. & Chow, Y. K. (2008). A comparison of the bearing capacity of flat and conical circular foundations on sand. Geotechnique, 58(10): 781-792.

Zaaijer, M.B. (2003). Comparison of monopile, tripod, suction bucket and gravity base design for a 6 MW turbine. *In* Proceedings of the European Seminar on Offshore Wind energy in Mediterranean and Other European Seas, OWEMES-2003, Naples, Italy.

Chapter 4

4 Numerical Investigation of Hybrid Monopile-Footing Foundation Systems under Undrained Loading Conditions

The bearing capacity of shallow foundations under combined loading has always been a problem of considerable importance, yet exact closed form solutions remain elusive (Houlsby and Puzrin, 1999). Laterally loaded structures, such as wind turbines, earth-retaining structures, bridge abutments and offshore structures impose complex loading regimes on their foundations. These foundations are typically subjected to a combination of vertical, horizontal and moment loadings as a result of the vertical self-weight of the foundation system, superstructure, soil fill and surface surcharge, in addition to lateral loads and moments due to horizontal soil pressures. Particularly in the offshore oil and gas industry, and recently in the renewable wind energy field, foundation design becomes more complex due to the added loads from the wind, waves and currents. Moreover, for clay soils, large loads applied on offshore foundations and the drainage characteristics of fine grained seabed soils (e.g.: permeability of soil, length of the drainage path, characteristic drainage time, etc...) require suitable design and construction approaches for such foundation systems.

The proper selection of a suitable foundation system is an important factor in the economic viability of a design, which depends on the nature of the applied loads, in addition to specific soil characteristics. Shallow foundations would represent the most economical solution in the case of relatively small loads and firm supporting soils, especially when the foundation level is above the ground water table. The weight and dimensions of the foundation must be sufficient to resist tilting and sliding, while at the same time preventing the failure of the subsoil and satisfying the serviceability conditions. These criteria are generally achieved by properly sizing the width and thickness of the shallow foundation. However, for large loads and/or low bearing capacity, it is essential to use large and thick footings, which can be a major construction challenge especially in locations with limited access. Additionally, for offshore

foundations, the presence of large gravity bases has a large influence on the currents and the movement of surrounding water, which can generate significant heave forces (Zaaijer, 2003).

Several studies have examined the response of shallow footings on clay soils under complex *V-H-M* load combinations considering various analytical approaches (e.g. Bransby and Randolph, 1998; Houlsby and Puzrin, 1999; Gourvenec and Randolph, 2003). Ukritchon *et al.,* (1998) developed upper and lower bound solutions to evaluate the undrained stability of surface strip footings on clay deposits under the effects of vertical, horizontal, and moment loading. Their study revealed that the existing empirical bearing capacity factors for inclined, eccentric loading (e.g. Meyerhof, 1953; Hansen, 1970; Vesic, 1975) are conservative and often underestimate the exact collapse loads for footings on homogeneous clay by more than 20%. In particular, the work conducted by Gourvenec and Randolph (2003) examined the influence of undrained soil strength heterogeneity on the shape of the *V-H-M* failure envelope of surface strip and circular footings fully bonded to an underlying bed of a Tresca soil. Subsequently, Gourvenec extended her work to cover the behavior of rectangular footings (Gourvenec, 2007) and embedded footings (Gourvenec, 2008) under general loading. Martin and Houlsby (2000) conducted a series of laboratory tests on spudcan foundations on clay under general planar loadings, and Martin and Houlsby (2001) extended their work to cover a full numerical analysis for the same problem. Further studies have investigated support structures for offshore wind turbines (e.g.: Byrne and Houlsby, 2002 and 2003; Stone *et al.*, 2007, 2010a and 2010b). Recent numerical modeling by Gourvenec and Randolph (2003) developed design aids for circular footings under combined loading. Horvath (1991) also discussed the effect of shear keys on the resistance of shallow footings to sliding.

In this thesis, a new technique is proposed to improve the lateral capacity of shallow footings bearing on clays by providing them with a central short monopile to create a 'hybrid' monopiled-footing arrangement.

4.1 Objectives and Scope of Work

The geometry and assumed loading state for the proposed innovative foundation system are shown in Figure 4-1, where a single central pile is employed. The pile diameter and length are (D) and (L) respectively, and the footing width is (W). The objectives of this study are twofold: to examine the undrained behavior of this foundation system under various combinations of vertical, horizontal and moment (V-H-M) loading; and to generate detailed information about the failure envelopes in the three-dimensional (V-H-M) load space.
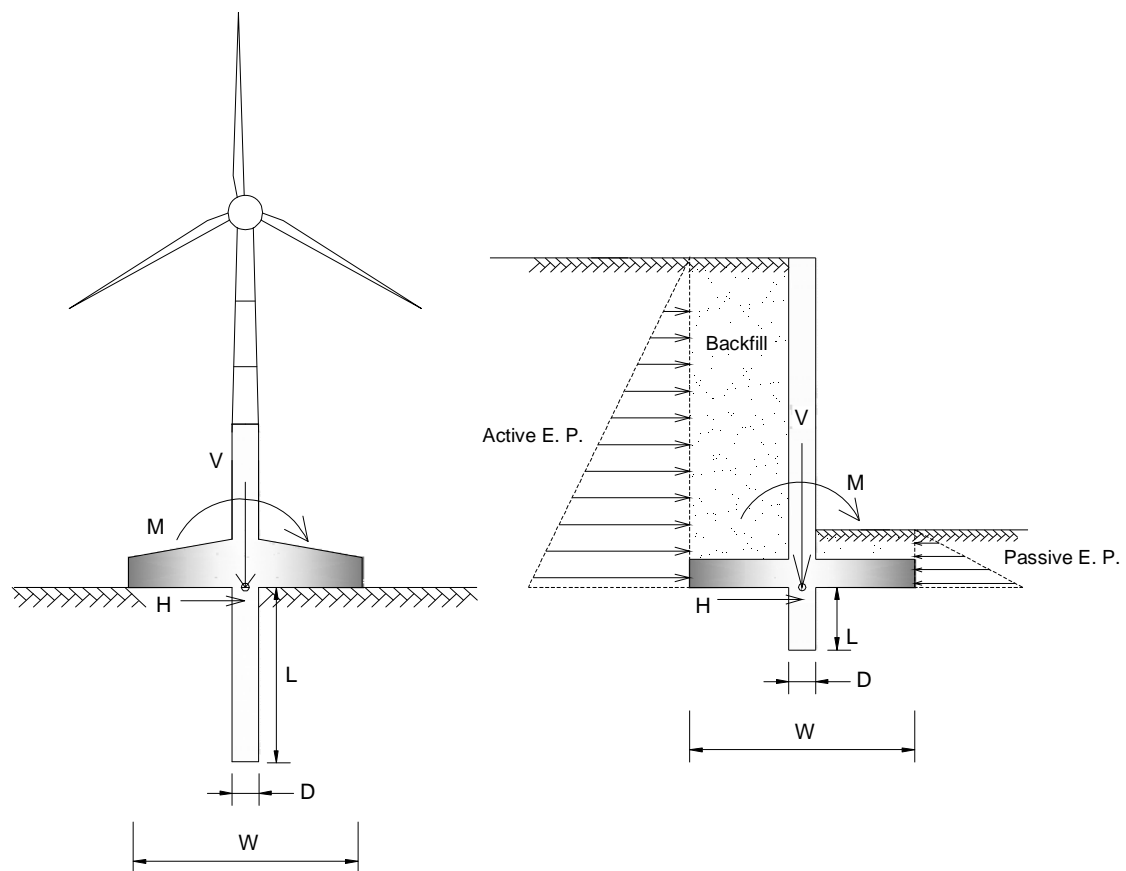
Figure 4-1 Examples of laterally loaded structures supported on the proposed hybrid system

An extensive numerical modeling investigation using the finite element program PLAXIS has been conducted to study the behavior of the system under various combinations of vertical, horizontal and moment (V-H-M) loading. In the finite element models, the width

of the footing and the diameter of the pile are kept constant with values of 5.0 and 0.5 m, respectively, while the pile length to footing width ratio is increased from 0 to 1.0. The results from the parametric study are used to understand the failure mechanisms and to generate information regarding the failure envelopes in the three-dimensional (*V-H-M*) load space.

4.2 Numerical Modeling

An extensive finite element investigation was performed using the finite element code PLAXIS V8 (Brinkgreve, 2002). The objective of this numerical modeling study was to better understand the role of the individual components of the hybrid system and consequently provide guidance towards choosing their optimum dimensions. The analysis of the numerical modeling results have provided the basis for developing the relationships between the acting vertical loads and the allowable horizontal and moment loads in the form of *V-H* and *V-M* failure envelopes. Consequently, the ultimate bearing capacity of the hybrid system under general combinations of *V-H-M* loadings may be established.

Given the substantial amount of computing involved in numerical modeling of such complex foundation problem, it was necessary to initiate the analysis considering the simple 2-D plane strain problem of a long, rigid strip footing resting on a continuous rigid wall. The insights gained from this analysis can then be extended to the more general and realistic 3D problem representing the envisioned hybrid system being composed of a circular footing with a central pile shaft using optimized scope of 3D numerical modeling. Hence, the majority of the numerical models used in this study deliberately represent a simple 2-D plane strain problem, but still capture the main features required to understand the characteristics of the new hybrid system, followed by limited 3D models designed to discern the features of the 3D behavior.

4.3 2D Finite Element Model

All structural elements and soils are modeled in this study using unstructured meshes with 15-noded plane strain triangular elements with 12 Gaussian points. The hybrid

structural system material is modeled as a very stiff, linear elastic, non-porous material with unit weight, $\gamma = 25$ kN/m^3, modulus of elasticity, $E = 10^7$ times the soil elastic modulus, and Poisson's ratio, $v = 0.15$. The soil bed has been modeled as a homogeneous bed of clay simulated by a Mohr-Coulomb, elastic-perfectly plastic constitutive model. The soil parameters used in the analysis are summarized in Table 4-1 below.

Table 4-1 Undrained Properties, Mohr-Coulomb model

Properties	Value	Unit
Saturated Unit Weight	18	kN/m^3
Young's Modulus, E	12500	kN/m^2
Poisson's Ratio, v	0.49	N/A
Cohesion Stress, c	25	kN/m^2
Friction Angle, ϕ	0.0	Degree
Material Model	Mohr-Coulomb	N/A

The typical mesh discretization used in the analysis is shown in Figure 4-2. The model exterior boundaries are simulated using standard fixities in PLAXIS, which are imposed to constrain the lateral displacements at the mesh sides and imply total fixity at the bottom.
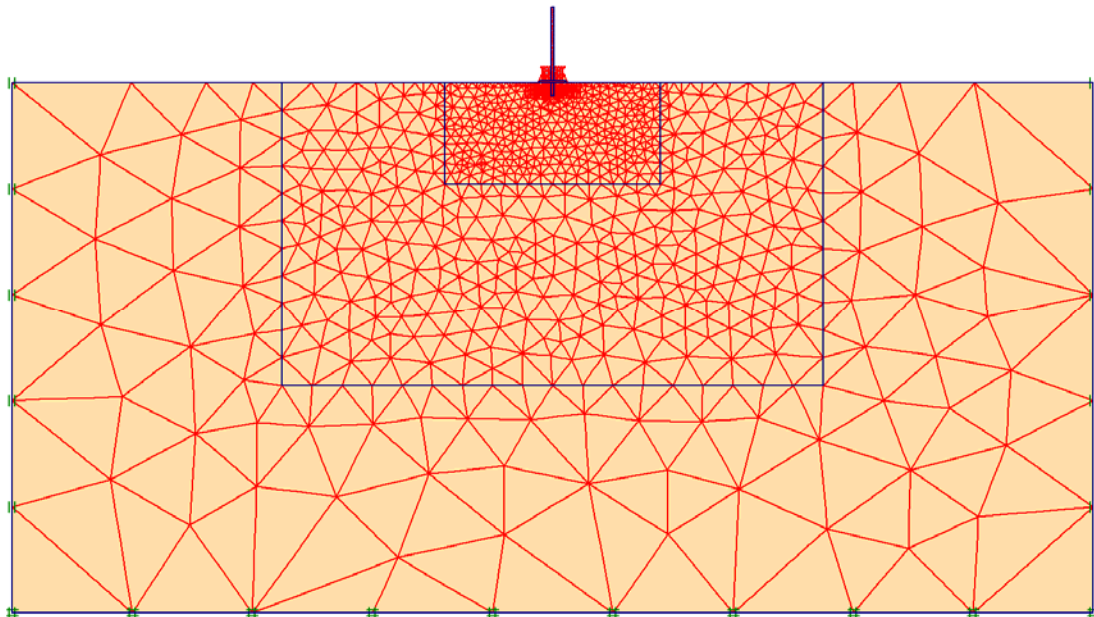
Figure 4-2 Mesh discretization applied in the finite element analysis

The location of the outer mesh boundaries was chosen to provide a sufficient distance from the foundation to eliminate any possible boundary effects, especially during the early stages of loading, before the onset of strain localizations associated with failure conditions. During the analysis, variable mesh density is employed to achieve acceptable accuracy while maintaining the computational efficiency of the solution. As shown in Figure 4-2, local refinements are assigned to areas where large stress concentrations or large deformation gradients are expected. These include the anticipated location of failure planes underneath and surrounding the strip footing and the continuous wall.

Frydman and Burd (1997) noted that a zone of high stress gradients develops at the singularity points at the foundation edges, which may impact the convergence of the solution and represents a challenging problem. Below the footing, the major principal stress acts vertically in the case of the smooth footing and at a variable inclination to the vertical in the rough footing case. However, the vertical stress at the soil surface just outside the footing edge is zero and thus the shear strength of the sand, and all other stresses, are zero. Close to the soil surface, the major principal stress acts horizontally. This abrupt transformation in the principal directions at the edge of the footing creates computational difficulties. This problem was addressed by using 10-noded interface elements that extend a little farther than the footing edges together with a concentration of small elements in the region of the footing edge (Frydman and Burd, 1997). In general, PLAXIS Reference Manual recommends extending the interface around the corners to allow sufficient freedom of deformation and to obtain more accurate stress distribution. Furthermore, the interface helped in modeling the interaction between the hybrid system and the soil. A rough interface (R_{inter} = 1.0) is used in the models. This factor relates the interface strength to the soil strength ($c'_{inter} = R_{inter} \times c'$ and $\tan \phi'_{inter} = R_{inter} \times \tan \phi'$).

4.3.1   Sign Convention and Notations

In this study, the sign convention for displacements and loads proposed by Butterfield *et al.*, (1997) demonstrated in Figure 4-1 is followed. The position of the reference point for loads and moments, which is positioned at the middle of the foundation at the ground level, is also shown in the same figure.

V_{max}, M_{max} and H_{max} represent the vertical ultimate bearing capacity, the horizontal ultimate bearing capacity, and the ultimate moment capacity, respectively. A complete list of symbols and annotations is displayed in Table 4-2.

Table 4-2 List of symbols and annotations

Parameter	Vertical	Horizontal	Moment
Load	V	H	M
Ultimate Load	V_{max}	H_{max}	M_{max}
Dimensionless Load	$v = V/A.S_u$	$h = H/A.S_u$	$m = M/A.W.S_u$
Dimensionless Ultimate Load	$v_o = V_{max}/A.S_u$	$h_o = H_{max}/A.S_u$	$m_o = M_{max}/A.W.S_u$
Normalized Load	v/v_o	h/h_o	m/m_o

4.3.2   Load Paths

For laterally loaded structures mounted on a shallow foundation, a piled foundation or the proposed hybrid system, the vertical loading on the foundation is nearly constant over the entire environmental loading period and is equal to the combined weights of the subsurface structure, in addition to the self-weight of the foundation system and any soil surcharge. On the other hand, the lateral loads may vary depending on their source, whether it is due to soil pressures only or combined with loads imposed by wind, waves, and currents. The presence of a lateral loading component that acts at a certain distance above the foundation level typically adds a complex combination of lateral load accompanied by a moment component to the vertical weights. In most cases, the load combination will occur in one plane of *V-H-M* space with a fixed ratio of *V/Vmax*. In this situation, both the horizontal and moment load components acting on the foundation will act in the same direction, so that this quadrant of the yield locus will be most critical for the foundation design.

The numerical investigation used displacement-controlled swipe tests to produce the *V-H* or *V-M* failure envelopes. Tan (1990) introduced the swipe test, and it was consequently used by many researchers (e.g. Bransby and Randolph, 1998; Gourvenec & Randolph, 2003; Bienen *et al*. 2006). In theory, a single swipe test would be sufficient to determine

a complete failure envelope in any two-dimensional loading plane. The swipe test typically consists of two loading stages. In the first stage, a prescribed displacement (typically vertical) is applied to the foundation until reaching the ultimate vertical load bearing capacity. Subsequently, the footing is swiped laterally (or rotated) while the vertical displacement is constant. The measured loads during the second phase generate a load path falling slightly within the true failure envelope, as reported by Gourvenec and Randolph (2003).

4.4 Effect of the Geometry of the Hybrid System on Loading Resistances

Preliminary studies by the author have indicated that the foundation width-to-pile diameter ratio (W/D) has an insignificant effect on the resistance of the hybrid system, since the additional capacity gained by increasing the wall thickness is counteracted by the reduction in the rotational constraints at the pile head in addition to the added weight. Hence this study has ignored the effect of W/D ratio. On the other hand, the effects of wall length-to-footing width ratio (L/W) on the pure vertical, lateral and rotational resistances were studied through series of displacement controlled tests. All of the geometries of the hybrid system had a constant normalized wall thickness ratio (W/D=10), and a range of L/W ratios varying from 0 to 1.

During the analysis, two different series of tests were examined. The first series assumed a fully bonded foundation-soil interface, where the soil at the interface can resist large tensile stresses. This assumption allows a reverse bearing capacity phenomenon to occur due to suction or negative pore water pressures generated during the undrained loading. The second series assumed an instant breakaway condition at the foundation-soil interface. This second series made use of the feature implemented in PLAXIS 2D to assign "zero tension cut-off" to the soil, which simply means that the soil have a zero resistance to tension.

4.4.1   Resistance to Vertical Loading

When the hybrid system is loaded vertically and the system settles, the pile starts to mobilize skin friction over its shaft. As the applied pressure increases, a failure zone is initialized at the edges of the footing and gradually extends downward and outward; similar behavior takes place below the pile toe.

Previous studies by Stone *et al.,* (2007) proposed that the vertical capacity of the hybrid system can be taken as the sum of the capacities of its individual components (pile and footing). This assumption may be acceptable in the case of long and slender pile connected to a relatively small footing (*L/W* ratio = 3 or more), where the resistance of the pile is dominating the behavior of the hybrid system. On the other hand, in the case of short piles or a continuous wall connected to a wide footing, the vertical capacity of the system is expected to fall below the sum of the resistances of the individual components of the system (Figure 4-3). This occurs because the stressed soil zones beneath the foundation tend to overlap, eliminating the development of the full capacity of the individual structural elements of the hybrid system.
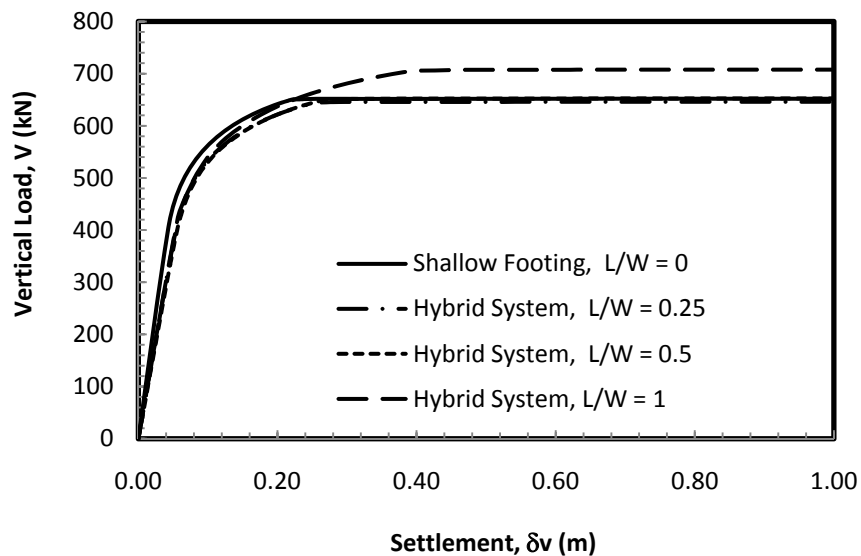

**Figure 4-3 Plot of vertical load (V) versus vertical displacement (δv)**

At failure, the rupture planes beneath the footing can be separated into three main zones; 1) a triangular elastic zone right underneath the footing; 2) a radial shear zone; and 3) a triangular passive resistance zone as shown in Figure 4-4a. For a hybrid system ($W/D=$ 10) with a short pile, the pile shaft would be fully embedded in the elastic soil zone developed right below the footing as can be noted from Figure 4-4b and c. For a hybrid system with a medium length pile, the majority of the pile shaft falls within the elastic soil zone as shown in Figure 4-4d. In this moving soil wedge, neither significant bearing pressure nor shaft friction could be mobilized. It can be concluded that for a hybrid system provided with a short pile, the vertical capacity of the hybrid system will always fall below the sum of the capacities of its structural elements (footing and pile) as shown in Figure 4-4d.

As a first order approximation, the vertical capacity of the hybrid system may be taken as the sum of 3 components: 1) the bearing load of the footing, which is calculated using the theoretical bearing capacity equations; 2) the end bearing of the pile (only if $L/W > 0.5$); and 3) the skin friction produced along the section of the pile shaft that extends outside the failure zones of the footing. The third term may be neglected with a low margin of error (for $L/W \leq 1$);. Another demonstration of the failure mechanisms due to vertical loading is displayed in Figure 4-5. From both figures, we can observe how the side angle of the triangular elastic soil wedge beneath the footing, which should be equal to 45° for a shallow footing on clayey soil, increases or decreases depending on the length of the central monopile. Accordingly, the size of the mobilized failure mechanism and thus the vertical load resistance are changed.

The V-load versus displacement curves plotted in Figure 4-3 show that the presence of the short pile does not affect the vertical stiffness of the hybrid system at the studied L/W ratios. Also the plots of the maximum vertical capacity versus the L/W ratio of the hybrid system in Figure 4-6a underscore the previous contention that the maximum vertical load resistance of the hybrid system is not affected by the presence of a short pile ($L/W \leq 0.5$). A minor gain in the vertical capacity of about 10% was only achievable at $L/W = 1$. The curves also demonstrate that the condition assigned to the foundation-soil interface (fully bonded vs. instant breakaway), has a minimal effect on the vertical capacity.
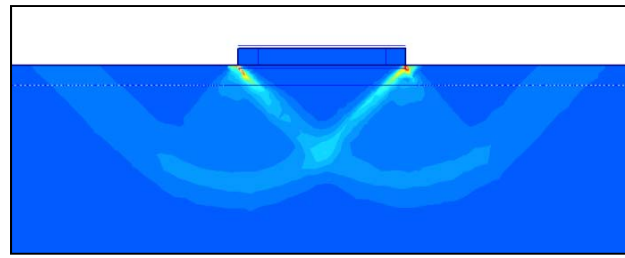
a) Shallow footing, L/W = 0
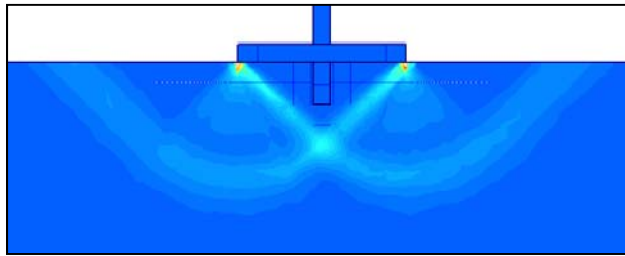
b) Hybrid system with L/W = 0.25
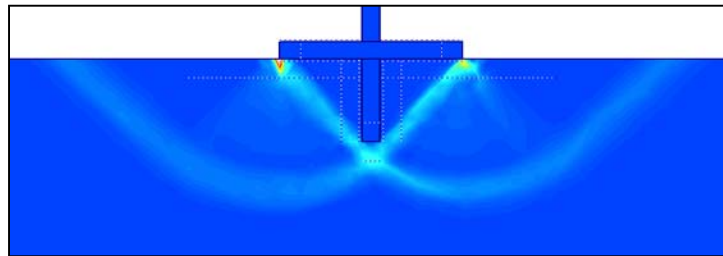
c) Hybrid system with L/W = 0.5
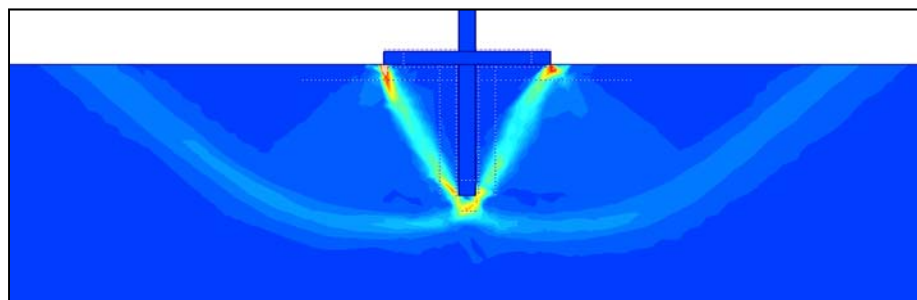
d) Hybrid system with L/W = 1

Figure 4-4 failure mechanisms, a) Shallow footing, b) Hybrid system with L/W=0.25, c) Hybrid system with L/W=0.5 and d) Hybrid system with L/W=1
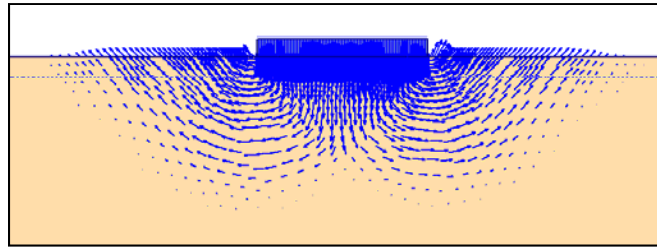
a) Shallow footing, L/W = 0
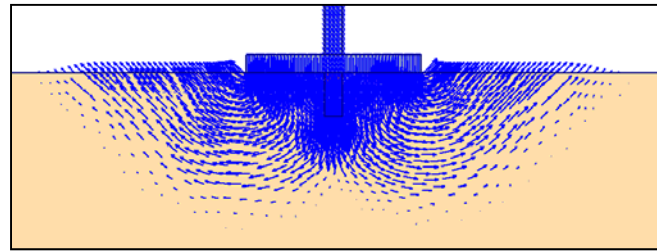
b) Hybrid system with L/W = 0.25
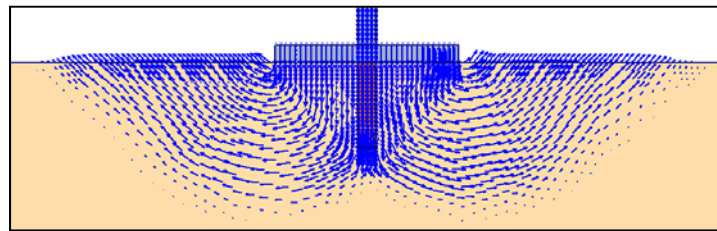
c) Hybrid system with L/W = 0.5
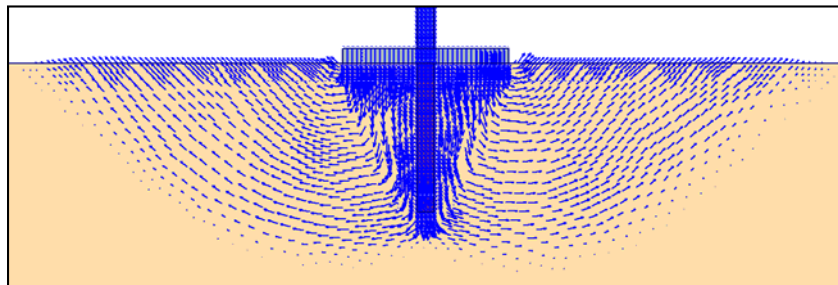
d) Hybrid system with L/W = 1

Figure 4-5 Displacement vectors at failure for: a) Shallow footing, b) Hybrid system with L/W=0.25, c) Hybrid system with L/W=0.5 and d) Hybrid system with L/W=1

4.4.2   Resistance to Lateral Loading

Gaining from the formation of passive soil wedges in front of the pile, the maximum lateral load capacity of the hybrid system seems to be highly dependent on: (1) the geometry of the hybrid system (L/W ratio) and (2) the conditions assigned to the foundation soil interface. Figure 4-6b demonstrates the significant influence of increasing the pile length on the increased maximum lateral load capacity of the hybrid system.

4.4.3   Resistance to Moment Loading

The rocking resistance of the hybrid system shows a dependency on: (1) the geometry of the hybrid system (L/W ratio) and (2) the condition assigned to the foundation soil interface (Figure 4-6c). In general, the rocking resistance increased with the increased pile length with the only exception for the case of the short monopile ($L/W = 0.25$), when the fully bonded interface foundation-soil interface is considered. In this particular situation, the short pile reduced the maximum rocking resistance by 33% below the shallow footing. This is attributed to strain localization below the short pile tip, which limits the propagation of the complete failure mechanism below the footing, thus reducing the rocking capacity.
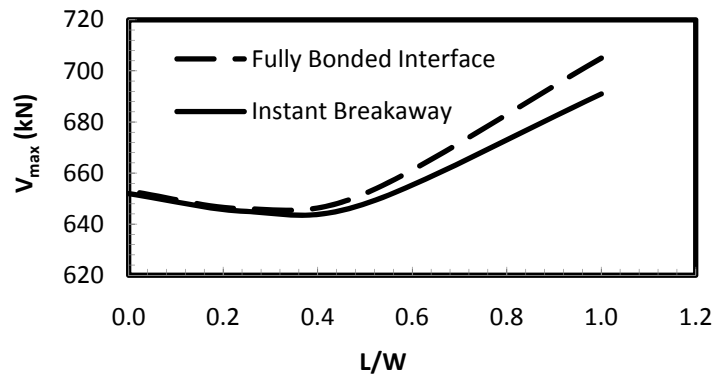
a) Effect of L/W ratio on the maximum vertical load resistance
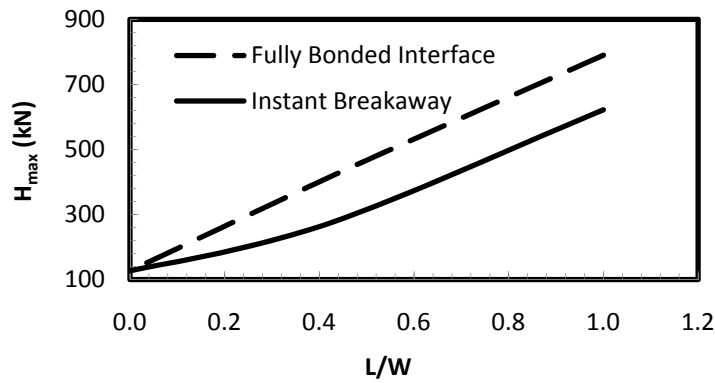
b) Effect of L/W ratio on the maximum lateral load resistance
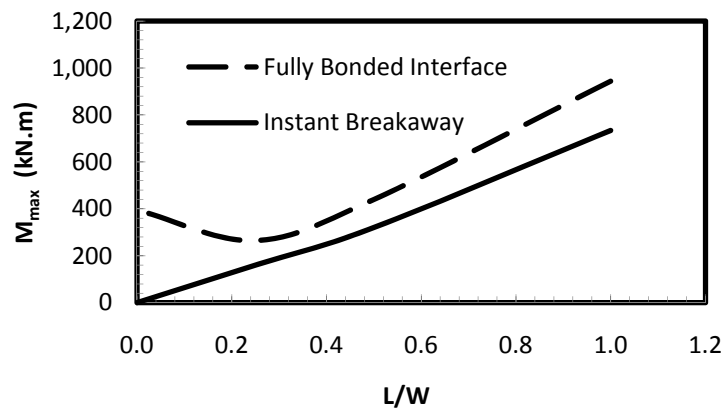
c) Effect of L/W ratio on the maximum moment resistance

Figure 4-6 Effect of the geometry of the hybrid foundation system on load resistance for: a) pure vertical loading, b) pure lateral loading and c) pure moment loading

4.5 Effect of the Geometry of the Hybrid System on the Size and Shape of V-H Failure Envelopes

Figure 4-7 displays a plot of the *V-H* failure envelopes for different *L/W* ratios (*L/W* = 0, 0.25, 0.5 and 1), which shows a similar behaviour as that observed in pure lateral loading. Increasing the pile length (i.e. increasing *L/W* ratio) has significantly increased the size of the *V-H* failure envelope, thus the capacity of the system. Even adding a short monopile (*L/W* = 0.25) can increase the resistance to sliding by 60% to 135% (for instant breakaway and fully bonded conditions, respectively). Since in many cases the sliding resistance is the governing factor in the design of the foundations supporting earth retaining structures, the use of the hybrid system can dramatically reduce the installation costs and foundation size. This improvement was more significant for higher *L/W* ratios. For *L/W* = 1, the hybrid system produced a maximum resistance to sliding of 5 to 6 times of that of a shallow footing (for instant breakaway and fully bonded conditions respectively).

In Figure 4-8, the *V-H* failure envelopes are displayed in a dimensionless form as *v-h*, by normalizing both the vertical and lateral loads by $A.S_u$, where A is the footing print area (*W* x 1m) and *Su* is the undrained shear strength of the clay. To emphasize the effect of the geometry of the hybrid system on the shape of *V-H* failure envelopes, Figure 4-9 displays plots of v/v_o versus h/h_o where, v_o and h_o are the maximum vertical and lateral load capacities reached at a specific geometry (V_{max} and H_{max}) normalized by $A.S_u$. It can be noted from this figure that the shape of the concave normalized envelopes for the fully bonded foundation-soil interface depends on the *L/W* ratio of the hybrid system.
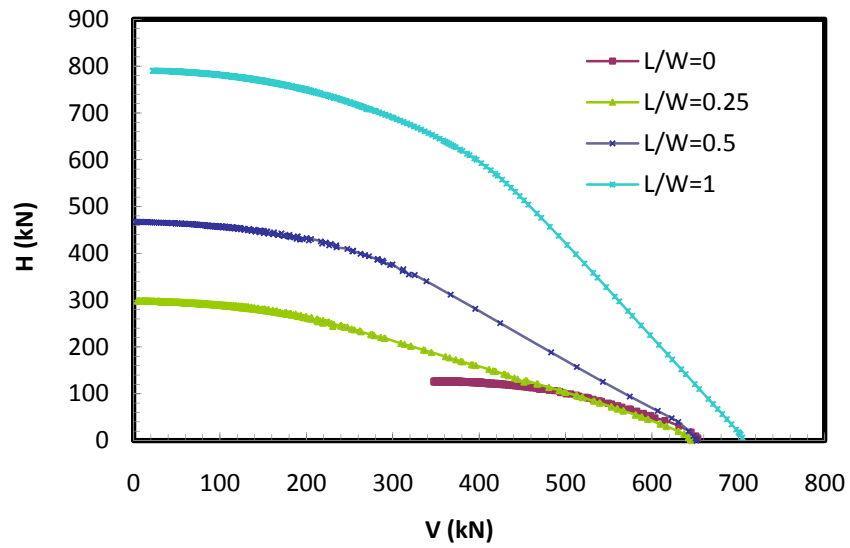
a) Fully bonded foundation - soil interface
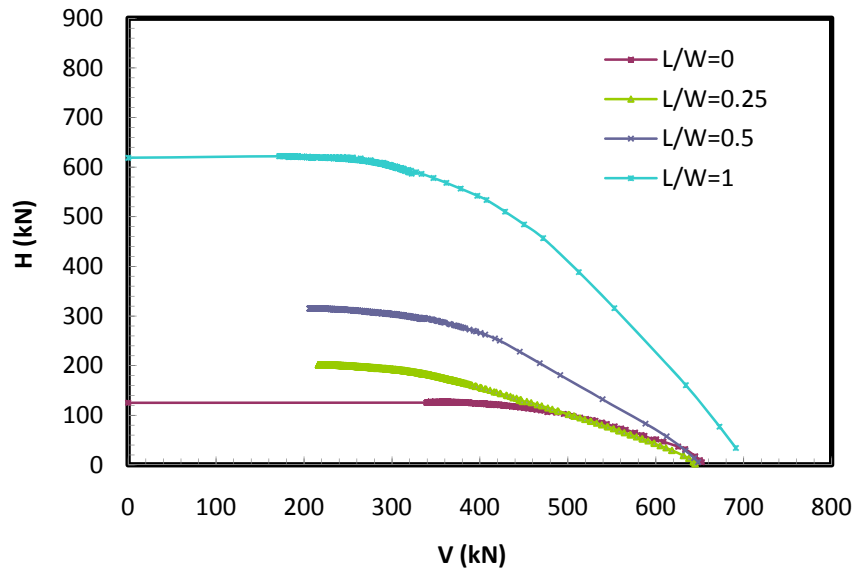
b) Foundation - soil interface with no bonding (instant breakaway)

Figure 4-7 Effect of the geometry of the hybrid system (L/W ratio) on the shape of the V - H failure envelopes, for the case of: a) Fully bonded foundation - soil interface, b) Foundation - soil interface with no bonding

a) Fully bonded foundation - soil interface

b) Foundation - soil interface with no bonding (instant breakaway)

Figure 4-8 Effect of the geometry of the hybrid system (L/W ratio) on the shape of the normalized v - h failure envelopes, for the case of: a) Fully bonded foundation - soil interface, b) Foundation - soil interface with no bonding

a) Fully bonded foundation - soil interface

b) Foundation - soil interface with no bonding (instant breakaway)

Figure 4-9 Effect of the geometry of the hybrid system (L/W ratio) on the shape of the normalized v/vo - h/ho failure envelopes, for the case of: a) Fully bonded foundation - soil interface, b) Foundation - soil interface with no bonding

The effect of the foundation-soil interface is readily noticed in Figure 4-10. For the fully bonded condition, it is noticeable that the lateral capacity is continuously increasing, when decreasing the applied V-load, as opposed to the plateau observed for the case of instant breakaway. The fully bonded and the instant breakaway conditions represent the range of values bounding the expected in-situ behavior. In general, depending on factors such as the rate of loading, characteristic drainage time and the boundary conditions, the actual behavior at the foundation-soil interface will fall somewhere between these two limiting conditions.
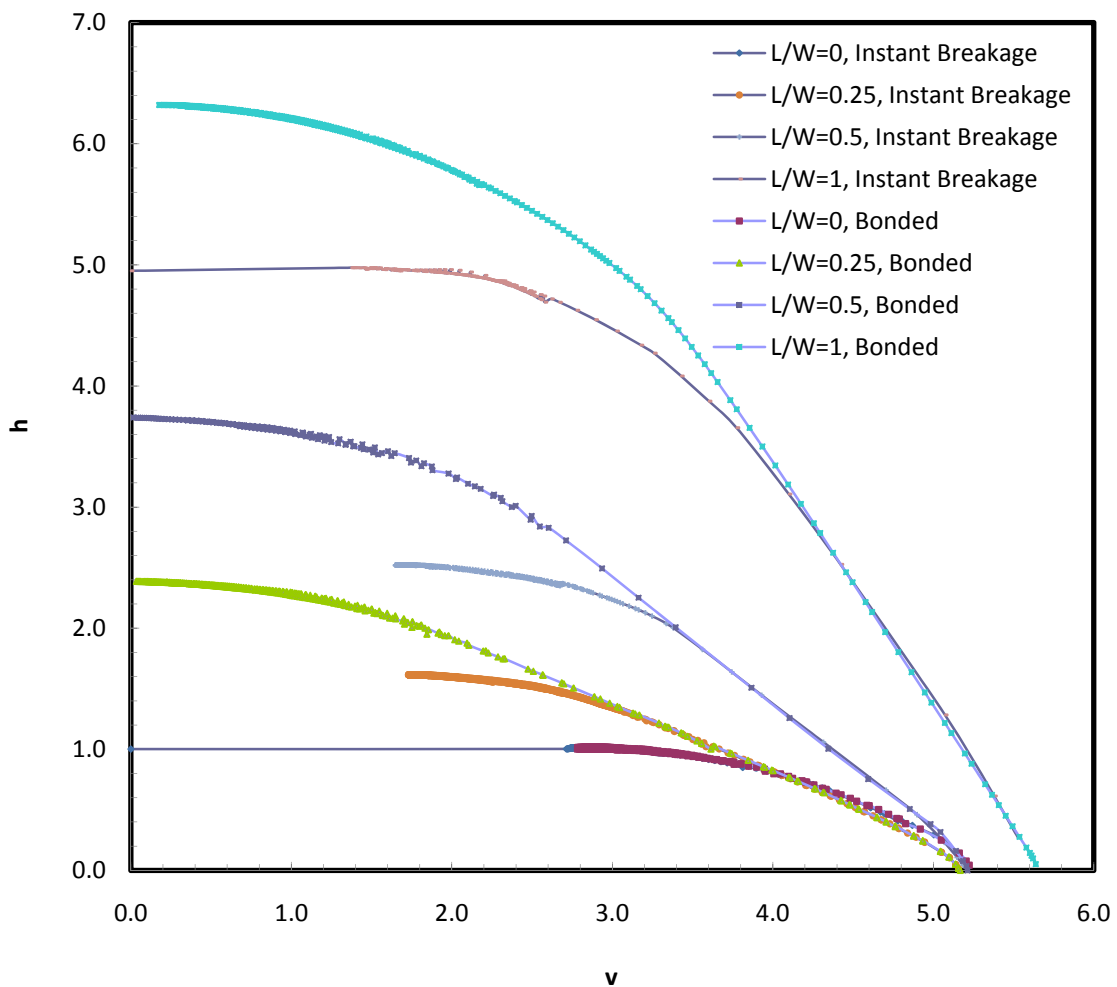
Figure 4-10 Effect of the condition of the soil - foundation interface on the shape of the normalized v - h failure envelopes

4.6 Effect of the Geometry of the Hybrid System on the Rocking Resistance

Figure 4-11 shows the *V-M* failure envelopes produced for different geometries of the hybrid system. Interestingly, the presence of a short monopile ($L/W = 0.25$) reduces the size of the *V-M* failure envelope below that of a shallow footing. Also, the peak rocking resistance was reduced by 18%. On the other hand for the case of instant breakaway, the presence of the short pile added an initial rocking strength to the hybrid system when subjected to low *V*-load values, which is useful when supporting a light structure subjected to considerable overturning moments such as wind turbine.

Increasing the pile length ($L/W \geq 0.5$) can produce a noticeable gain in the maximum rocking resistance by 20% to 34% at $L/W = 2$ and 100% to 144% at $L/W = 1$, for the conditions of instant breakaway and full bond at the foundation-soil interface respectively. This is because a long pile extending outside the initial failure zones of the un-stiffened shallow footing would force an extended soil zone to contribute to producing a wider and deeper soil failure mechanism.

In Figure 4-12, the *V-M* failure envelopes are displayed in a dimensionless form as *v-m*, by normalizing both the vertical loads by $A.S_u$, as before, while the moment loads where normalized by $A^2.S_u$. Again, to study the effect of the geometry of the hybrid system on the shape of the *V-M* failure envelopes, Figure 4-13 displays plots of v/v_o versus m/m_o, where m_o is the maximum moment capacity reached for a specific geometry (L/W ratio) normalized by $A^2.S_u$. The figure shows that the L/W ratio of the hybrid system has a minor effect on the shape of the normalized envelopes, which may be practically ignored.
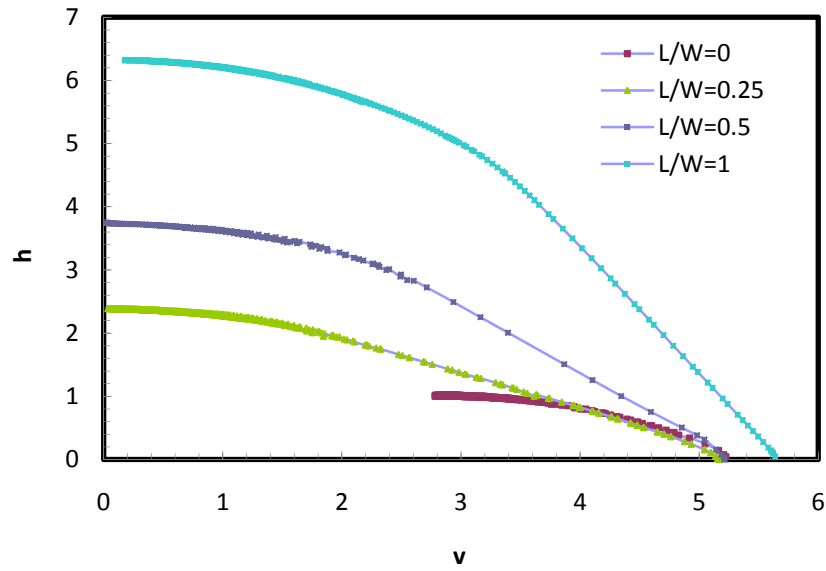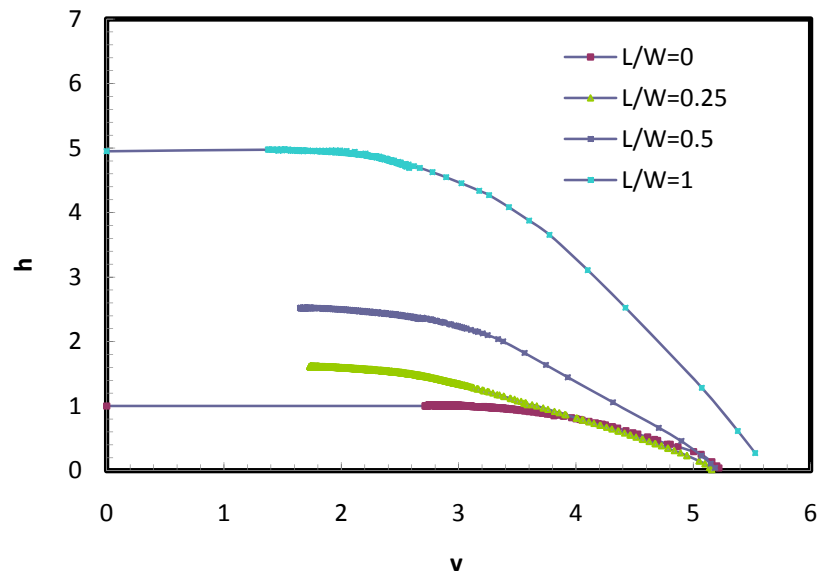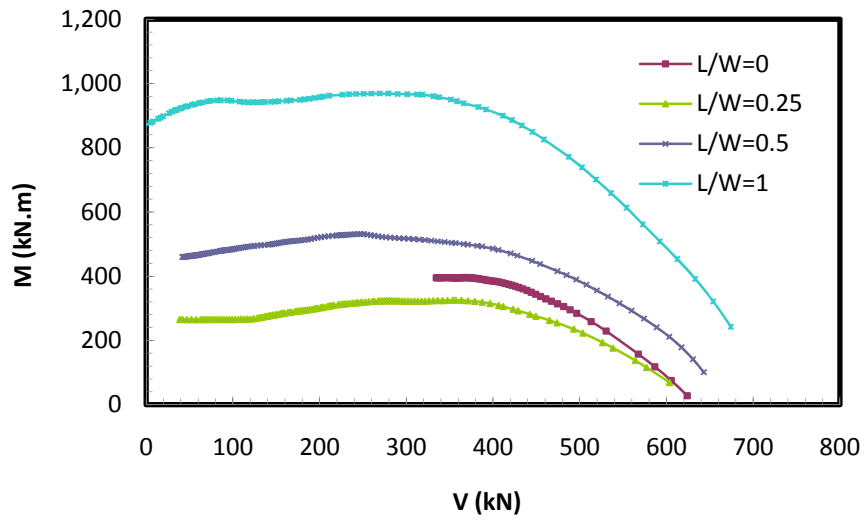
a) Fully bonded foundation - soil interface
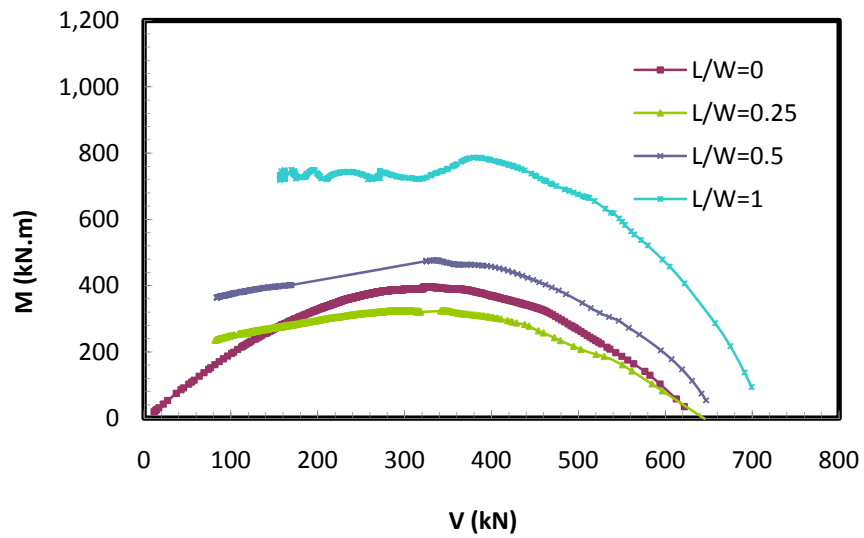
b) Foundation - soil interface with no bonding (instant breakaway)

Figure 4-11 Effect of the geometry of the hybrid system (L/W ratio) on the shape of the V - M failure envelopes, for the case of: a) Fully bonded foundation - soil interface, b) Foundation - soil interface with no bonding
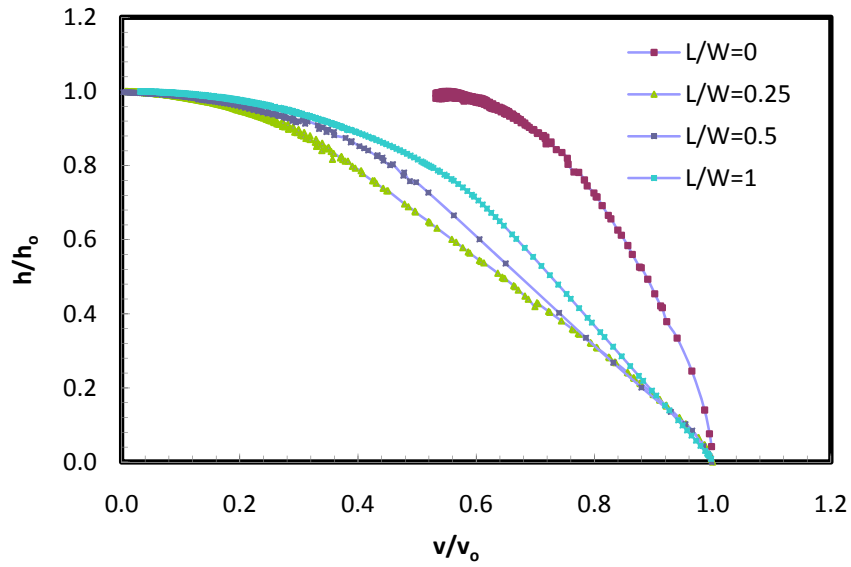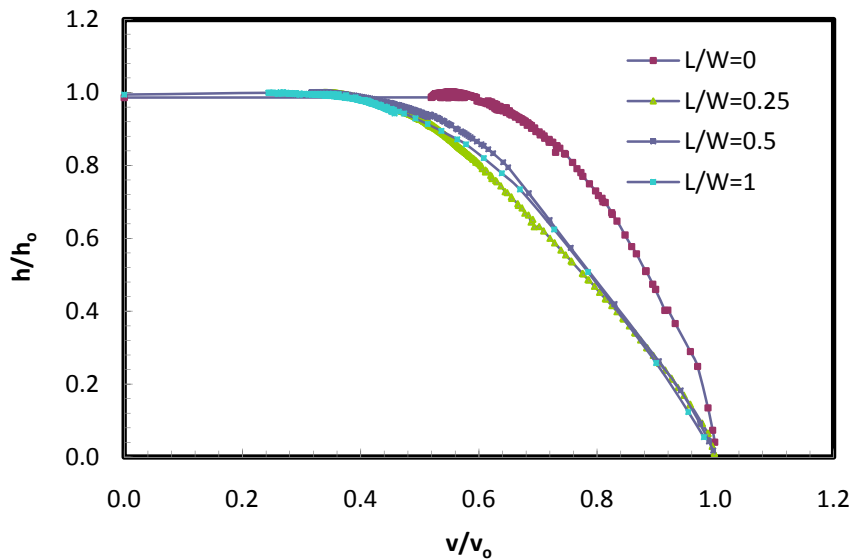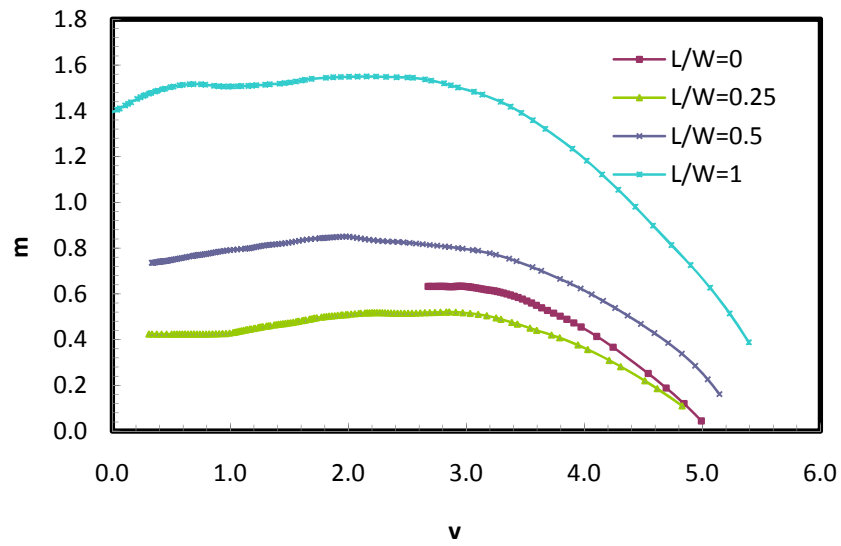
a) Fully bonded foundation - soil interface
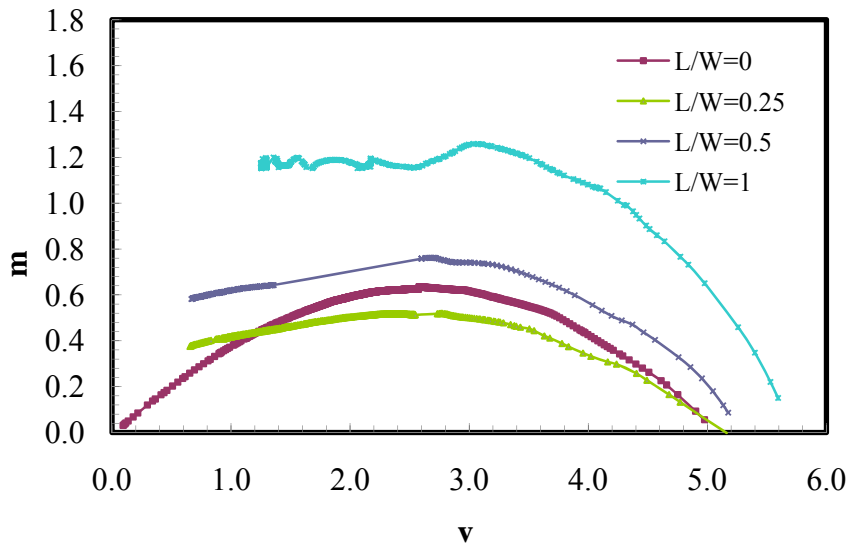
b) Foundation - soil interface with no bonding (instant breakaway)

Figure 4-12 Effect of the geometry of the hybrid system (L/W ratio) on the shape of the normalized v - m failure envelopes, for the case of: a) Fully bonded foundation - soil interface, b) Foundation - soil interface with no bonding
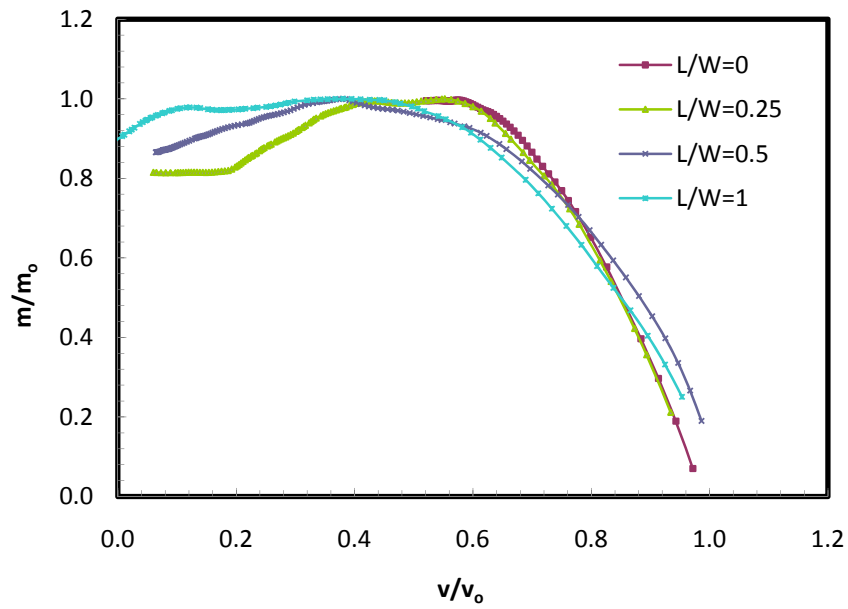
a) Fully bonded foundation - soil interface
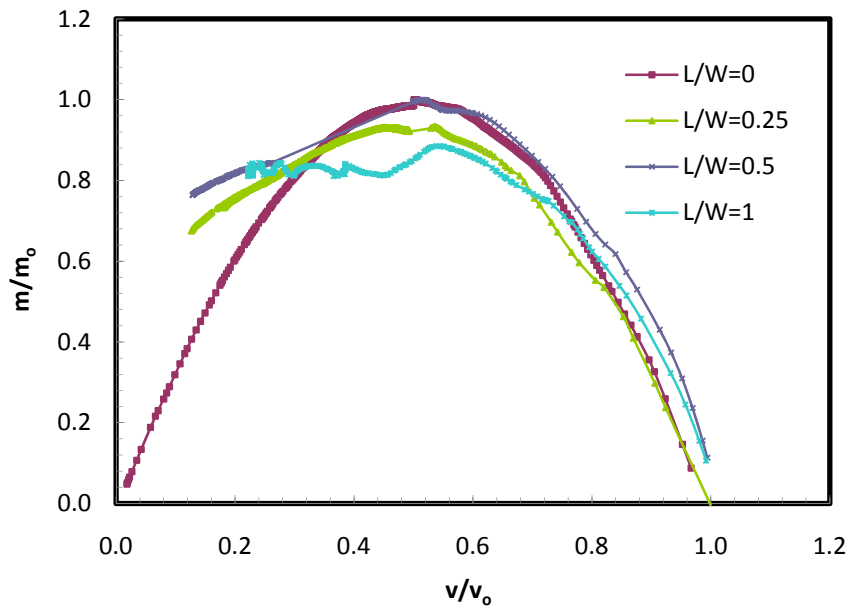
b) Foundation - soil interface with no bonding (instant breakaway)

Figure 4-13 Effect of the geometry of the hybrid system (L/W ratio) on the shape of the normalized v/vo - m/mo failure envelopes, for the case of: a) Fully bonded foundation - soil interface, b) Foundation - soil interface with no bonding

The effect of the foundation-soil interface on the *V-M* failure envelopes can be observed in Figure 4-14. Similar to the case of *V-H* envelopes, the moment capacity is higher for the fully bonded condition especially at lower *V*-load values.
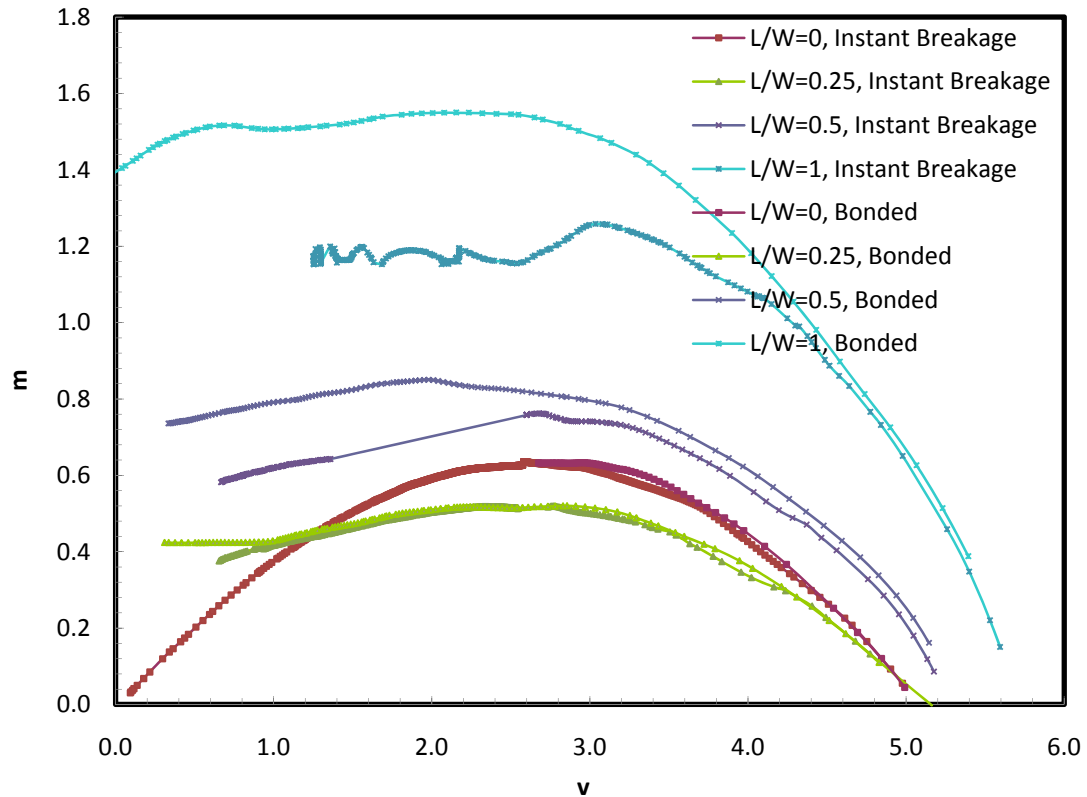

Figure 4-14 Effect of the condition of the soil - foundation interface on the shape of the normalized v - m failure envelopes

4.7 Comparison of the Shape of Normalized V-H and V-M Failure Envelopes of Shallow Footings to Previously Published Studies

To compare the results of this current numerical study to previously published data; the normalized *v-h* failure envelope produced for a shallow footing, in case of instant breakaway condition assigned to the interface, was plotted in Figure 4-15 alongside with envelopes previously produced in the literature. The shape of the *v-h* envelope produced in this study appear to be in good agreement with the previous studies especially with the

envelope produced by Gourvenec (2007). The same level of agreement appeared in the normalized *V-M* failure envelopes plotted in Figure 4-16.
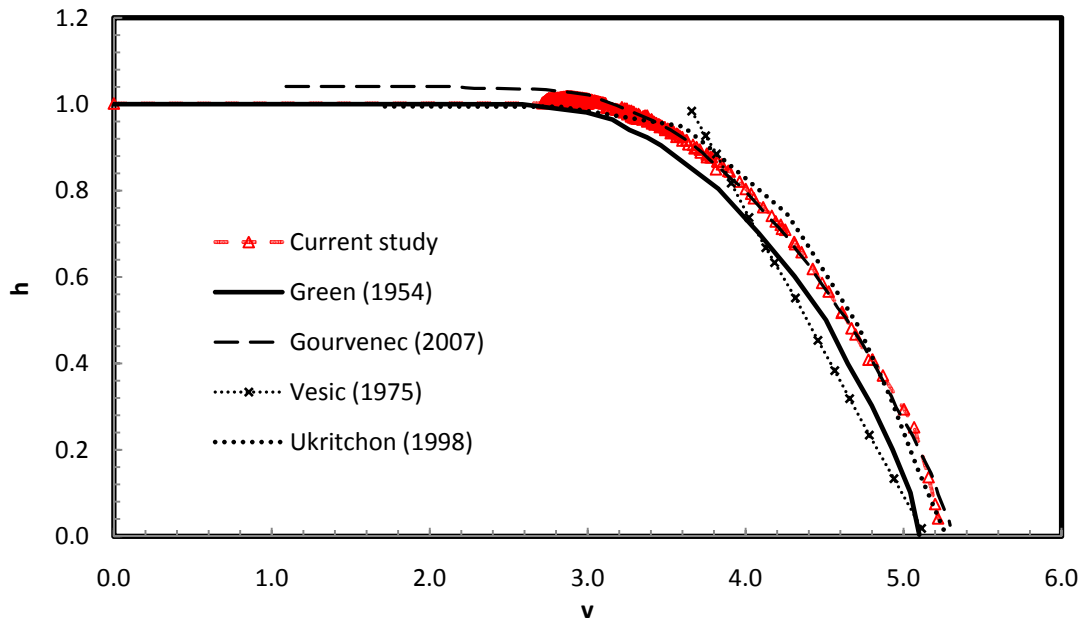
Figure 4-15 The shape of the normalized V-H failure envelope for shallow footings on undrained clays - a comparison to previously published studies
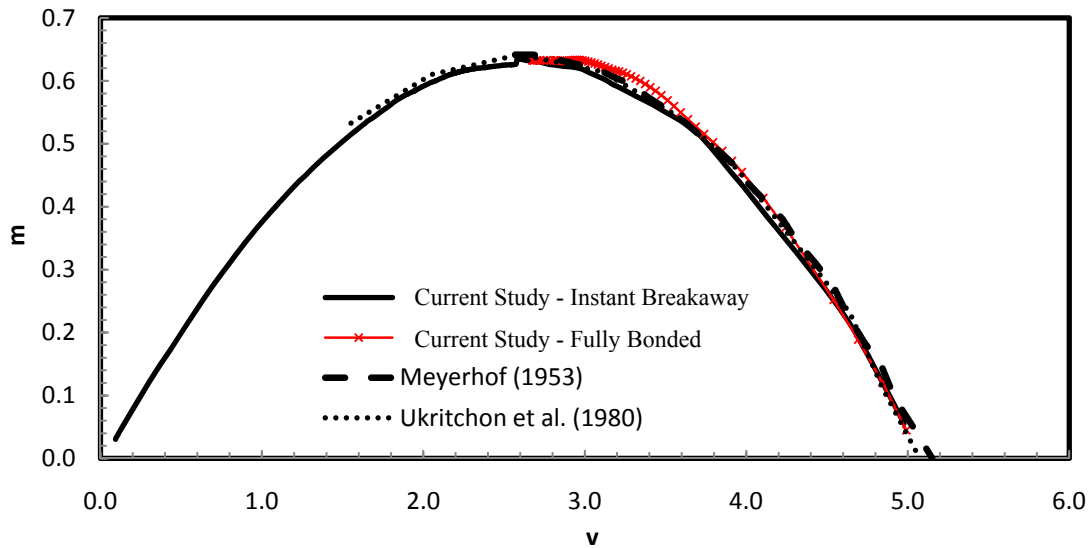
Figure 4-16 The shape of the normalized V-M failure envelope for shallow footings on undrained clays - a comparison to previously published studies

4.8 Closed Form Expressions for the V-H Failure Envelopes

4.8.1 Case 1: Fully Bonded Foundation-Soil Interface Condition

Equation 4-1 is proposed to describe the shape of the V-H failure envelopes of the shallow strip footings, regardless of the foundation-soil interface condition.

For $v/v_o > 0.5$:

$$\frac{h}{h_o} = \frac{H}{A.Cu} = 3.08 \, \frac{v}{v_o} \left[1 - \left(\frac{v}{v_o}\right)^{1.5} \right] \qquad \text{Shallow footing, } L/W = 0.0 \quad (4\text{-}1)$$

For $v/v_o < 0.5$:

$$h/h_o = 1.0$$

 The following general function (Equation 4-2) is capable of producing the normalized V-H failure envelopes of the hybrid monopile-footing foundation systems while taking account for the geometrical configuration of the foundation.

$$\frac{h}{h_o} = 1 - \left(\frac{v}{v_o}\right)^{\beta_2} \left[(1 + \beta_1) - \beta_1 \left(\frac{v}{v_o}\right)^{\beta_2} \right] \qquad \text{General Function} \qquad (4\text{-}2)$$

Where, the parameters β_1 and β_2 can be evaluated from the curve fitting of the normalized V-H failure envelopes. The following equations describe the failure envelopes of the hybrid systems at L/W ratios of 0.25, 0.50 and 1.0, respectively.

$$\frac{h}{h_o} = 1 - \left(\frac{v}{v_o}\right)^2 \left[1.35 - 0.35 \left(\frac{v}{v_o}\right)^2 \right] \qquad \text{Hybrid System, } L/W = 0.25 \quad (4\text{-}3)$$

$$\frac{h}{h_o} = 1 - \left(\frac{v}{v_o}\right)^2 \left[1.017 - 0.017 \left(\frac{v}{v_o}\right)^2 \right] \qquad \text{Hybrid System, } L/W = 0.50 \quad (4\text{-}4)$$

$$\frac{h}{h_o} = 1 - \left(\frac{v}{v_o}\right)^2 \left[0.74 + 0.26 \left(\frac{v}{v_o}\right)^2 \right] \qquad \text{Hybrid System, } L/W = 1.00 \quad (4\text{-}5)$$

The graphs produced from the previous failure envelope equations are plotted in Figure 4-17.

c) $L/W = 0.00$

b) $L/W = 0.25$

d) $L/W = 0.50$

d) $L/W = 1.00$
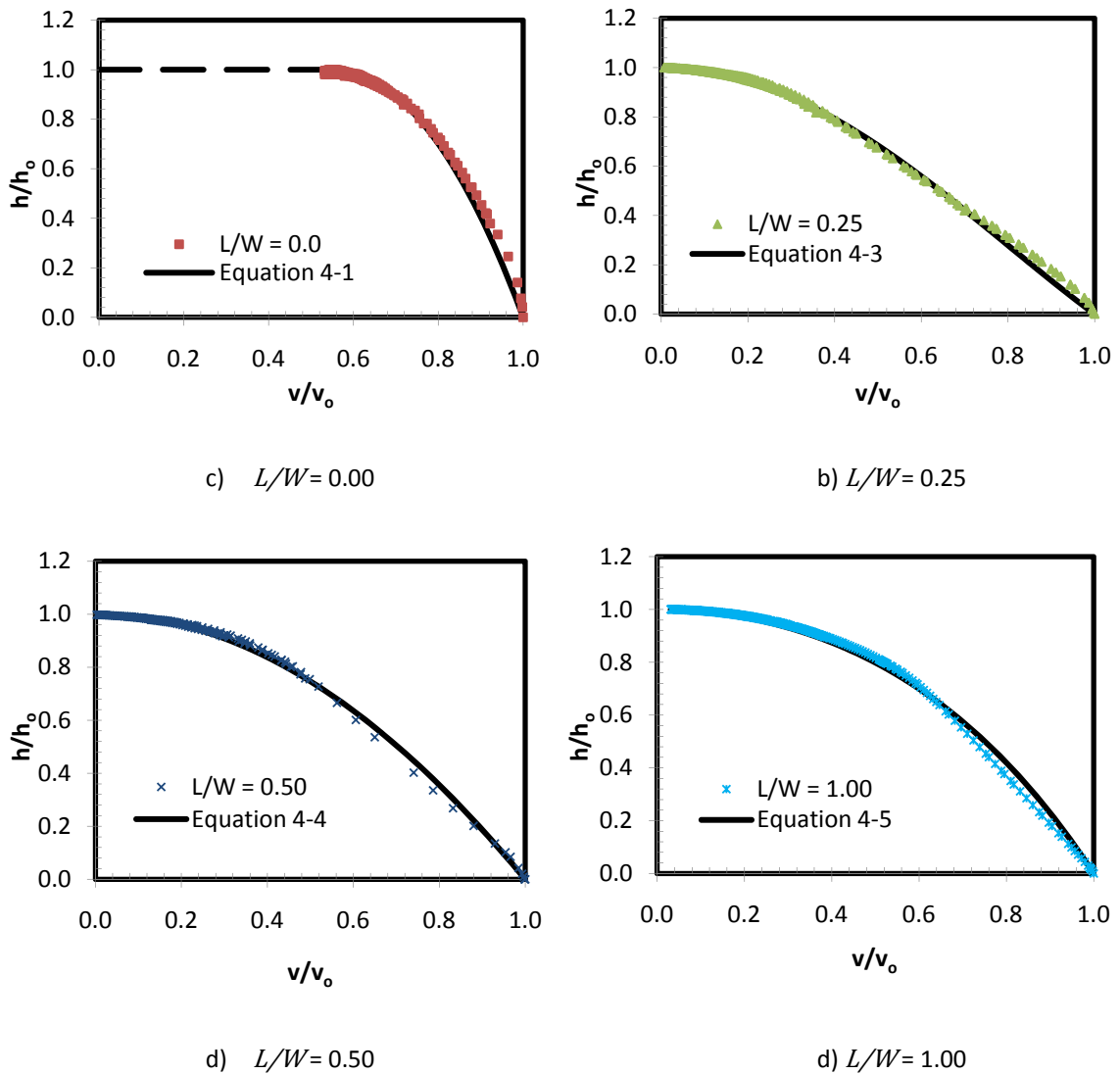
Figure 4-17 Curve fitting of the normalized V-H failure envelopes of hybrid systems – Fully bonded condition

4.8.2   Case 2: Instant Breakaway Condition

Equation 4-6 is capable of describing the shape of the normalized *V-H* failure envelopes of the hybrid monopile-footing foundation systems for the instant breakaway condition,

while taking account of the *L/W* ratio. The general failure envelope, produced by Equation 4-6, is plotted in Figure 4-18.

For $v/v_o > 0.3$:

$$\frac{h}{h_o} = 2.6 \left(\frac{v}{v_o}\right)^{0.5} \left[1 - \frac{v}{v_o}\right] \qquad \qquad (4\text{-}6)$$

For $v/v_o < 0.3$:

$h/h_o = 1.0$
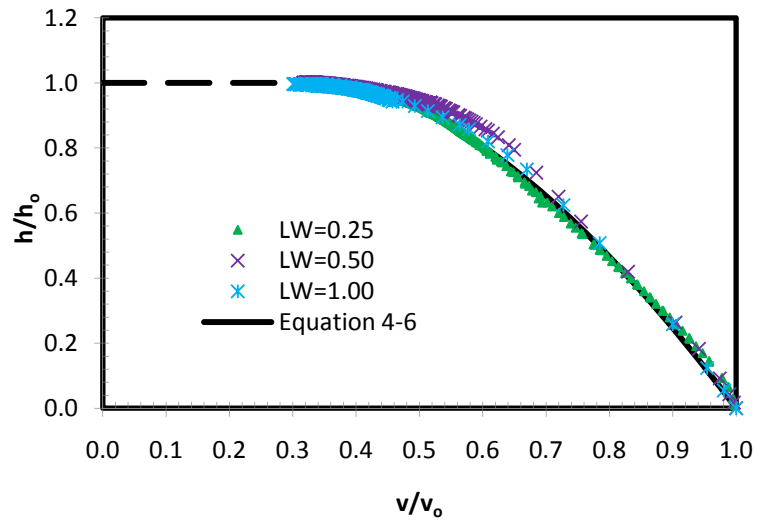
Figure 4-18 Curve fitting of the normalized V-H failure envelopes of hybrid systems - Instant breakaway condition

4.9 Closed Form Expressions for the V-M Failure Envelopes

4.9.1 Case 1: Fully Bonded Foundation-Soil Interface Condition

Equation 4-7 is suggested by the curve fitting of the normalized *V-M* failure envelope of the shallow footing at a fully bonded foundation-interface condition (Figure 4-19 below).

For $v/v_o > 0.5$:

$$\frac{m}{m_o} = 4\,\frac{v}{v_o}\left[1 - \frac{v}{v_o}\right]$$
Shallow footing, $L/W = 0.0$ (4-7)

For $v/v_o < 0.5$:

$m/m_o = 1.0$
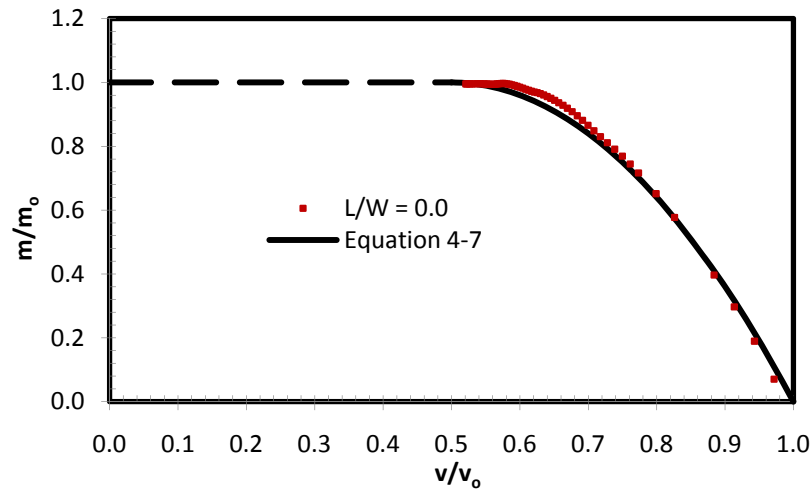
Figure 4-19 Curve fitting of the normalized V-M failure envelope of shallow footing - Fully bonded condition

The V-M failure envelopes of the hybrid monopile-footing foundation systems are described by Equation 4-8. The generated envelope is plotted in Figure 4-20.

For $v/v_o > 0.3$:

$$\frac{m}{m_o} = 0.89 + \left(\frac{v}{v_o}\right)^2 \left[0.78 - 1.71\left(\frac{v}{v_o}\right)^2\right]$$
(4-8)
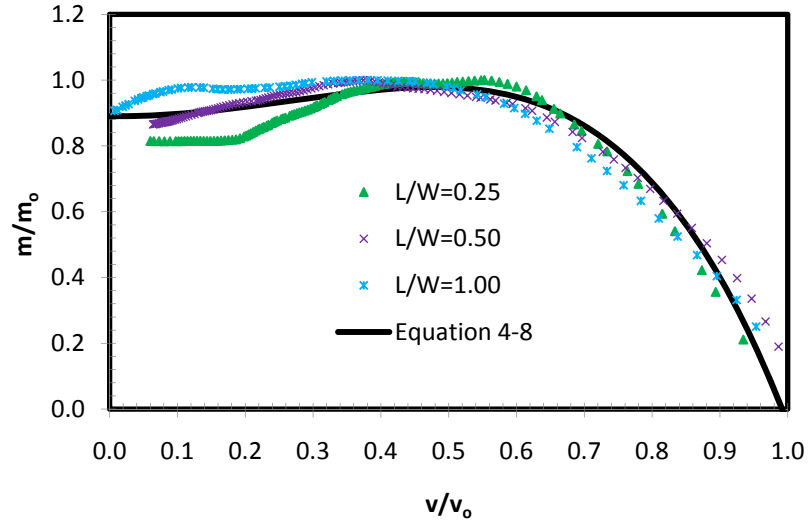
Figure 4-20 Curve fitting of the normalized V-M failure envelopes – Fully bonded condition

4.9.2 Case 2: Instant Breakaway Condition

For the instant breakaway condition, the normalized *V-M* failure envelope of the shallow footing can still be described using Equation 4-7 for the full range of *V/V$_{max}$* values (from 0.0 to 1.0) as demonstrated in Figure 4-21.
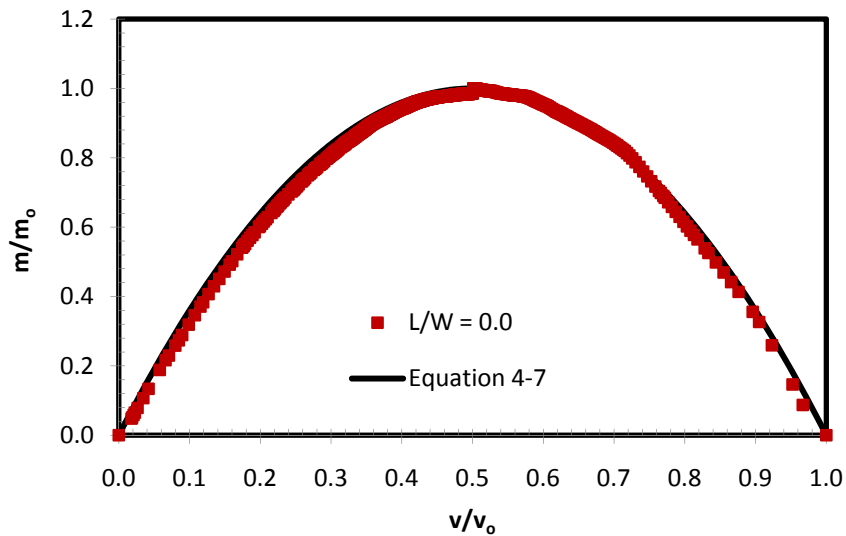
Figure 4-21 Curve fitting of the normalized V-M failure envelope of shallow footing - Instant breakaway condition

Equation 4-9 below is able to describe the normalized *V-M* failure envelopes of the hybrid monopile-footing foundations for the studied range of *L/W* ratios.

For $v/v_o > 0.3$:

$$\frac{m}{m_o} = 0.72 + \left(\frac{v}{v_o}\right)^2 \left[5.36 - 6.09 \left(\frac{v}{v_o}\right)^2\right] \qquad (4\text{-}9)$$

Figure 4-22 shows a plot of the normalized envelopes alongside with the graph produced from Equation 4-9.
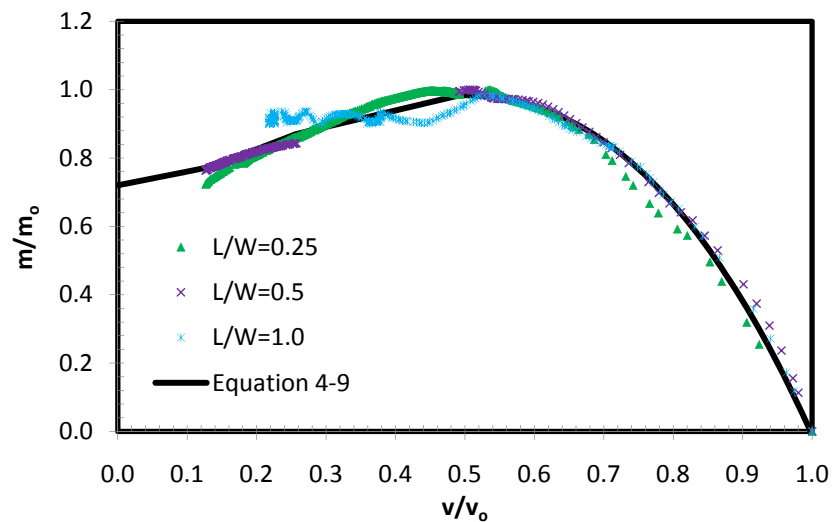
Figure 4-22 Curve fitting of the normalized V-M failure envelopes of hybrid systems - Instant breakaway condition

4.10 Failure Mechanisms

The combined *V-H* loading acting on the hybrid foundation systems results in complex asymmetrical failure mechanisms, as displayed in Figure 4-23 to Figure 4-26.

For the instant breakaway condition at low *V*-load levels ($V/V_{max} < 0.2$), the figures show the formation of narrow failure mechanisms consisting of a rigid rectangular soil block sliding laterally beneath the compression side of the footing, followed by a rotating shear fan and a passive triangular wedge (as shown Figure 4-23). In the presence of the monopile/key, the resistance to sliding becomes the result of the passive earth pressures

applied on the pile, in addition to the shear resistance produced beneath the sliding soil block, which is a significantly larger resistance than the resultant of the shear strength at the footing-soil interface for the case of shallow footings. It can also be noticed that increasing the pile length generates deeper and wider mechanisms of failure and thus a higher resistance to sliding.

A different failure mechanism appeared for the fully bonded foundation soil interface condition. This mechanism formed at both the tension and compression sides consisted of; a sliding soil block, a radial shear fan and a soil wedge (as shown Figure 4-25). Obviously, the fully bonded interface cracks bigger mechanisms and higher resistances. It can also be seen that the shape and extent of the failure mechanism beneath the shallow footing is independent of the conditions assigned to the foundation-soil interface.

At high V-load levels (V/V_{max} >0.8), the shape and extent of the failure mechanisms seem to be independent of the conditions assigned to the foundation-soil interface (Figure 4-24 and Figure 4-26), which explains the compatibility of the V-H failure envelopes observed at V-load values in Figure 4-10. In general, the generated failure mechanisms for either the shallow footing or the hybrid system consisted of an asymmetrical triangular wedge formed beneath the footing followed by a radial shear zone and a passive soil wedge. Once again it can be noticed that increasing the pile length generated deeper and wider mechanisms of soil failure.

a) Shallow footing

b) Hybrid system with L/W =0.25

c) Hybrid system with L/W =0.5

d) Hybrid system with L/W =1
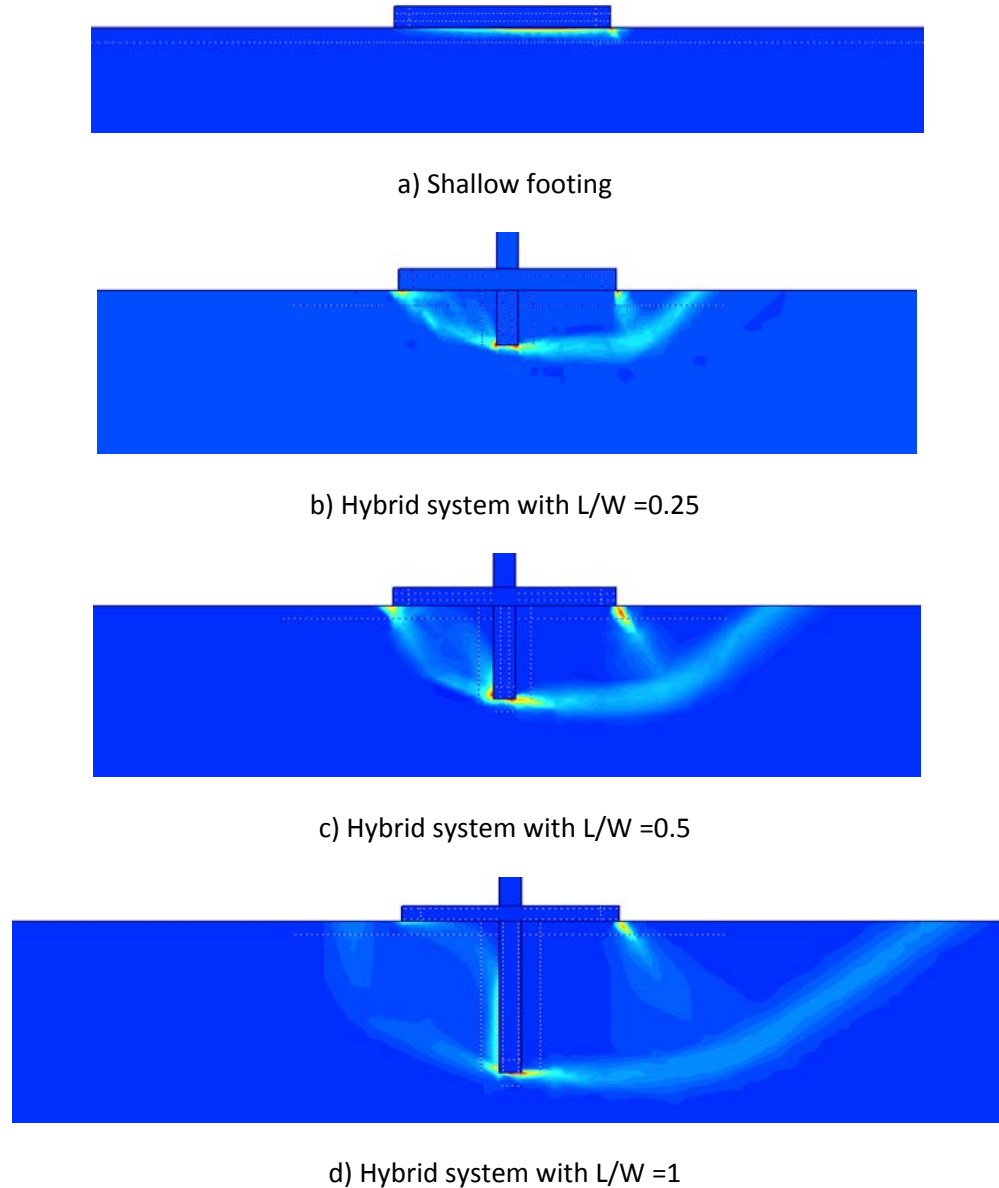
Figure 4-23 Failure mechanisms under combined V-H loading at V/Vmax < 0.2 in case of foundation - soil interface with no bonding, for: a) Shallow footing, b) L/W =0.25, c) L/W =0.5 and d) L/W=1
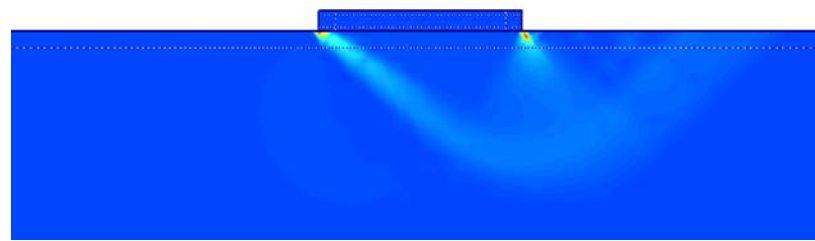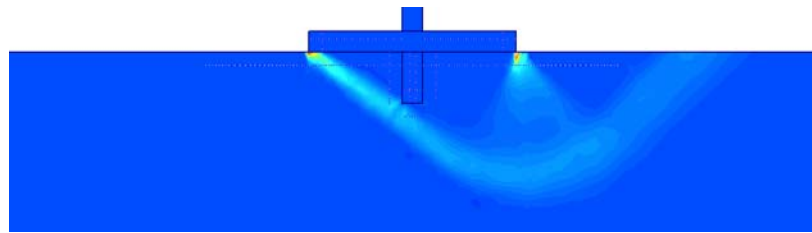
a) Shallow footing

b) Hybrid system with L/W =0.25
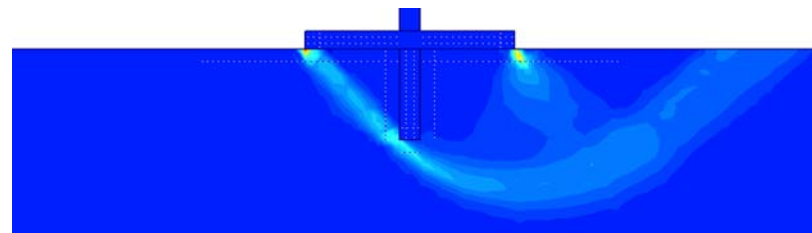
c) Hybrid system with L/W =0.5
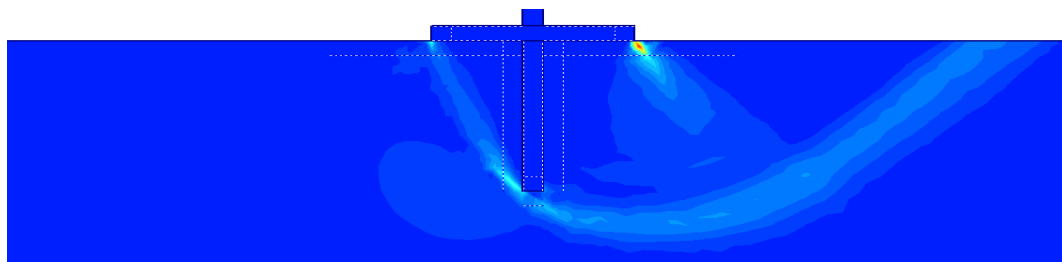
d) Hybrid system with L/W =1

Figure 4-24 Failure mechanisms under combined V-H loading at V/Vmax > 0.8 in case of foundation - soil interface with no bonding, for: a) Shallow footing, b) L/W =0.25, c) L/W =0.5 and d) L/W=1

a - Shallow footing

b - Hybrid system with L/W =0.25

c - Hybrid system with L/W =0.5

d - Hybrid system with L/W =1
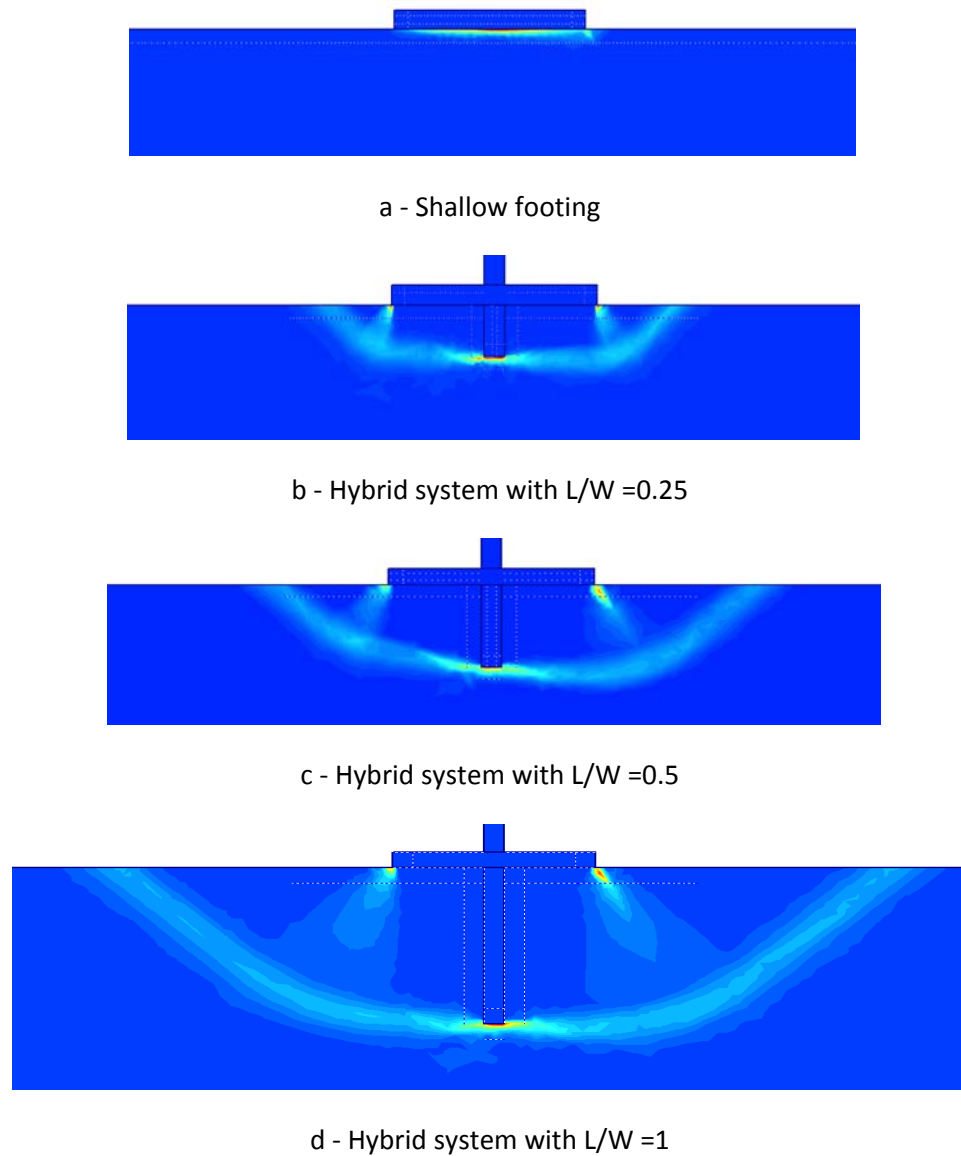
Figure 4-25 Failure mechanisms under combined V-H loading at V/Vmax < 0.2 in case of fully bonded foundation - soil interface, for: a) Shallow footing, b) L/W =0.25, c) L/W =0.5 and d) L/W=1

a) Shallow footing

b) Hybrid system with L/W =0.25

c) Hybrid system with L/W =0.5

d) Hybrid system with L/W =1
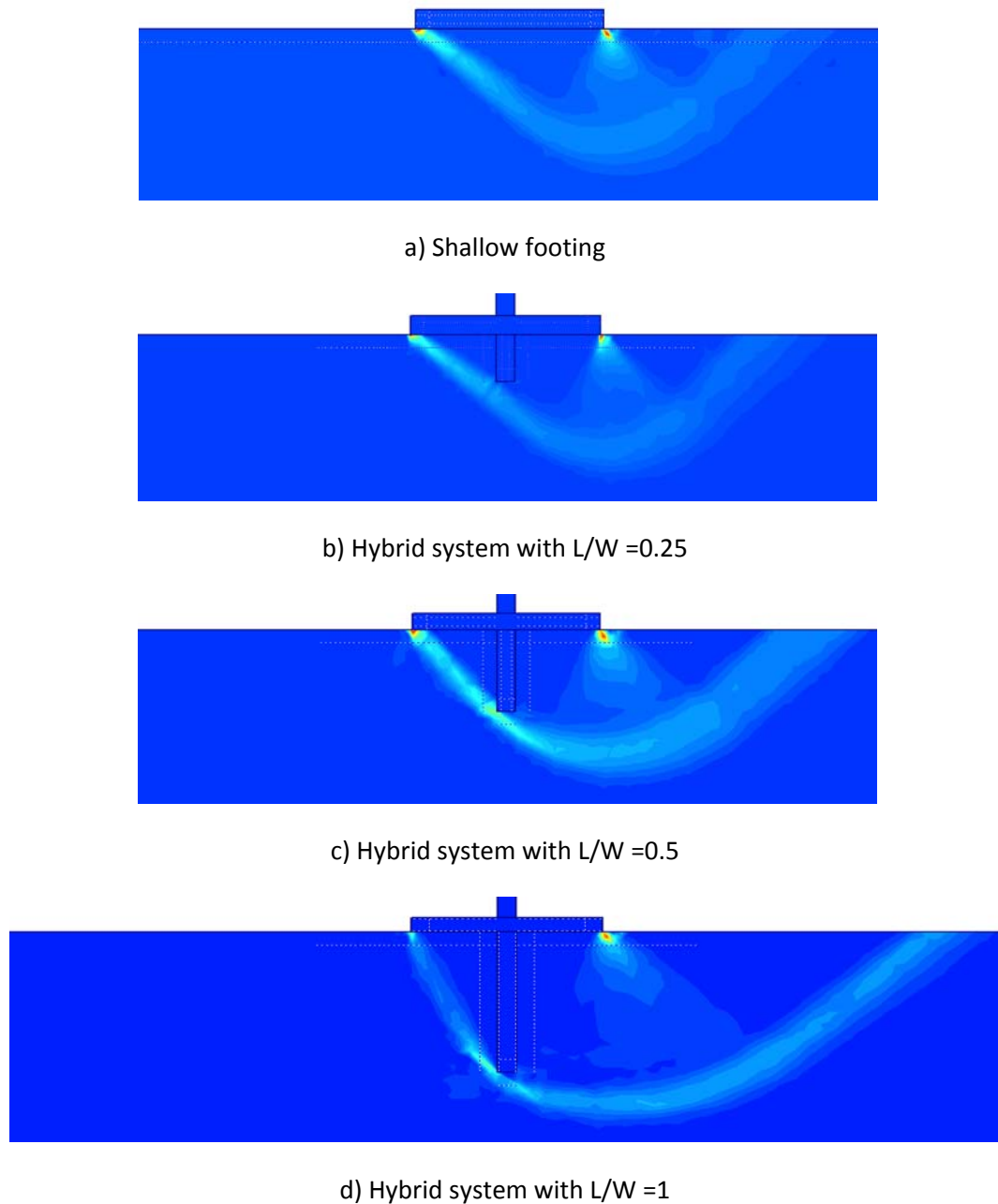
Figure 4-26 Failure mechanisms under combined V-H loading at V/Vmax > 0.8 in case of fully bonded foundation - soil interface, for: a) Shallow footing, b) L/W =0.25, c) L/W =0.5 and d) L/W=1

The failure mechanisms generated due to combined *V-M* loading are displayed in Figure 4-27 to Figure 4-30. For the fully bonded foundation-soil interface condition and at low V-load ratios (V/V_{max}<0.2), the failure mechanisms displayed in Figure 4-27consisted of

a simple rotating scoop that increased in diameter and depth as the pile length was increased. A more complex asymmetrical scoop failure mechanism took place at the instant breakaway condition (Figure 4-29).

Once again, at high V-load levels (V/V_{max}>0.8) the shape and extent of the V-M failure mechanisms seem to be independent of the conditions assigned to the foundation-soil interface (Figure 4-28 and 24). In this case, the generated failure mechanisms for either the shallow footing or the hybrid system are a combination of rotating scoops and rigid soil wedges as displayed in Figure 4-28 and 24. As seen previously, increasing the pile length resulted in deeper and wider mechanisms of failure.
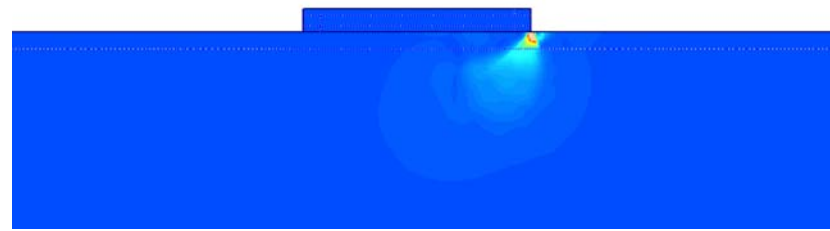
a) Shallow footing
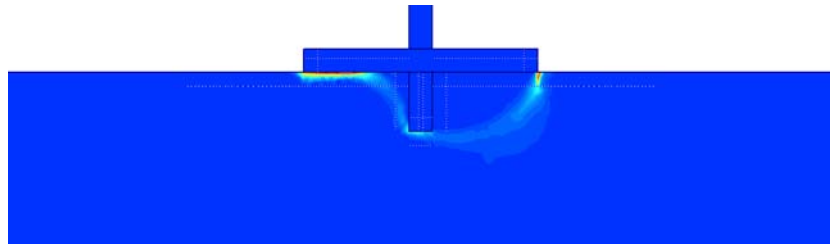
b) Hybrid system with L/W =0.25
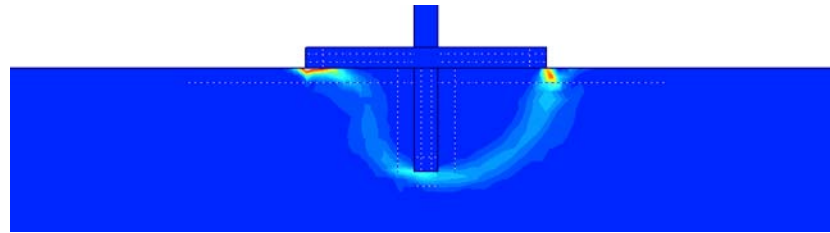
c) Hybrid system with L/W =0.5
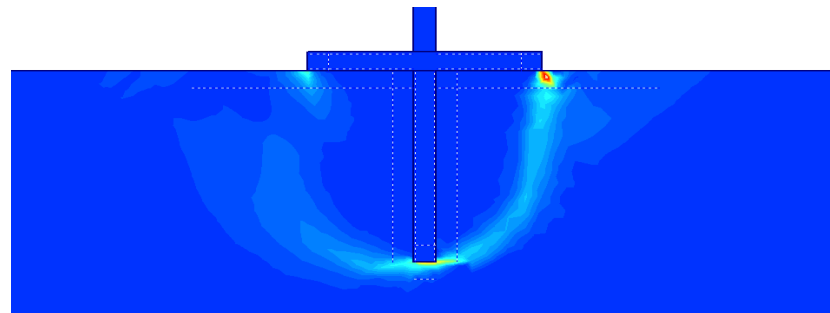
d) Hybrid system with L/W =1

Figure 4-27 Failure mechanisms under combined V-M loading at V/Vmax < 0.2 in case of foundation - soil interface with no bonding, for: a) Shallow footing, b) L/W=0.25, c) L/W=0.5 and d) L/W=1

a) Shallow footing

b) Hybrid system with L/W =0.25

c) Hybrid system with L/W =0.5

d) Hybrid system with L/W =1
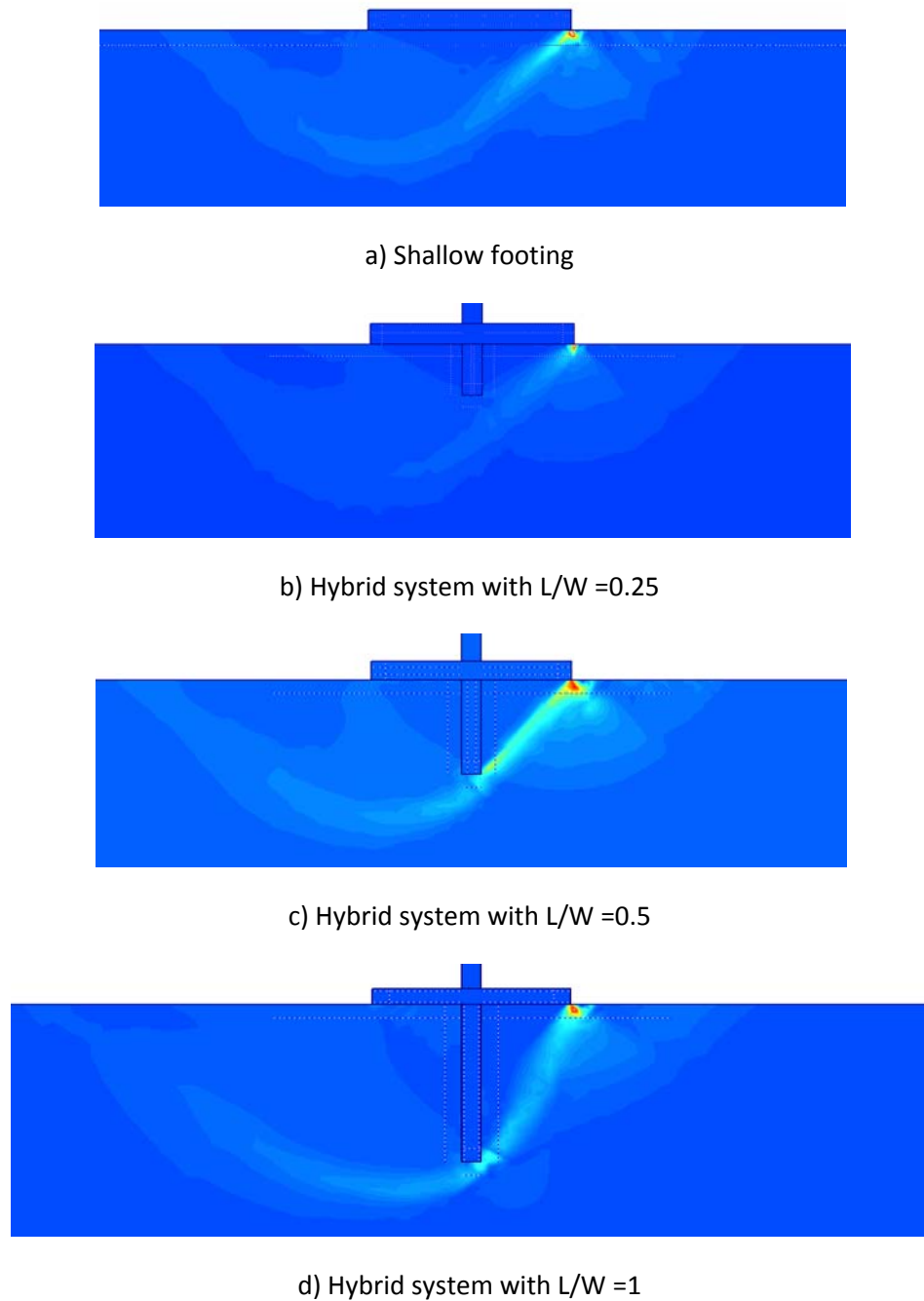
Figure 4-28 Failure mechanisms under combined V-M loading at V/Vmax > 0.8 in case of foundation - soil interface with no bonding, for: a) Shallow footing, b) L/W=0.25, c) L/W=0.5 and d) L/W=1
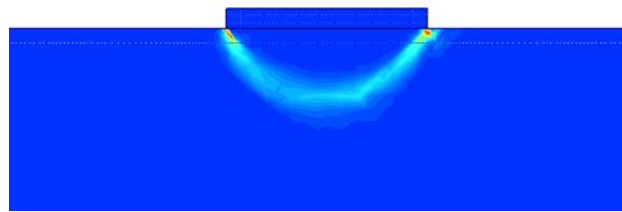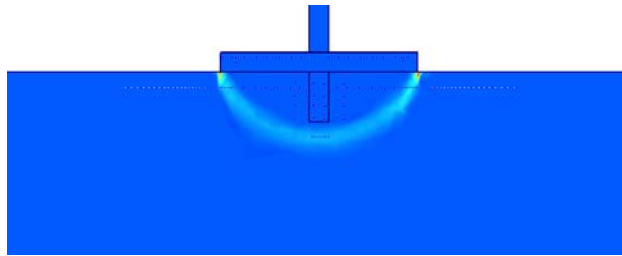
a) Shallow footing

b) Hybrid system with L/W =0.25
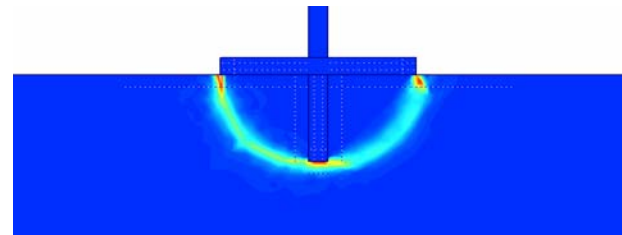
c) Hybrid system with L/W =0.5
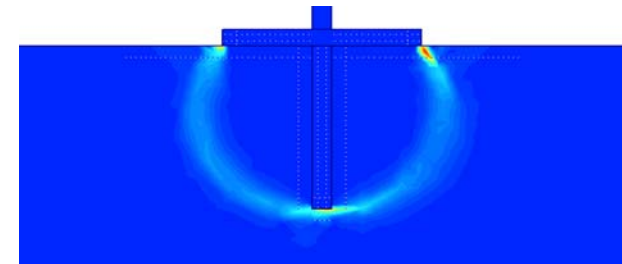
d) Hybrid system with L/W =1

Figure 4-29 Failure mechanisms under combined V-M loading at V/Vmax < 0.2 in case of fully bonded foundation - soil interface, for: a) Shallow footing, b) L/W =0.25, c) L/W =0.5 and d) L/W=1
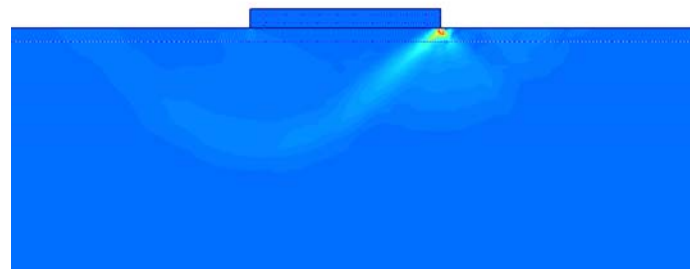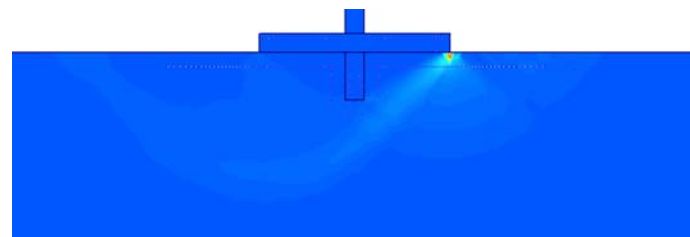
a) Shallow footing

b) Hybrid system with L/W =0.25
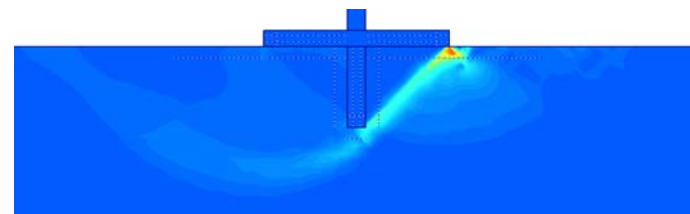
c) Hybrid system with L/W =0.5
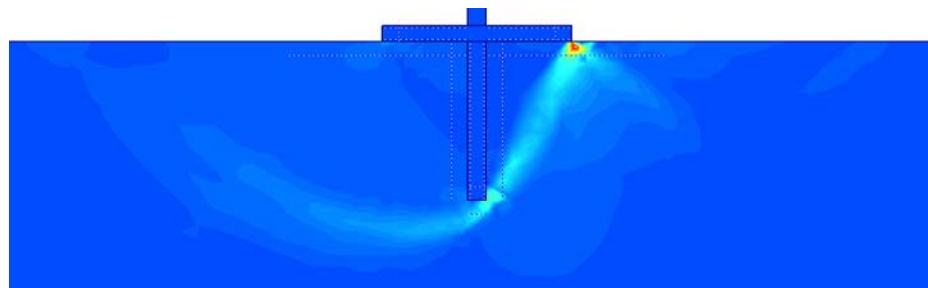
d) Hybrid system with L/W =1

Figure 4-30 Failure mechanisms under combined V-M loading at V/Vmax > 0.8 in case of fully bonded foundation - soil interface, for: a) Shallow footing, b) L/W =0.25, c) L/W =0.5 and d) L/W=1

4.11 2D versus 3D Modeling of Monopiled-Footing Hybrid Systems

In practice, the implementation of the proposed monopiled-footing hybrid foundation system to wind turbine foundations is expected to be close to circular in plan. Whilst the simple 2-D plane strain problem presented an essential precursor to the understanding of the governing parameters affecting the behaviour of circular hybrid systems, an advanced 3D numerical study was required to verify the outcomes of the 2D parametric study.

4.11.1 3D Numerical Modeling

The 3D finite element study was carried out using PLAXIS 3D-Foundations V2.2 on three geometrical configurations, namely: a circular footing; and two hybrid systems with L/W ratios of 0.5 and 1.0. In all 3D models, constant diameters of 5.0m and 0.5m were assigned to the footing and pile respectively, whilst the L/W ratio was varied as required. The typical mesh used in the analysis is shown in Figure 4.25. The shallow footing was modeled by removing the embedded portion of the pile while retaining the footing.

The 3D finite element mesh was modeled using 15-node wedge elements. Each element consisted of a 6-node triangle in the horizontal direction and 8-node quadrilateral in the vertical direction. The location of the outer mesh boundaries was selected based on the results of sensitivity analysis to ensure a sufficient distance from the foundation in order to eliminate any possible boundary effects while keeping the required calculation time on mind. A typical mesh discretization used in the analysis is shown in Figure 4-31. Again, the model boundaries were simulated using the standard fixities in PLAXIS (constrained lateral displacements at the mesh sides and total fixity at the bottom).

To simplify the comparison between the results of the 3D models and those of the 2D study, soils and foundations were assigned the same material properties in both cases. The soil profile has been modeled as a homogeneous bed of clay simulated by a Mohr-Coulomb, elastic-perfectly plastic constitutive model. The soil parameters used in the analysis are summarized in Table 4-1. Also, the foundation system (footing and pile) was modeled as very stiff, linear elastic, non-porous material with Poisson's ratio, ν of 0.15

and Young's modulus, E of 10^7 times the soil's elastic modulus. This condition ensured the full rigidity of the foundation in comparison to the surrounding soils.
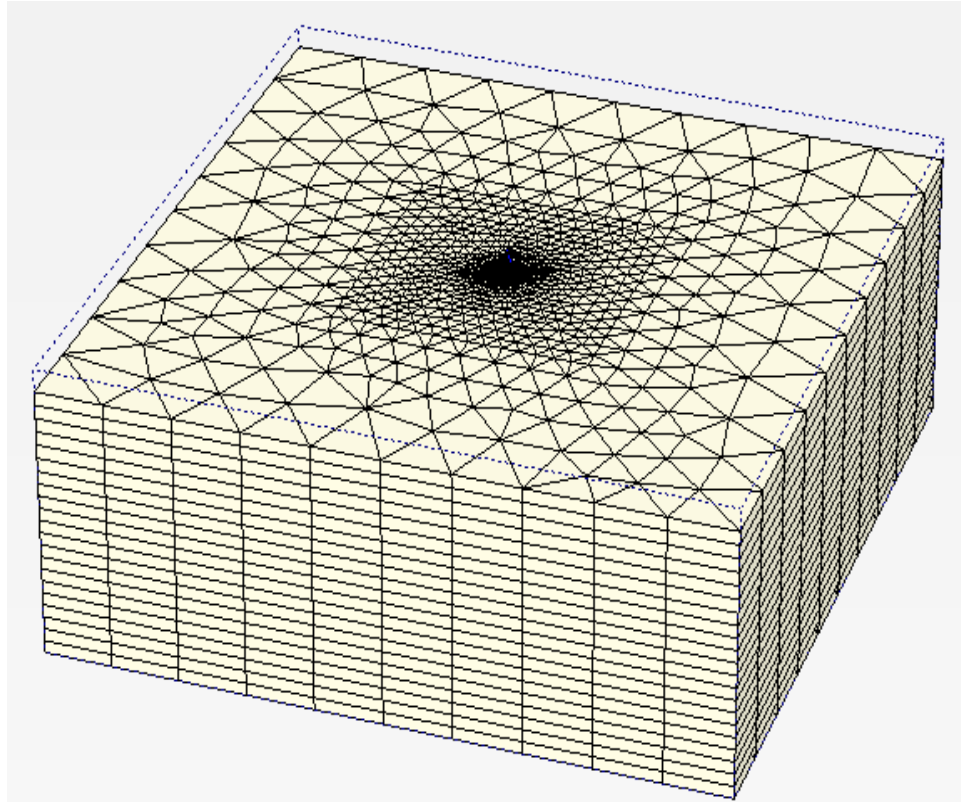
Figure 4-31 Typical mesh discretization applied in the finite element analysis

4.11.2 Load Paths

In the V-H loading space, the load was applied in the form of a single inclined resultant applied at the load reference point previously described. This load resultant was gradually increased until the failure was reached and the V-load and H-load values at failure were plotted as a single point on the V-H failure envelope. The shape of the V-H failure envelope was identified by repeating this same loading procedure using different inclinations of the load resultants. The angle of inclinations of the load resultants varied from a 0.0° angle to the vertical axis (for purely vertical load), to 90.0° (for purely lateral load).

In the *V-M* loading space, the load was applied in the form of a single vertical eccentric resultant. The load eccentricity $e = V/M$, was increased from 0.0 (for the case of purely vertical loading) to 2.25. In each time, the vertical eccentric load was gradually increased until reaching failure and the vertical load and associated moment were plotted as a single point on the *V-M* failure envelope.

In the 3D numerical models, failure load was taken as the maximum load reached in the plot of the load - displacement curves.

4.11.3 Effect of the Geometry of the Hybrid System (*L/W* ratio) on the Lateral Load and Rocking Resistance

The plots of the *V-H* and *V-M* failure envelopes in Figure 4-32 and 4-27 prove that the presence of the short monopile has a minor effect on the maximum vertical capacity of the hybrid system and conform the findings of the 2D models previously discussed in Subsection 4.4.1, with an observed maximum gain in the vertical capacity of no more than 10% at *L/W*=1.

The *V-H* failure envelopes plotted in Figure 4-32 show the significant influence of increasing the pile length on the increased maximum lateral load capacity of the hybrid system. The observed gain in the maximum lateral capacity of the hybrid systems over the circular footing reached 60% and 90% at *L/W* = 0.5 and 1, respectively. The same findings were observed for the 2D plane strain problem of wall footings fitted with a shear key as previously discussed in Subsection 4.5.

The *V-M* failure envelopes plotted in Figure 4-33 show that the rocking resistance of the hybrid system is dependent on the pile length-to-footing width ratio. The observed increase in the maximum rocking resistance of the hybrid systems over the circular footing reached 20% and 130% at *L/W* = 0.5 and 1, respectively. Again, these observations support the findings of the 2D analysis previously discussed in section 4.6.

The normalized *V-H* and *V-M* failure envelopes plotted in Figure 4-34 and 4-29 show that increasing the pile length expanded the size of the normalized failure envelopes and

increased both, the maximum lateral and rocking capacities. However, it should be noted that whereas in a 2D situation, the presence of a relatively short row of piles (shear key) in a wall foundation can dramatically improve the capacity, these effects would be reduced in a 3D situation. This difference in the behavior is attributed to fact that for a circular hybrid system, where the diameter of the pile is 1/10 of the footing width, the action of the shallow foundation is anticipated to dominate the behavior of the hybrid foundation system. Nonetheless, it is safe to conclude that the outcomes of the 2D study are still valid in the 3D modeling. There is still a noticeable effect of increasing the pile length (increasing L/W ratio) on expanding the failure envelopes and increasing the maximum lateral and rocking capacities of the hybrid system.
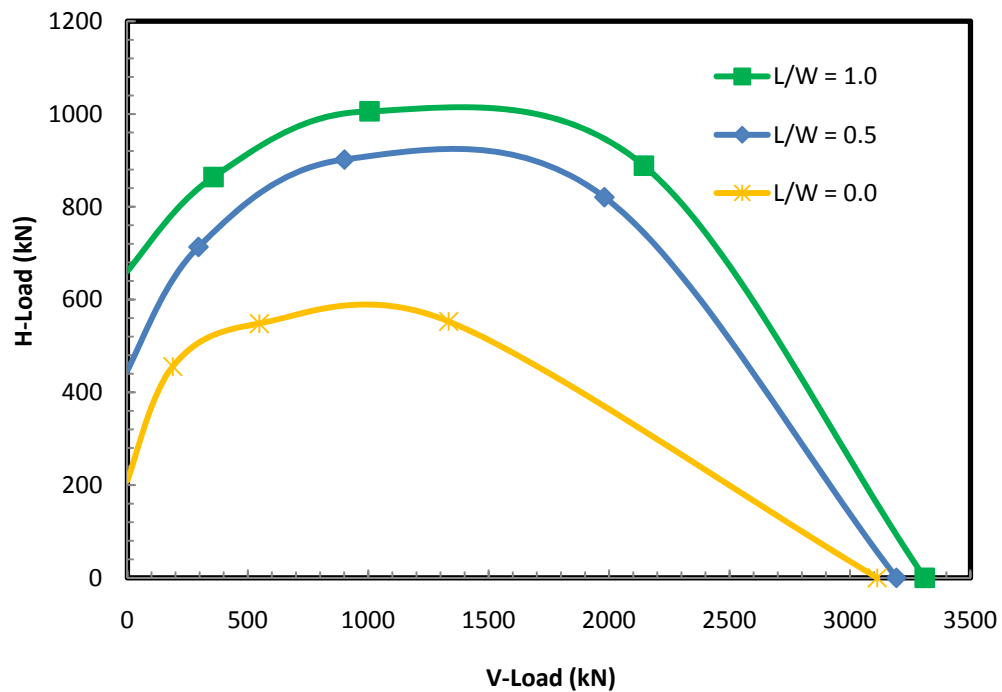
Figure 4-32 Effect of the L/W ratio on the shape of V-H failure envelopes in undrained loading
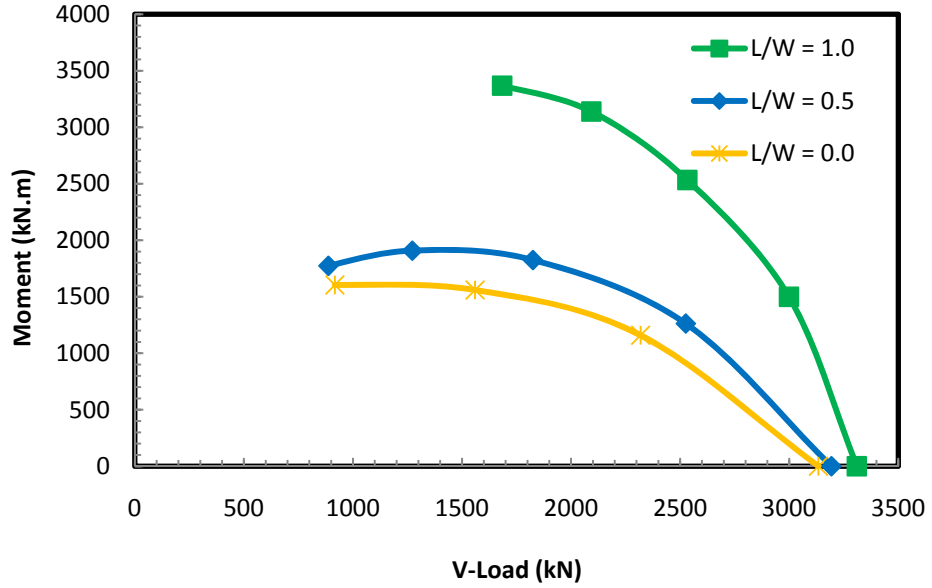
Figure 4-33 Effect of the L/W ratio on the shape of V-M failure envelopes in undrained loading
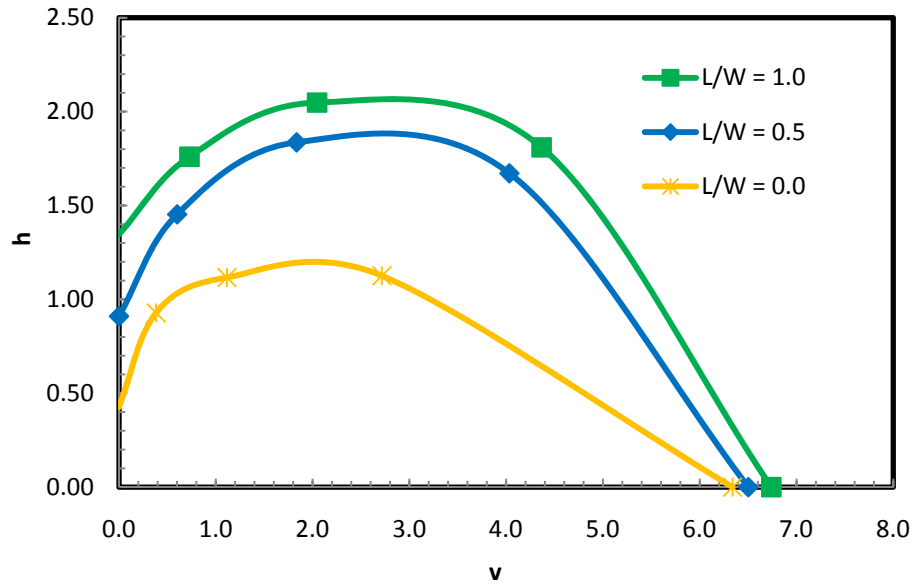
Figure 4-34 Effect of the L/W ratio on the shape of the normalized V-H failure envelopes in undrained loading
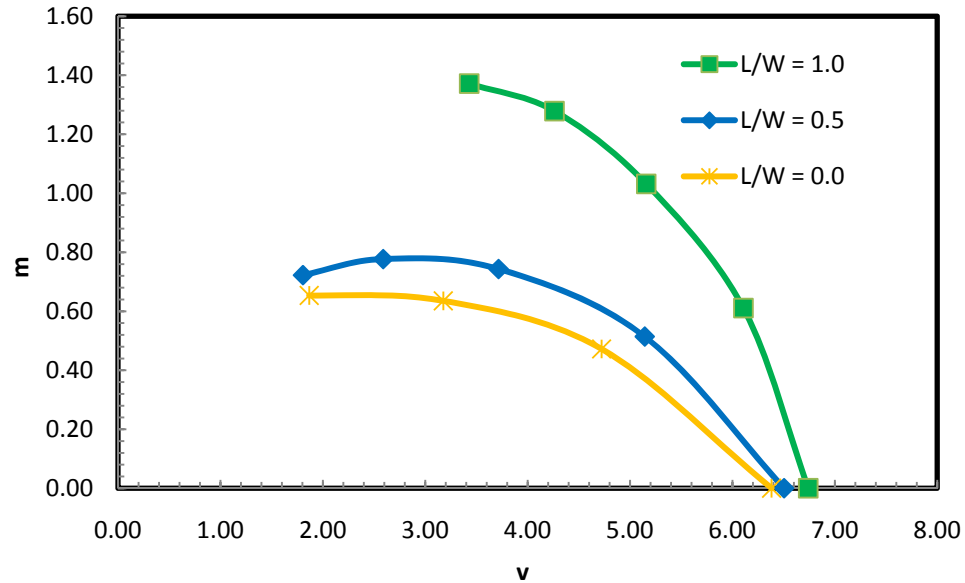
Figure 4-35 Effect of the L/W ratio on the shape of the normalized V-M failure envelopes in undrained loading

4.12 Closed Form Expressions for the V-H and V-M Failure Envelopes

The normalized *V-H* failure envelopes are represented by Equation 4-10, which is capable of describing the failure envelopes of shallow foundations and hybrid systems.

For $v/v_o > 0.3$:

$$\frac{h}{h_o} = 1 + \left(\frac{v}{v_o}\right)^2 \left[0.14 - 1.14\left(\frac{v}{v_o}\right)^2\right] \tag{4-10}$$

The normalized *V-H* failure envelopes of a shallow footing and a hybrid monopile footing foundation at *L/W* ratio of 0.5 and 1.0 are plotted in Figure 4-36.
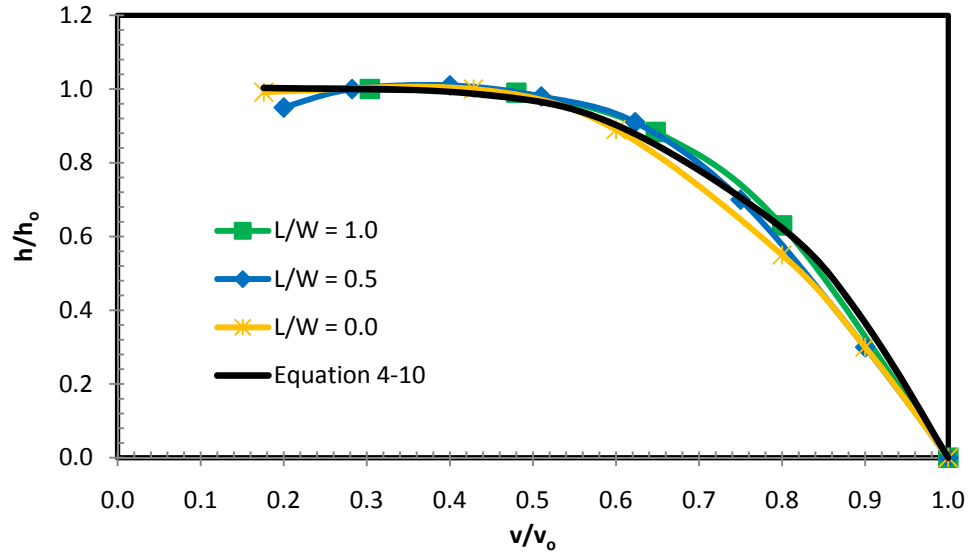
Figure 4-36 Curve fitting of the normalized V-H failure envelopes

Equation 4-11 describes the shape of the normalized *V-M* failure envelopes of shallow foundations and hybrid systems.

For $v/v_o > 0.3$:

$$\frac{h}{h_o} = 0.945 + \left(\frac{v}{v_o}\right)^2 \left[0.485 - 1.423\left(\frac{v}{v_o}\right)^2\right] \tag{4-11}$$

The normalized *V-M* failure envelopes of the shallow footing and the hybrid monopile footing foundation at an *L/W* ratio of 0.5 and 1.0 are plotted in Figure 4-37.
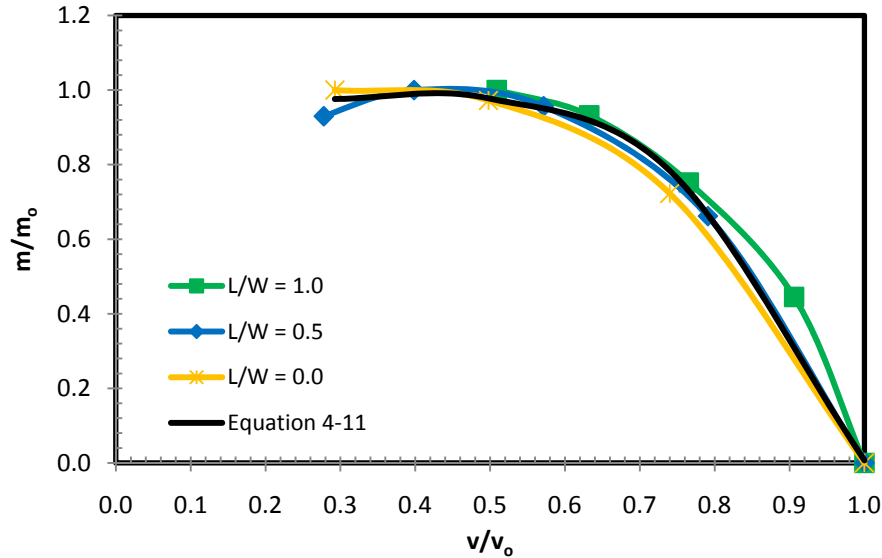
Figure 4-37 Curve fitting of the normalized V-M failure envelopes

4.13 Conclusions

This study has proposed a new shallow footing – monopile hybrid foundation system. The behavior of the hybrid system under general planar load combinations has been characterized through an extensive program of numerical modeling, which produced the following major findings:

The finite element results demonstrated that the presence of a short monopile ($L/W \leq$ 0.5) has an insignificant effect on the maximum vertical capacity and the vertical stiffness of the hybrid system. A minor gain in the vertical capacity of the system of about 10% can be achievable at $L/W = 1$. The study also revealed that the vertical resistance of the hybrid system does not depend on the foundation-soil interface conditions (fully bonded versus instant breakaway).

Adding a short shear key to a wall footing ($L/W = 0.25$) can increase the resistance to sliding by 60% to 135% (for instant breakaway and fully bonded conditions respectively), however it would slightly reduce the rocking resistance. This improvement reached 150% to 290% at $L/W = 0.5$, and up to 400 to 500% at $L/W = 1.0$ (for instant breakaway and fully bonded foundation-soil interface, respectively). In a circular hybrid system, where the diameter of the pile is 1/10 of the footing width, the action of the

shallow foundation is expected to dominate the behavior of the hybrid foundation system; the improvement in the lateral capacity was reduced to 60 and 85% at L/W equals 0.5 and 1.0, respectively.

The gain in the rocking resistance of the hybrid system can be achieved by having a minimum L/W ratio of 0.5. The pile must be long enough to extend outside of the original failure zones of the shallow footing, which triggers wider and deeper soil failure mechanisms and provides higher capacities. The gain in the maximum rocking resistance was 20% to 34% at $L/W = 0.5$, and 100% to 144% at $L/W = 1$ (for instant breakaway and fully bond conditions, respectively).

In plane strain loading conditions, a hybrid system of $L/W \geq 0.25$ produced a maximum rocking resistance falling slightly below the resistance of the un-stiffened shallow footing. On the other hand, the system had a superior initial rocking resistance at low V/V_{max} values. This is particularly advantageous when the loading conditions involve a relatively small vertical load accompanied by significant lateral loads. This initial gain in the rocking resistance at low V/V_{max} values is not expected for circular hybrid systems. The achieved gain in the rocking resistance was 20 and 135% at $L/W = 0.5$ and 1.0, respectively.

At $V/V_{max} < 0.4$, the shape and size of the generalized V-H and V-M failure mechanisms are highly affected by the condition of the foundation-soil interface, which is in contrast to the case of high V-load values.

The study suggests that the use of hybrid foundations systems, such as the one investigated here, may provide viable alternatives to conventional laterally loaded foundations. However, further work needs to be conducted on a wider range of materials, cyclic and monotonic load cases and for full three dimensional conditions.

4.14 References

Bienen, B., Byrne, B. W., Houlsby, G. T. & Cassidy, M. J. (2006). Investigating six-degree-of-freedom loading of shallow foundations on sand. Geotechnique, 56 (6): 367-379.

Bransby, M. F. and Randolph, M. F. (1998). Combined loading of skirted foundations. Geotechnique, 48 (5): 637-655.

Brinkgreve, R.B.J. (2002). PLAXIS user's manual - Version 8.2. Delft University of Technology and PLAXIS b.v., The Netherlands. ISBN 9058095088.

Butterfield, R., Houlsby, G. T. and Gottardi, G. (1997). Standardized sign conventions and notation for generally loaded foundations. Geotechnique, 47(5): 1051-1054.

Byrne, B.W. and Houlsby, G.T. (2002). Investigating novel foundations for offshore wind turbines. *In* proceedings of the 21st International Conference on Offshore Mechanics and Arctic Engineering (OMAE'02), Oslo, Norway, Paper No. OMAE2002-28423.

Byrne, B.W. and Houlsby, G.T. (2003). Foundations for offshore wind turbines. *In* proceedings of the Philosophical Transactions of the Royal Society of London, Series A, 361, pp. 2909-2930.

Frydman, S. and Burd, H.J. (1997). Numerical studies of bearing capacity factor $N\gamma$. Journal of Geotechnical and Geoenvironmental Engineering, ASCE, 123(1): 20-29.

Georgiadis, M., and Butterfield, R. (1988). Displacements of footings on sand under eccentric and inclined loads. Canadian Geotechnical Journal. 25(2): 199-212.

Gottardi, G., and Butterfield, R. (1993). On the bearing capacity of surface footings on sand under general planar load. Soils and Foundations. 33(3): 68-79.

Gottardi, G., Houlsby, G. T. & Butterfield, R. (1999). Plastic response of circular footings on sand under general planar loading, Geotechnique, 49(4): 453-469.

Gourvenec, S. and Randolph, M. F. (2003). Effect of strength nonhomogeneity on the shape and failure envelopes for combined loading of strip and circular foundations on clay. Geotechnique, 53(6): 575-586.

Hansen, J. B. (1970). A Revised and Extended Formula for Bearing Capacity. Available from the Danish Geotechnical Institute, Copenhagen, Bul. No. 28, 21 pp. (successor to Bul. No. 11).

Horvath, J.S. (1991), Effect of footing shape on behaviour of cantilever retaining wall. Journal of Geotechnical Engineering, 117(6): 973-978.

Houlsby, G. T. & Puzrin, A. M. (1999). The closed-form solutions for the bearing capacity of strip footing under combined loadings. *In* Proceedings of the Royal Society Conference, London, UK, pp. 893-916.

Loukidis, D., Chakraborty T., and Salgado R. (2008), Bearing capacity of strip footings on purely frictional soil under eccentric and inclined loads. Canadian Geotechnical Journal, 45(2): 768-787.

Martin, C.M. and Houlsby, G.T. (2000). Combined loading of spudcan foundations on clay: laboratory tests. Geotechnique, 50 (4): 325-338.

Martin, C.M. and Houlsby, G.T. (2001). Combined loading of spudcan foundations on clay: numerical modelling. Geotechnique, 51(8): 687-699.

Stone, K., Newson, T. and Sandon, J. (2007). An Investigation of the Performance of a 'Hybrid' Monopile-Footing Foundation for Offshore Structures. *In* Proceedings of the 6th International Offshore Site Investigation and Geotechnics Conference, London, UK, 391-396.

Tan, F. S. C. (1990). Centrifuge and theoretical modelling of conical footings on sand. Ph.D. thesis, University of Cambridge, London, UK.

Vesic, A. S. (1975). Bearing capacity of shallow foundations, Chapter 3. *In* Foundation Engineering Handbook. *Edited by* H. F. Winterkorn and H.-Y. Fang. Van Nostrand Reinhold Co., New York, N.Y., U.S.A., pp. 121-147.

White, D. J., Teh, K. L., Leung, C. F. & Chow, Y. K. (2008). A comparison of the bearing capacity of flat and conical circular foundations on sand. Geotechnique, 58(10): 781-792.

Zaaijer, M.B. (2003). Comparison of monopile, tripod, suction bucket and gravity base design for a 6 MW turbine. *In* Proceedings of the European Seminar on Offshore Wind energy in Mediterranean and Other European Seas, OWEMES-2003, Naples, Italy.

Chapter 5

5 Physical Centrifuge Testing of Hybrid Monopile-Footing Foundation Systems on Drained Sands

The growth of the wind energy sector in Canada has been very rapid and the majority of wind farms constructed so far have been onshore. However, the growing opposition to the construction of wind farms in suburban areas has led to the delay or cancellation of many projects, prompting a threat to Ontario's energy security. For this reason, the strategic switch to the development of offshore wind farms in the Great Lakes is a promising opportunity for further significant energy generating projects and allows the access to highly desirable wind environments.

The economic viability of offshore wind is highly dependent on the installation costs and so the selection of a suitable foundation design is a crucial factor in the economic viability of a wind farm. The requirements for such foundations are more demanding than for onshore developments, since they will experience complex loading patterns as the result of combined wind, wave, currents and self weight loading effects, all of which must be accommodated with sufficiently small displacements to maximize the operational envelope of the turbines.

Currently, there are several types of foundation systems available to the designer of offshore wind turbines. The preferred foundation system will be dependent on the local seabed soil conditions and size of the turbine. Generally speaking, the choice will be between surface or near surface type foundation solutions, such as gravity base or suction caisson systems (including tripods), or large diameter mono-piles. Gravity bases can be quite large, with typical diameters of 10 to 20 m and weights of up to 2000 tons. On the other hand, monopiles are typically made of very large steel pipes with a diameter of 3 to 4m or more and length of 20m to 35m (Bransby and Randolph, 1998). Since both foundation types require substantial installation equipment, jack-up barges or ship hire, both foundation types are expensive to install and this often constitutes the major component of wind farms installation costs. Hence a reduction in the width or length of

foundations required to resist these complex loading cases has significant economic benefits.

Clearly there is scope to develop foundation systems, which are more efficient, economic and satisfactory for the particular case of resisting the combined loading induced by a wind turbine. One such approach is to develop foundation systems which combine several foundation elements to create a 'hybrid' system. This study concerns the investigation of such a 'hybrid' foundation system, which combines a mono-pile and circular footing or foundation plate to produce a 'hybrid' monopiled-footing arrangement (as displayed in Figure 5-1).
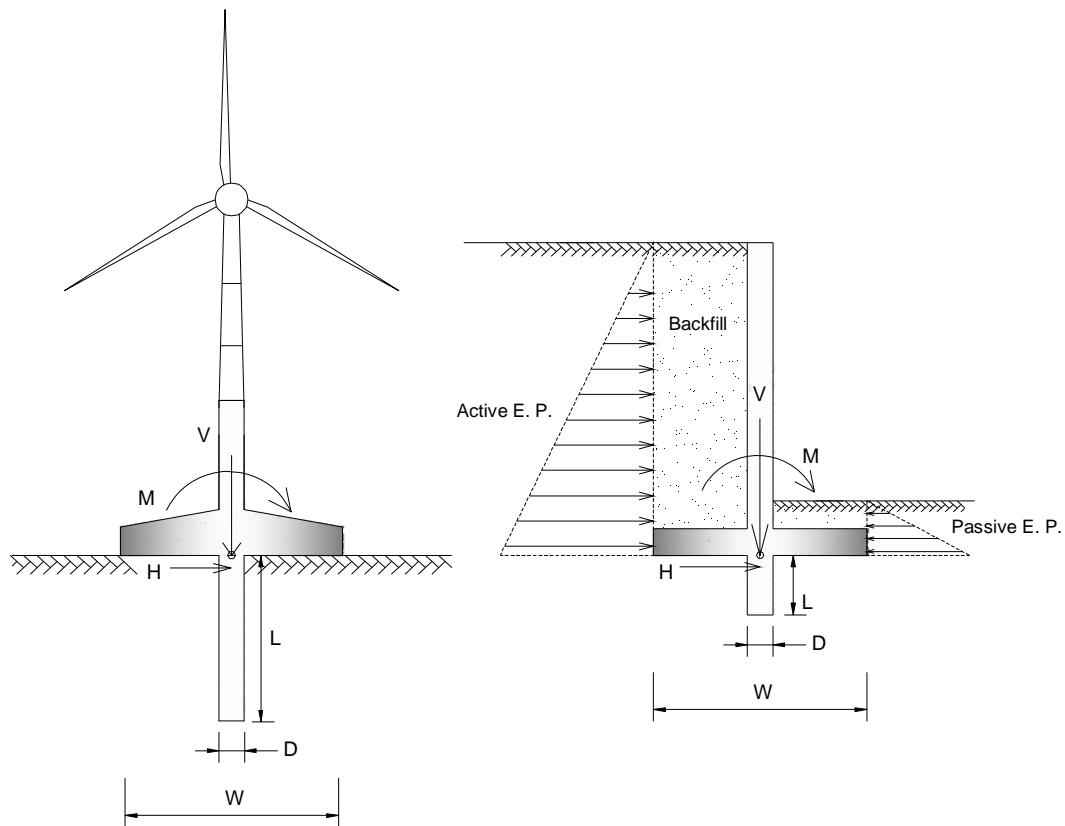
Figure 5-1 Examples of laterally loaded structures supported on the proposed hybrid system

Despite the apparently obvious advantages of such hybrid systems, with the exception of recent work reported by Stone *et al.,* (2007), which has indicated that the lateral capacities of a single pile can be considerably increased through the use of a foundation plate, there is no information available in the literature to suggest that such systems have been explicitly studied. On the other hand, there is a significant body of literature available in respect to the component elements i.e. a pile and surface footing. In particular, research on the response of shallow foundations to combined loading (Bransby and Randolph, 1998; Houlsby and Puzrin, 1999; Gourvenec and Randolph, 2003). Similarly, several methods for the analysis of piles, and in particular their response to lateral loads have been developed (e.g. Matlock and Reese, 1960; Broms, 1964; Poulos, 1971; Reese *et al.,* 1974; Randolph 1981; Duncan *et al.,* 1994; Zhang *et Al.,* 2005).

The proposed foundation system has 2-dimensional analogy in the case of a retaining wall with a stabilizing base (Powrie and Daly, 2007), and in 3-dimensional case that of a single capped pile. Poulos and Randolph (1983) developed methods for analyzing the relative influence of the pile and pile cap under axial loading, and some studies of the influence of the pile cap on the lateral performance of single piles has also been reported by Kim *et al.,* (1979), Mokwa and Duncan (2001, 2003) and Maharaj (2003). The dimensions of pile caps are generally relatively small, but the role they play in determining restraint conditions at the pile head is significant. It has also been demonstrated that for individual piles, the presence of a relatively thick pile cap can provide a significant contribution to lateral resistance through the development of passive soil wedges. A similar resistance mechanism develops where a skirt is present (Bransby and Randolph, 1998).

It should also be noted that a 'hybrid' foundation system composed of a monopiled-footing is an attractive combination from an installation point of view since the plate can be located first, and then used as a sea-bed guide for the installation of the pile, although the reality of such a procedure remains to be investigated. Furthermore, it has also been suggested (Stone *et al.,* 2007) that existing monopile turbine towers could be retrospectively fitted with footing or stabilizing plates as a way of upgrading their capacity to carry larger (heavier) generators.

The overall aim of this study is to undertake a 'proof of concept' or feasibility study of a novel foundation system for wind turbines. Canada's natural abundance of potential wind farm sites makes wind energy a particularly attractive source of renewable energy. The proposed 'hybrid' monopiled-footing foundation system has the potential to significantly improve the performance of current turbine foundation design while minimizing the installation costs and time. The proposed test program follows on from studies previously reported (Stone *et al.,* 2007), which demonstrated that combining a foundation plate to the mono-pile, provides additional vertical capacity provides as well as significant increase in lateral capacity and stiffness over that of a single pile.

The model tests are intended to investigate the influence of the bearing plate on the lateral load response of the monopile. The centrifuge model was instrumented with strain gauges to provide some qualitative information concerning the contribution to lateral resistance from the soil reaction on the pile. The lateral resistance contributed by the bearing plate can then be deduced by considering the overall lateral capacity of the combined pile and bearing plate.

The study proposed here is directly relevant to those working in this industry since it explores a methodology towards adapting existing offshore design (from the oil and gas industry) to the particular requirements of wind turbines. In terms of economic value, the wind energy sector is now firmly established as one of the largest sectors in the energy market. There is no doubt that any technological advantage for Canada in the wind energy sector would result in significant economic gains to Ontario and Canada. The project also has much relevance to the oil and gas industry where the operating requirements (tolerable displacements) are less severe.

5.1 Centrifuge Modeling

The behavior of soils is highly non-linear and dependent on the stress and strain conditions. For this reason, using small-size models in scaled experimental testing under 1-g conditions cannot reproduce the prototype behavior. This discrepancy is attributed to the stress levels produced by self-weights in a scaled test, which are much lower than those in a field scale prototype. Centrifuge testing recreates true prototype behavior by

producing the same stress and strain level within the scaled model by testing a 1:N scale model at N times earth's gravity, created by centrifugal force.

It should be noted that all the results and dimensions are expressed at model scale and can be easily converted to prototype scale using the scaling factors shown in Table 5-1.

Table 5-1 Scaling Factors

Quantity	Ratio*
Length	1/N
Stress	1
Strain	1
Mass Density	1
Gravity	N
Mass	$1/N^3$
Force	$1/N^2$
Stiffness	1/N

*Ratio: model value / prototype value.

5.2 Beam Centrifuge at London Geotechnical Centrifuge Centre

The centrifuge model tests were conducted in the London Geotechnical Centrifuge Centre at City University (London, UK) on an Acutronic 661 balanced beam centrifuge (displayed in Figure 5-2). This centrifuge has a platform radius of 1.8 m and a capacity of 40 g tons. Payloads up to a mass of 200 kg can be accelerated to 200 g. The swinging platform has a plan area of 700 x 500 mm. The full description of the balanced-beam centrifuge can be found in Schofield and Taylor (1988). The beam centrifuge operates with the model package on the swinging platform and balanced counterweights on the other. The centrifuge model is first prepared outside the centrifuge pit, then transferred to the swinging platform and mounted on the beam centrifuge using a crane. The swinging platform swings outwards and upwards as the centrifuge arm gains speed, consequently the direction of the resultant acceleration field passes through the pivot and the centroid of the package.
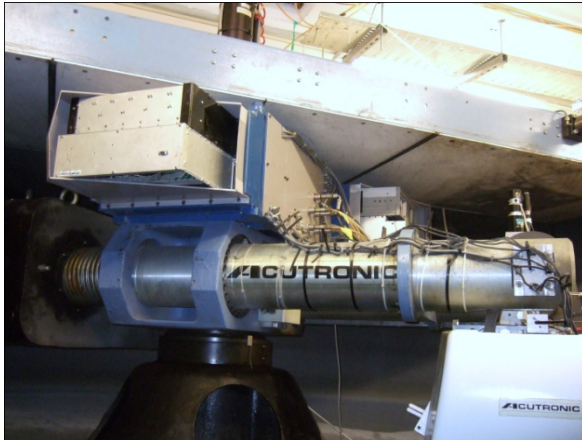
a) Centrifuge beam and central axis
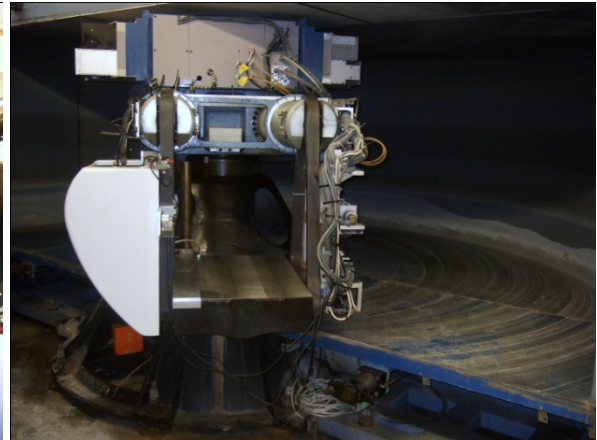
b) Swinging platform
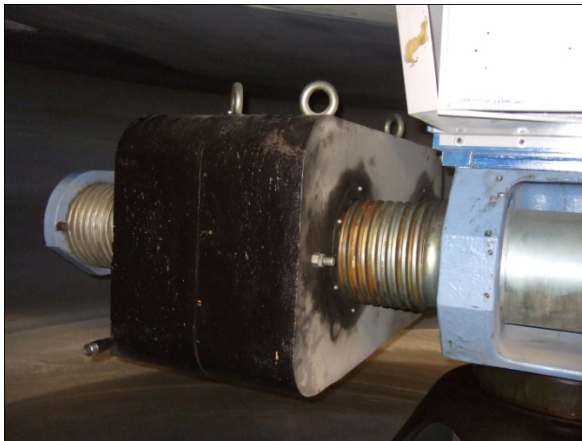
c) Counterweight

d) Centrifuge chamber

Figure 5-2 Acutronic 661 balanced beam centrifuge at the Centre for Geotechnical Modeling of City University, London, UK

5.3 Centrifuge Test Program

The testing program consisted of six centrifuge tests carried out on a model scale of 1/50 at a nominal centrifugal acceleration of 50g. The testing program was aimed to study the behaviour of monopiled-footing hybrid systems under pure vertical loading and combined vertical, horizontal and moment loading. In addition, the behaviour of the constituent elements of the hybrid system (i.e. pile and foundation plate) was tested for

comparison. Table 5-2 summarises the test program giving information on the pile's embedment length and the initial dead weight applied as a vertical load during the tests.

Table 5-2 Summary of centrifuge model tests

Test ID	Test Type	Pile Embedment (mm)	Vertical Load (N)
FV	Footing only - vertical load	N/A	N/A
PV	Pile only - vertical load	200	N/A
PL1	Pile only - lateral load	180	600
HL1	Hybrid system	180	600
HL2	Hybrid system	180	1100
HS1	Hybrid system	50	600

5.4   Materials and Model Preparation

5.4.1   Fraction D Silica Sand

The sand used in this study was a rounded to sub-rounded fine grained, uniformly graded, silica sand with an average particle size of 0.25 mm (Fraction D from David Ball UK Ltd.). The maximum and minimum void ratios were determined to be 1.06 and 0.61 respectively and $Gs = 2.65$, which corresponds to dry unit weights of 12.6 and 16.1 kN/m^3. The critical state friction angle, determined from direct shear testing, was 32°. The complete properties of Fraction D sand are listed in Table 5-3.

Table 5-3 Soil Properties

Properties	Value	Unit
D_{10}	0.20	mm
D_{50}	0.27	mm
D_{90}	0.32	mm
e_{max}	1.06	n/a
e_{min}	0.61	n/a
Critical angle of friction, ϕ_{crit}	32	Degree
Specific gravity of solids, G_s	2.65	n/a

5.4.2   Model Foundation

The model pile was fabricated from a 19 mm diameter thin-walled, open-ended steel tube (t=0.5 mm) and was instrumented with foil strain gauges at four locations along its length (refer to Figure 5-3). The bearing plate was 100 mm in diameter and formed from a 5mm thick aluminum plate with a clamping arrangement allowing the location of the plate to be varied in relation to the pile, i.e. the length of pile protruding below the plate can be adjusted (refer to Figure 5-3).
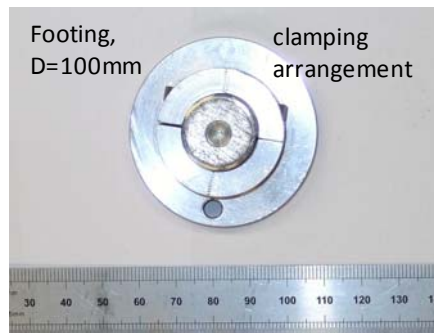
a) Plate Footing
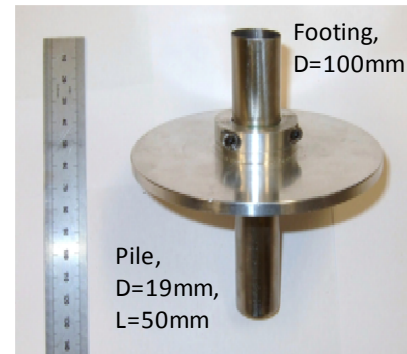
b) Short Hybrid System
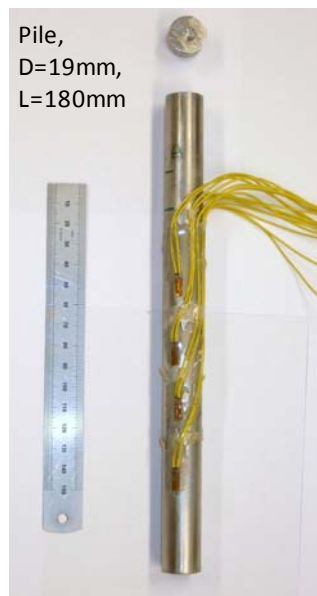
c) Instrumented Pile

d) Long Hybrid System

Figure 5-3 Model Foundations

5.4.3   Calibration of Model Foundation

In view of the fact that the calibration of transducers in centrifuge model testing does not change during the test regardless of the acceleration, the calibration of model foundation system for bending in the pile was performed at 1g prior to centrifuge testing. All load cell transducers were calibrated in the appropriate data-logging channels on the centrifuge and not with any other source of amplification or signal conditioning. This involved clamping the bearing plate vertically to a rigid support. The instrumented pile was then loaded as a cantilever beam by the application of discrete weights, and the output from the strain gauges was recorded. Since the strain gauges are located on opposite external faces of the pile their signal can be subtracted to eliminate the effect of axial loading.

5.4.4   Soil Model Preparation

The first stage of model preparation involved the formation of the soil test bed, which was undertaken using air pluviation of dry Fraction D silica sand at a controllable drop height over two large sieves overlying a 420 mm diameter circular container. This procedure insured the formation of a medium dense homogeneous sand bed with a unit weight of 13.7 kN/m^3, void ratio of 0.89 and a relative density of 36%. On completion of pouring the sand bed, the container was mounted onto the centrifuge platform and the surface of the sand bed was carefully leveled.

5.4.5   Model Installation

The model foundation was installed in the soil bed by pushing the pile by hand to about 80% of its desired penetration depth and then final driving of the pile was accomplished by light tapping with a hammer to the desired depth of installation. For tests involving the combined pile and bearing plate, care was taken while placing the bearing plate to ensure a firm contact with the soil surface upon completion of installation. For tests when only the single pile response was required, the bearing plate was fixed to the pile shaft some 20-25 mm clear of the soil surface.
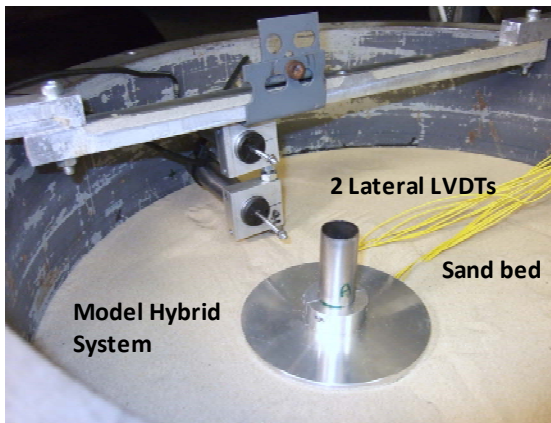
a) Centrifuge model embedded in sand
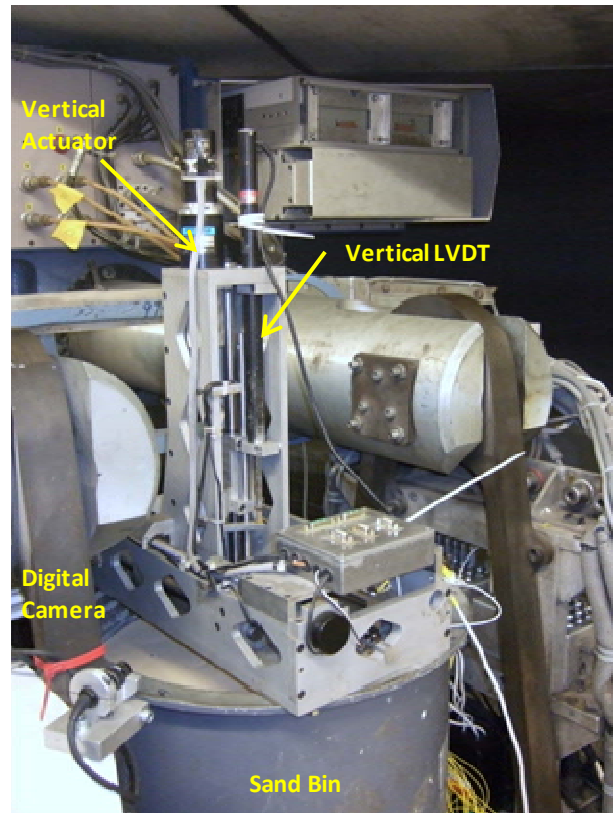
b) Actuator mounted on soil bin

Figure 5-4 Model foundation installation and test setup

5.4.6   Centrifuge Modeling Considerations

According to Taylor (1995), in a typical centrifuge test there are some sources of error that may affect the integrity of the results, which include the reproducibility of the prepared model, the acceleration history, deviation of acceleration from the prescribed value, boundary conditions such as the loading system, base roughness and freedom of movement of the foundation. Gemperline (1988) reported a deviation in the test results by up to 9.5% based on the results of 26 centrifuge tests.

The vertical response of a pile is highly sensitive to the installation procedure. Installing the pile in flight can establish a stress regime in the soil surrounding the pile that is comparable to the field prototype. Up to 50 % of reduction in the vertical capacity can

result of 1g installation (Taylor, 1995). The testes carried on piles installed at 1g are still capable of giving an insight on the system response and can be used in a comparative study; however these results require special care in the analysis.

For laterally loaded piles installed at 1g, the effect of pile installation is generally less pronounced. Craig (1984) reported a reduction in the observed lateral capacity of up to 10% for piles installed at 1g as opposed to installations at 52.5g. Craig (1984) also concluded that the installation effect on the overall behaviour of the laterally loaded pile is less significant.

5.4.7   Load Tests

In pure vertical loading tests (FV and PV), the actuator shown in Figure 5-5 was used to push the foundation with a predetermined constant rate of strain, while a vertical LVDT was used to track the vertical displacement. In the remaining tests the lateral loading of the model foundation was provided using a steel wire looped around the pile and connected to a lateral load actuator (as displayed in Figure 5-5b). At the same time, the vertical loading was provided using dead weights placed on a bearing plate fixed at the top of the pile shaft. Two linear variable differential transformers (LVDT) were used to record the lateral displacement at the pile head.

b) Plan view showing dead weights and lateral LVDTs

a) Actuator mounted on top of the
soil container
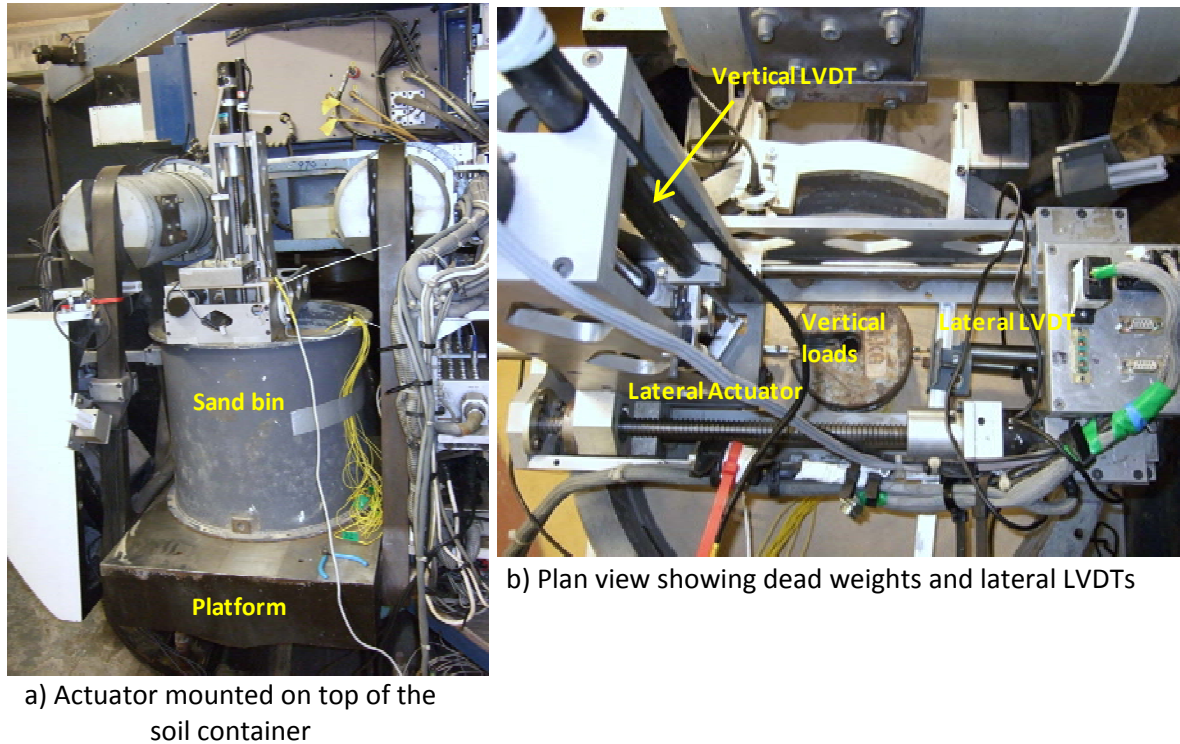
Figure 5-5 Testing setup for the centrifuge load tests

5.5   Results of Centrifuge Model Testing

5.5.1   Vertical Loading

To obtain basic information on the vertical capacity of the pile and the bearing capacity of the plate, vertical loading tests were conducted. Due to the limitations of the actuation system it was necessary to estimate the ultimate bearing capacity of the foundation plate using a smaller, 50mm, diameter plate. Figure 5-6 shows the results of the two vertical loading tests (refer to Table 5-2). The ultimate capacity of the bearing plate can be estimated to be between 880 and 1250 N (line FV), depending on the methodology used. These equate to ultimate bearing stresses of 448-637 kPa and back analysis with the bearing capacity equation (Terzaghi, 1943) gives values of the bearing capacity factor $N\gamma$ of 44 to 62. These bearing capacity factors correspond to mobilized friction angles of 36 to 38 degrees for rough foundations (Davis & Booker, 1971; Hansen, 1961). Allowing for increasing capacity with settlements (Ovesen, 1975) and stress level related dilation effects (Kimura *et al.*, 1985), this seems reasonable for this loose material state. Given

the same foundation behavior, the ultimate capacity of the larger 100 mm diameter bearing plate would therefore be within the range of 4480 to 6365 N.
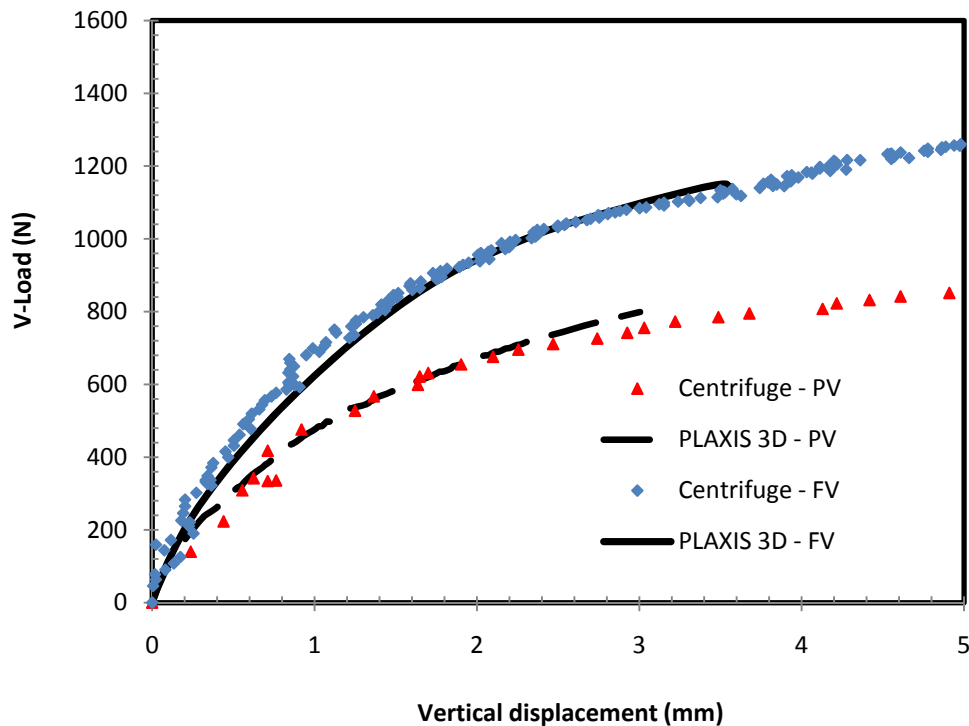
Figure 5-6 Vertical load vs. vertical displacement for 50mm diameter plate (FV) and single pile (PV)

From the same plot, it is apparent that the ultimate capacity of the pile is approximately 850 N (line PV). Back analysis using the pile equation (Meyerhof, 1976; Berezantsev *et al.*, 1961) and assuming only skin friction (i.e. no plugging of the open pile), gives a mobilized friction angle of 32-33°. This agrees well with the observations of Craig and Sabah (1994) who found that mobilized pile friction angles fell between the peak and critical state friction angles.

5.5.2   Combined Loading

The results of the combined vertical and lateral loading tests are best represented through plots of lateral load versus lateral displacement for a given vertical load level. Figure 5-7 presents the lateral load versus lateral displacement for the hybrid monopiled footing (HL

1) and single pile (PL 1) with a vertical load of 600 N at 50 g. The horizontal loads were applied at 30 mm above the ground level, giving eccentricities e/L for these foundations of 0.17. It is apparent from this plot that the initial lateral stiffness of the monopiled footing and pile are similar for the first 1 - 1.5 mm of lateral displacement. However, the hybrid monopiled footing continues to exhibit a stiffer response than the single pile as the lateral displacement increases.

When the lateral capacity of the soil adjacent to the pile is fully mobilized, solutions of Zhang *et al.* (2005) or Broms (1964) solution for 'short' piles in cohesionless soils can be applied. Assuming a friction angle of 32°(with the appropriate L/D ratio) for the two pile systems, suggests that the behavior of the hybrid system falls between a fully restrained pile and one with $e/L = 0$, whereas the pile alone behaves in a manner consistent with a pile foundation loaded horizontally with the appropriate eccentricity. This also suggests a reduction in rotation of the hybrid pile system as it begins to fail, since a fully restrained pile would be expected to fail in horizontal translation, rather than rotation.
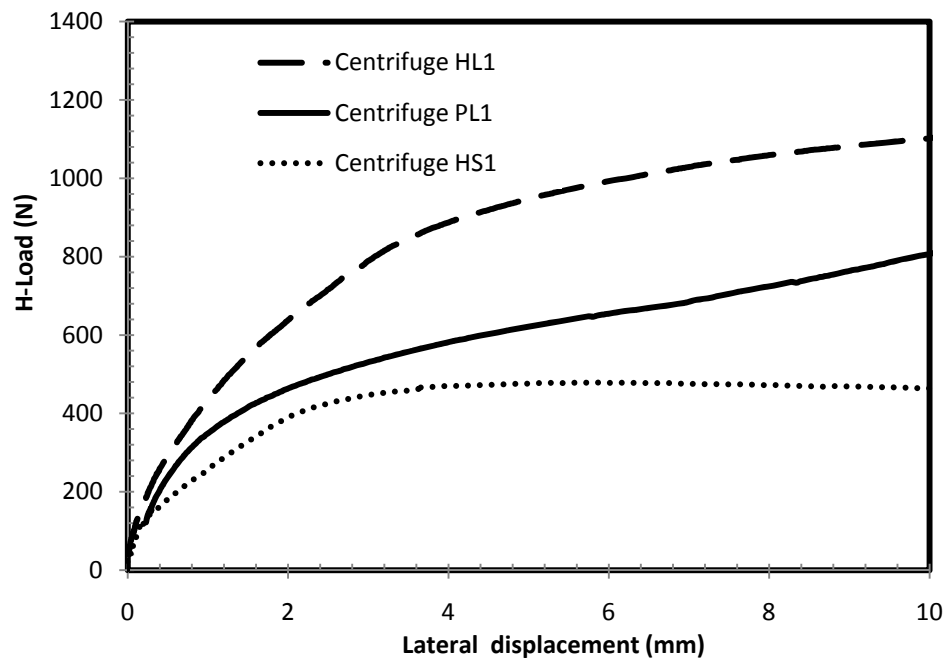
Figure 5-7 Lateral load vs. lateral displacement response for monopile-footing (HL1) and single pile (PL1) with a vertical load of 12N

Also presented in Figure 5-7 is the response for a hybrid footing with a short 50mm pile embedment depth (HS1). Unfortunately, no data are available for the lateral response of the single short pile, although the use of Broms approach again suggests a behavior somewhere between a fully restrained pile and one loaded horizontally at the surface (*e/L* = 0.6). It is also apparent from the shorter pile behavior that the embedment depth has a significant influence on the lateral response of the monopiled footing and highlights the significant influence that the geometry of the respective foundation elements have on the response of the foundation system.

5.5.3   Bending Moments

Figure 5-8 presents the measured bending moment distribution along the instrumented pile as determined from the readings of the strain gauges installed along the pile for test HL1 (pile with bearing plate) and test PL1 (pile only). The bending moment distributions were plotted at pile head displacements through the testing progress. The distributions plotted in Figure 5-8 were measured at pile head displacements-to-pile diameter ratios of 0.05, 0.1, 0.2 and 0.4. From these data, it is apparent that the pile bending moment increases more rapidly in the pile only case.

Figure 5-9 presents the measured bending moments for test HL1 (pile with bearing plate) and test PL1 (pile only) against the applied lateral load. The plotted moments represent the observed moment readings of the strain gauges that were taken at 4 different levels along the pile shaft, at depths of 4D, 6D, 7.5D and 9D below the pile head level. From these data, it is apparent that the flattening out of the moment curve is consistent with a rotational failure mechanism of the pile as the lateral resistance of the soil is exceeded. A less rapid increase in the pile bending moment is observed with the bearing plate present. It is also apparent that the presence of the bearing plate leads to the generation of higher moments in the pile as the plate rotates into the soil surface. The rigid connection between the pile and the bearing plate results in the transfer of the moments, developed by the rotating plate into the pile, such that even as the ultimate lateral resistance of the foundation is being reached, bending in the pile is still increasing.
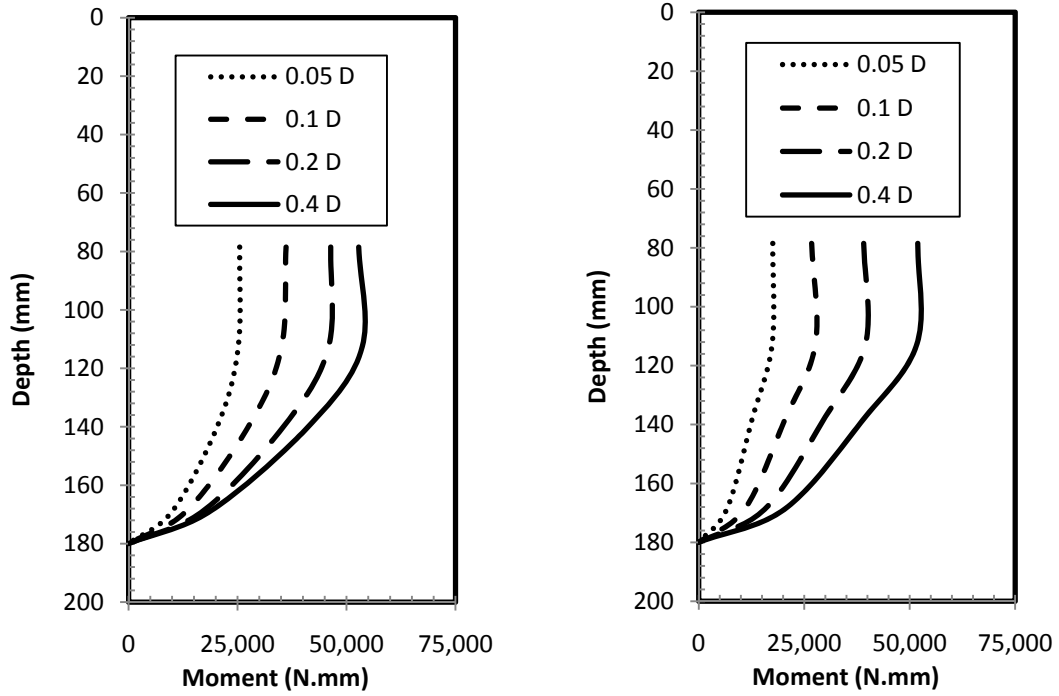
a) Bending moment profile for Pile only (PL1)   b) Bending moment profile for Hybrid system (HL1)

Figure 5-8 Bending moment profiles at various pile head displacements for: a) Pile only (PL1) and b) Hybrid system (HL1)
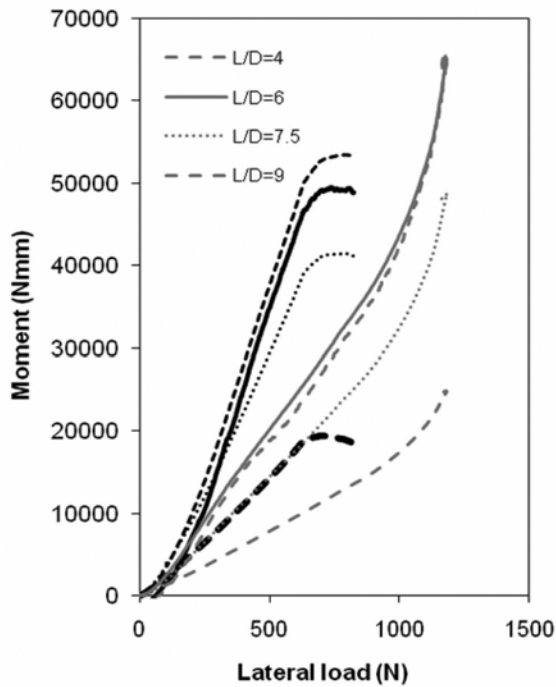
Figure 5-9 Pile bending moment vs. applied lateral load (black lines for single pile, grey for pile with bearing plate)

5.6 3D Numerical modeling of the centrifuge testing results

The results of the centrifuge tests were simulated in a 3D numerical model using the software PLAXIS 3D Foundations. In the numerical models, the material parameters and the characteristic parameters of the foundation soil interface were established from the interpretation of the centrifuge test results. The soil has been modeled as a uniform bed of drained sand simulated by a Mohr-Coulomb, elastic-perfectly plastic constitutive model. The sand parameters used in the analysis are summarized in Table 5-4 below. The foundation was modeled at the prototype scale; the plate footing was modeled as a 2500 mm diameter, 250 mm thick aluminum plate of $E = 70$ GPa, $v = 0.2$ and $\gamma = 27$ kN/m^3. The pile was modeled as a 475 mm diameter, 25 mm thick, open ended, hollow steel pipe of $E = 210$ GPa, $v = 0.1$ and $\gamma = 77$ kN/m^3 .

Table 5-4 Soil parameters implemented into PLAXIS 3D model

Properties	Value	Unit
Saturated Unit Weight	13.6	kN/m^3
Young's Modulus, E	2850	kN/m^2
Poisson's Ratio, v	0.3	N/A
Cohesion Stress, c	0.01	kN/m^2
Critical Friction Angle, ϕ_{cr}	32	Degree
Dilatancy Angle, ψ	1 – 6*	Degree
Material Model	Mohr-Coulomb	N/A

For the vertical loading tests (tests PV and FV), the load tests were modelled in three loading stages. The first stage represented the in-situ soil conditions before the foundation installation. In the second loading stage, the foundation construction was simulated, and finally in the third loading stage the vertical load was gradually increased until reaching failure. The vertical load was applied in the form of a uniform vertical stress applied on an annulus area fixed on the pile at an elevation of 1500 mm above the sand surface. This was the loading technique adapted in the centrifuge tests; moreover this procedure prevents the formation of highly concentrated stresses as a shadow effect of using a single concentric point load. For the combined loading tests, the same modeling methodology was adapted; however the loading was applied over 2 separate stages; in the first loading stage the vertical load was applied with the same previously described methodology, whereas in the second loading stage, lateral distributed stresses

were gradually increased over the loaded area, while the vertical stresses were kept constant.

Figure 5-6 shows the results obtained from the 3D numerical model, plotted alongside with the measured load displacement curves of the centrifuge curves. The 3D numerical models were capable of simulating both the initial vertical stiffness and the ultimate capacities in the two modeled cases.

The lateral load – lateral displacement curves produced by the 3D numerical analysis are plotted in Figure 5-10 below. The numerical models showed a stiffened response for the hybrid system from the initial loading stages. This may be attributed to preloading the hybrid foundation system in the construction and vertical loading stages, prior to the lateral loading stage. This preloading insured the generation of contact stress below the footing, which insured the engagement of the footing action from the initial stage of the lateral loading. As previously mentioned, the installation procedures have an inherent effect on the test results. Any preloading of the hybrid system during or after the installation is expected to stiffen the response and increase the load resistance capacity; however the practicality of adapting such an approach on a prototype scale is questionable.
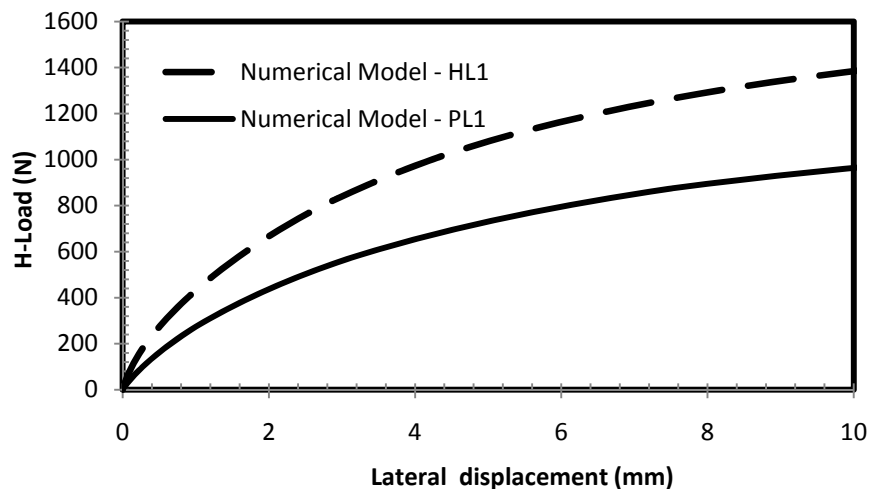
Figure 5-10 Lateral load vs. lateral displacement response for monopile-footing (HL1) and single pile (PL1) as estimated by PLAXIS 3D

Figure 5-11 shows the failure mechanisms under combined loading of tests PL1 and HL1. The mechanisms demonstrate that the presence of the plate footing fixed rigidly on top of the pile head helped producing a wider failure mechanism thus allowed to generate a higher lateral capacity.

a) Failure mechanism of test PL1   b) Failure mechanism of test HL1

c) Failure mechanism of test PL1   d) Failure mechanism of test HL1
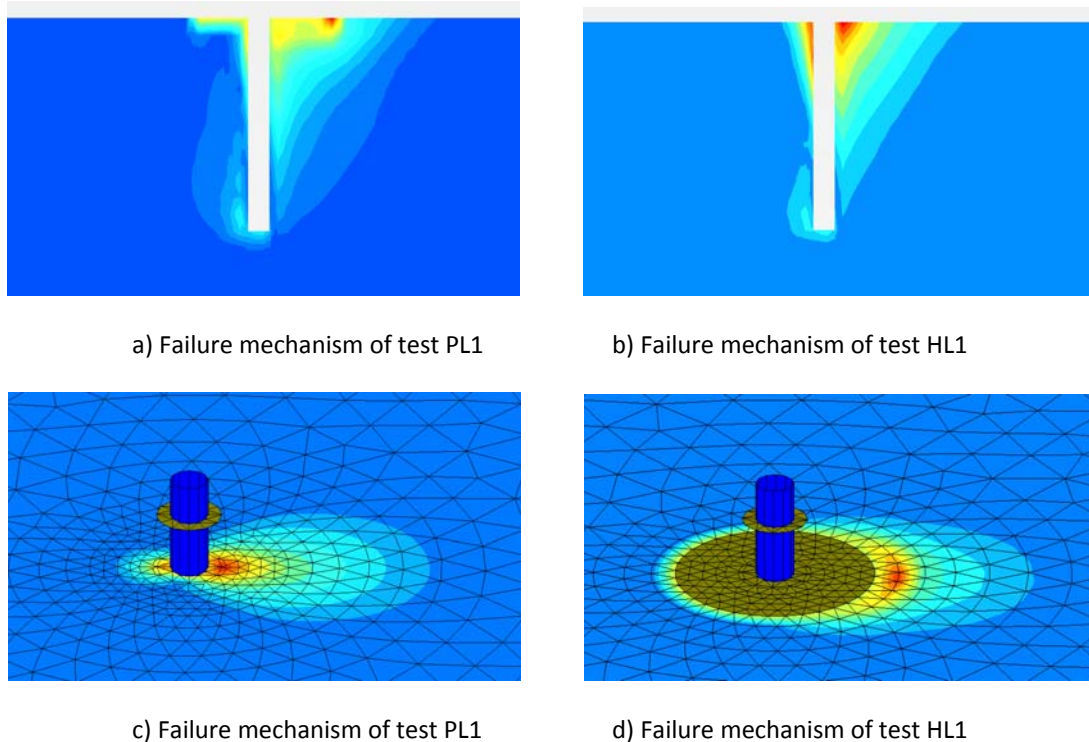
Figure 5-11Failure mechanism under combined loading

5.7 Discussion and Conclusions

The presence of the foundation plate rigidly attached to a monopile provides a degree of moment restraint to the pile head through the soil reaction acting on the underside of the bearing plate. For this soil reaction to be generated, it is necessary that the plate rotates into the soil surface. Consequently, it is likely that the very initial response of the hybrid foundation remains governed by the lateral stiffness of the pile, but as the foundation system rotates the lateral stiffness of the hybrid foundation response is influenced by the moment restraint provided by the bearing plate. The efficiency of the bearing plate to stiffen the response of the hybrid foundation will be greatly influenced by the initial

contact between the bearing plate and the soil, and any vertical pre-stress acting under the plate.

In the tests conducted as part of this program, it is evident that the axial capacity of the pile was significantly greater that the applied vertical load acting on the foundation. Consequently, there would not be any initial vertical pre-stress acting on the underside of the bearing plate. Also, any gap between the soil and the plate would eliminate any influence of the bearing plate on the initial lateral response. Nevertheless, the small number of tests conducted did provide some valuable information from which the following conclusions can be drawn:

- The presence of a foundation plate rigidly attached to a monopile provides a degree of moment restraint to the pile head by the restoring moment produced by the contact stresses between the plate and the soil.
- The centrifuge testing results showed that the very initial response of the hybrid foundation is governed by the lateral stiffness of the pile. The lateral stiffness beyond this initial movement was significantly enhanced by the presence of the bearing plate.
- The efficiency of the bearing plate to stiffen the response of the hybrid foundation is highly influenced by the initial contact between the bearing plate and the soil
- Further research is required to explore the influence of the geometry of the respective foundation elements, and the response of hybrid monopile-footing foundation systems in different soils.

5.8 References

Berezantsev et al. (1961). Load bearing capacity and deformation of piled foundations. *In* Proceedings of the 5th International Conference of Soil Mechanics and Foundation Engineering, Paris, 2, 11-12.

Bransby, M. F. and Randolph, M. F. (1998). Combined loading of skirted foundations. Geotechnique, 48 (5): 637-655.

Brinch Hansen, J. (1961). The ultimate resistance of rigid piles against transversal forces. The Danish Geotechnical Institute Bulletin (12): 5-9.

Broms, B.B. (1964). Lateral resistance of piles in cohesionless soils. ASCE Journal of the Soil Mechanics and Foundation Division Proceedings (JSMFD), 90(SM3), 123-156.

Craig, W.H. (1984). Installation studies for model piles. *In* Proceedings of Application of Centrifuge Modelling to Geotechnical Design, pp. 440-455, Balkema, Rotterdam.

Craig, W.H. and Sabagh, S.K. (1994). Stress-level effects in model tests on piles. Canadian geotechnical journal. 31(1): 28-41.

Davis, E.H. and Booker, J.R. (1971). The bearing capacity of strip footings from the standpoint of plasticity theory. *In* Proceedings of the 1st Australia-New Zealand Conference on Geomechanics, Melbourne (Australia), 276-282.

Duncan, J. M., Evans, L. T., and Ooi, P. S. (1994). Lateral load analysis of single piles and drilled shafts. ASCE Journal of Geotechnical Engineering, 120(6): 1018-1033.

Gemperline, M.C. (1998) Coupled effect of common variables on the behavior of shallow foundations in cohesionless soils. Centrifuge '88. 285-292. Balkema, Rotterdam.

Gourvenec, S. and Randolph, M. F. (2003). Effect of strength nonhomogeneity on the shape and failure envelopes for combined loading of strip and circular foundations on clay. Geotechnique, 53(6): 575-586.

Houlsby, G. T. & Puzrin, A. M. (1999). The closed-form solutions for the bearing capacity of strip footing under combined loadings. *In* Proceedings of the Royal Society Conference, London, UK, pp. 893-916.

Kim, J. B., Singh, L. P., and Brungraber, R. J. (1979). Pile cap soil interaction from full scale lateral load tests. ASCE Journal of Geotechnical Engineering, 105(5): 643-653.

Kimura, T., Kusakabe, O. and Saitoh, K. (1985). Geotechnical Model Tests of Bearing Capacity Problems in a Centrifuge. Géotechnique, 35(1): 33-45.

Maharaj, D.K. (2003). Load-Deflection Response of Laterally Loaded Single Pile by Nonlinear Finite Element Analysis. EJEG .

Matlock, H., and Reese, L. C. (1960). Generalized solutions for laterally loaded piles. ASCE Journal of Soil Mechanics and Foundations Division, 86(SM5), 63-91.

Meyerhof, G.G. (1976). Bearing capacity and settlement of pile foundations. ASCE, Journal of Geotechnical Engineering. 102(GT3), 197-228.

Mokwa, R.L. (1999). Investigation of the Resistance of Pile Caps to Lateral Loading. Ph.D Thesis, Virginia Polytechnic Institute, Blacksburg, Virginia.

Mokwa, R.L., and Duncan, J.M. (2001). Experimental evaluation of lateral-load resistance of pile caps, Journal of Geotechnical and Geoenvironmental Engineering, ASCE, 127(2): 185 -192.

Mokwa, R.L., and Duncan, J.M. (2003). Rotational restraint of pile caps during lateral loading, Journal of Geotechnical and Geoenvironmental Engineering, ASCE, 129(9): 829-837.

Ovesen, N.K. (1975). Centrifugal testing applied to bearing capacity problems of footings on sand. Geotechnique, 25(2): 394–401.

Poulos, H.G and Randolph, M.F. (1983.) Pile group analysis: a study of two methods, Journal of Geotechnical and Geoenvironmental Engineering, ASCE, 109(3), 355-372.

Poulos, H. G. (1971). Behaviour of laterally loaded piles: Part I - single piles. ASCE Journal of the Soil Mechanics and Foundations Division, 97(SM5), 711-731.

Poulos, H.G. (1988). Marine Geotechnics. Unwin Hyman, London.

Powrie, W. and Daly, M.P. (2007). Centrifuge modeling of embedded retaining wall with stabilizing bases. Geotechnique, 57(6): 485-497.

Randolph, M. F. (1981). The response of flexible piles to lateral loading. Géotechnique, 31(2): 247-259.

Reese, L. C., Cox, W. R., and Koop, F. D. (1974). Analysis of laterally loaded piles in sand. Offshore Technology Conference, Vol. II, Paper No. 2080, Houston, Texas, 473-484.

Schofield, A.N. and Taylor, R.N. (1988). Development of standard geotechnical centrifuge operations. Centrifuge 88, pp. 29-32.

Stone, K., Newson, T. and Sandon, J. (2007). An Investigation of the Performance of a 'Hybrid' Monopile-Footing Foundation for Offshore Structures. *In* Proceedings of the 6th International Offshore Site Investigation and Geotechnics Conference, London, UK, 391-396.

Taylor, R.N. (1995). Geotechnical Centrifuge Modeling. Blackie Academic and Professional, An Imprint of Chapman and Hall, Glasgow, ISBN 0 7514 0032 7

Terzaghi, K. (1943). Theoretical Soil Mechanics. John Wiley, New York.

Zhang, L., Silva, F. and R Grismala, R. (2005). Ultimate Lateral Resistance to Piles in Cohesionless Soils. Journal of Geotechnical and Geoenvironmental Engineering, Vol. 131(1): 78–83.

Chapter 6

6   Conclusions and Recommendations

6.1   Introduction

In this thesis, numerical and experimental investigations were conducted with an emphasis to undertake a 'proof of concept' or feasibility study of a novel monopile - footing hybrid foundation system to support laterally loaded structures including wind turbines. The study gave an insight on the behavior of the proposed system under various vertical, horizontal and moment load combinations for both drained and un-drained loading conditions. An extensive finite element analysis using the commercial software packages PLAXIS 2D and PLAXIS 3D Foundations was used to provide good interpretation of the behavior of the hybrid foundation system and to further extend the database of findings through parametric analysis. Furthermore, the findings of the numerical results were supported by experimental testing on scaled physical model foundations at enhanced gravity (on a centrifuge).

The measurable objectives associated with the conducted test program were as follows:

- Undertake a 'proof of concept' or feasibility study of a novel foundation system to support laterally loaded structures.
- Evaluate the performance of the proposed 'hybrid' systems under drained and undrained loading conditions
- Develop guidelines for the design of HMFF at different soil conditions, while taking account of the influence of the relative geometry of the constituent elements of the 'hybrid' system (i.e. the pile length and plate diameter) on the performance characteristics of the system.

6.2 Main Findings

The study revealed the feasibility of using the proposed hybrid monopile-footing foundation system as an efficient foundation option to support structures subjected to combinations of vertical, horizontal and moment loads under drained and undrained loading conditions.

The hybrid monopile-footing foundation system provides a significant improvement in the sliding and rocking resistances. This is very useful when constructing a laterally loaded foundation on weak bearing soil, where it becomes essential to reduce the vertical loads applied to the soil, especially when sliding resistance is the governing factor in the foundation design.

The study developed guidelines for the design of the hybrid foundation system on different drained and undrained loading conditions, while taking account of the influence of the relative geometry of the constituent elements of the 'hybrid' system (i.e. the pile length and plate diameter)

The study produced the design guidelines required to predict the vertical and lateral ultimate capacities of the hybrid foundation system in addition to expressions of the *V-H* and *V-M* failure envelopes in the 2D and 3D loading conditions.

The produced failure envelopes serve as a design tool that allows designing the hybrid foundation system, depending on the required ultimate capacity and the in-situ soil conditions. Moreover, for a given geometry, the failure envelopes and/or the provided equations can estimate the ultimate lateral and rocking capacities of the hybrid foundation systems as well as for shallow foundations.

The following subsections summarize the main findings of the study of the behavior of hybrid monopile - footing foundation system under combined drained loading, undrained loading in addition to the findings of the experimental centrifuge testing.

6.2.1 Main Findings of Chapter 3: Numerical Investigation of Hybrid Monopile-Footing Foundation Systems under Drained Loading Conditions

2D Plane Strain Loading Conditions:

- The maximum lateral load resistance of the hybrid monopile-footing foundation system exceeded the lateral capacity of the shallow foundation by 27% at L/W = 0.25, 127% at L/W = 0.5 and 218% at L/W = 1.0.
- A minimum L/W ratio of 1.0 is recommended, to achieve a significant improvement of 33% in the rocking resistance of the hybrid monopile-footing foundation system.

3D Loading Conditions:

- A minimum L/W ratio of 1.0 is recommended, to achieve a significant improvement in the sliding and rocking capacities of the hybrid monopile-footing foundation system.
- At this L/W ratio of 1.0, the observed increase in the lateral loading and rocking resistances were 27% and 34% respectively.

6.2.2 Main Findings of Chapter 4: Numerical Investigation of Hybrid Monopile-Footing Foundation Systems under Undrained Loading Conditions

2D Plane Strain Loading Conditions:

- The maximum lateral resistance of the hybrid monopile-footing foundation system exceeded the lateral capacity of the shallow foundation by 60 to 135% at *L/W*= 0.25, 150% to 290% at *L/W*= 0.5, and by up to 400 to 500% at *L/W*= 1.0 (for instant breakaway and fully bonded foundation-soil interface, respectively).

- Increasing the pile length ($L/W \geq 0.5$) produced a noticeable gain in the maximum rocking resistance by 20% to 34% at $L/W=0.5$ and 100% to 144% at $L/W=1$.
- At $L/W \leq 0.25$ the presence of the short pile / key is expected to reduce the rocking capacity by up to 25%.
- At low vertical load values ($V/V_{max}<0.2$), both the shape and size of the generalized V-H and V-M failure mechanisms are highly affected by the condition of the foundation-soil interface, which is in contrast to the case of high V-load values ($V/V_{max}>0.8$).

3D Loading Conditions:

- The observed gain in the maximum lateral capacity of the hybrid monopile-footing foundation system exceeded the lateral capacity of the shallow foundation by 60% at $L/W= 0.5$, and 85% $L/W= 1.0$ (fully bonded foundation-soil interface).
- The maximum rocking resistance of the hybrid monopile-footing foundation system exceeded the rocking capacity of the shallow foundation by 20% at $L/W= 0.5$, and 135% $L/W= 1.0$ (fully bonded foundation-soil interface).

6.2.3 Main Findings of Chapter 5: Physical Centrifuge Testing of Hybrid Monopile-Footing Foundation Systems on Drained Sands

- The presence of a foundation plate rigidly attached to a monopile provides a degree of moment restraint to the pile head.
- The very initial response of the hybrid foundation is governed by the lateral stiffness of the pile.
- The efficiency of the bearing plate to stiffen the response of the hybrid foundation is highly influenced by the initial contact between the bearing plate and the soil.

6.3 Discussion

From the previous findings, it was observed that the sliding resistance in particular was highly affected by the loading and strains conditions. In a 2D plane strain condition, which is applicable for long shallow foundations such as wall footings, adding a short shear key or a row of short piles to create a short hybrid system of $L/W = 0.25$ improved the lateral by 25 to 60% (for drained and undrained soils, respectively). However, in a 3D condition involving a circular hybrid foundation system with a pile diameter of 1/10 the footing width; the response of the hybrid foundation system is dominated by the footing action. The presence of a short pile in circular hybrid systems did not increase the lateral capacity of the foundation but rather helped reducing the dependency on the vertical load ratio by allowing the hybrid foundation system to produce the maximum lateral resistance at a V/V_{max} ratio of 0.4, as opposed to 0.5 for shallow footings. The same behavior was observed for the rocking capacity.

At L/W ratio of 1.0, comparing the 2D to the 3D results revealed that the percentage of improvement in the lateral capacity dropped from 218 to 27% in drained soils and from 500 to 85% in undrained soils (the reduction was about 85%). The results also showed that the improvement in the rocking was unaffected by the 3D loading effects.

In this same context, the observed results show that the improved resistance provided by the hybrid monopile-footing foundation systems tends to be more pronounce in undrained soils. Nonetheless, the proposed hybrid systems proved to be a feasible foundation solution and were capable of improving the rocking and sliding resistances for both drained and undrained conditions.

6.4 Recommendations for Future Research

The proposed 'hybrid' monopiled-footing foundation system is most timely since it has the potential to significantly improve the performance of current foundation design. This study demonstrated that the hybrid monpile footing foundation system provides a significant increase in lateral capacity and stiffness over that of a single pile.

Some features which have not been taken into account or have not given satisfactory answers are described as motivations for future research and presented in the following sections.

- The study was restricted to the application of monotonic load combination with the emphasis being on the investigation of the basic system performance, and the interaction of the constituent foundation components in resisting the applied loads. Further investigation on the behavior the proposed hybrid system under cyclic and transient loading may be required.

- The study produced a fair amount of data in the form of V-H and V-M failure envelopes and produced closed form expressions to describe these envelopes, which are important in evaluating the ultimate limit states of the hybrid system. It could be necessary to study in more detail the behavior of the system under service loading conditions and generate expressions to describe the vertical, lateral and rotational stiffness of the hybrid system.

- The conducted numerical study provided a good understanding on the influence of the relative geometry of the constituent elements of the 'hybrid' system performance characteristics of the system. However, the design and construction of an instrumented prototype monopile-footing hybrid system that supports a scaled wind turbine may be a crucial step in the way of establishing the design guidelines of the proposed system.

6.5 Conclusion

This dissertation has investigated an innovative monopile - footing hybrid foundation system, which has proved to be a promising foundation option for offshore wind turbines. It is expected that the successful performance of the proposed hybrid system, which was observed in this study, will lead to a significant interest in the research community. This would accelerate the research and development of such systems and further enhance offshore foundation technology.

The hybrid system proposed here is directly relevant to those working in the wind energy industry since it explores a methodology towards adapting existing offshore design (from

the oil and gas industry) to the particular requirements of wind turbines. In terms of economic value, the wind energy sector is now firmly established as one of the largest sectors in the energy market. There is no doubt that any technological advantage for Canada in the wind energy sector would result in significant economic gains to Ontario and Canada.

Curriculum Vitae

Name: Mohamed El-Marassi

Post-secondary   Alexandria University
Education and   Alexandria, Egypt
Degrees: 1996-2001 B.Sc.

                    Alexandria University
                    Alexandria, Egypt
                    2001-2006 M.Sc.

                    The University of Western Ontario
                    London, Ontario, Canada
                    2006-2011 Ph.D.

Honours and   John Booker Award
Awards: Geotechnical Research Centre, The University of Western Ontario
                    2010

                    Milos Novak Memorial Award
                    Geotechnical Research Centre, The University of Western Ontario
                    2009

                    Nomination for "The Graduate Student Teaching Awards"
                    The University of Western Ontario
                    2007

                    Western Graduate Research Scholarships
                    The University of Western Ontario
                    2006-2010

                    The Engineer of the Year
                    The Engineers Syndicate, Egypt
                    2001

                    Scholarship for Outstanding Undergraduates
                    Alexandria University
                    1996-2001

                    Quonswa award for Excellency in Hydraulics
                    Alexandria University
                    1999 - 2000

Related Work Experience   Lecturer
Civil & Env. Eng. Dept., The University of Western Ontario
2008

Research Assistant
Civil & Env. Eng. Dept., The University of Western Ontario
2006-2010

Teaching Assistant
Civil & Env. Eng. Dept., The University of Western Ontario
2006-2010

Assisstant lecturer
Structural Engineering Department, Alexandria University
2006

Instructor
Structural Engineering Department, Alexandria University
2001-2006

Geotechnical/Structural Design Engineer
FACB Fathi Abdrabbo Consulting Bureau, Alexandria, Egypt
2001-2005

Publications:

Stone, K.J.L., Newson, T.A., **El-Marassi, M.**, El-Naggar, H., Taylor, R.N. and Goodey, R.J. (2010). An investigation of the use of a bearing plate to enhance the lateral capacity of monopile foundations. *In* Proceedings of the 2nd International Symposium on Frontiers in Offshore Geotechnics (ISFOG 2010), Perth, pp. 623 - 628.

Stone, K.J.L., Newson, T. and **El-Marassi, M.** (2010). An investigation of the performance of a monopiled-footing foundation. *In* Proceedings of the 7th International Conference on Physical Modelling in Geotechnics (ICPMG 2010), Zurich, pp. 829 - 833.

El-Marassi, M., Newson, T., El-Naggar, H. and Stone, K. (2008). Numerical modeling of the performance of a hybrid monopiled-footing foundation. *In* Proceedings of the 61st Canadian Geotechnical Conference (GeoEdmonton 2008), Paper n. 420, pp. 97-104.

Abdrabbo, F. M., Abouseeda, H. M., Gaaver, K. E. and **El-Marassi, M. A.,** (2005). Behavior of strip footings resting on sand reinforced with tire-chips. *In* ASCE Geotechnical Special Publication No.140: Slopes and Retaining Structures under Seismic and Static Conditions (Geo-Frontiers 2005 Congress, Austin, Texas, January 2005), pp. 130-142.